THE UNIVERSITY OF HULL

How does grain size distribution impact the mobility and deposition of analogue pyroclastic density currents?

being a Thesis submitted for the Degree of

MSc (by Research) Geology

in the University of Hull

by

Thomas Johnston

November 2022

Abstract

Pyroclastic density currents (PDCs) are hot, density-driven flows of gas, rock and ash generated during explosive volcanic eruptions or from the collapse of lava domes. PDCs are able to travel for tens of km, traversing topographic barriers hundreds of metres high. They are notably more mobile than other gravity currents of comparable size. Gas fluidisation has been attributed as a major contributor to this high mobility. Experimentation on non-fluidised granular flows has assessed the influence of grainsize on mobility, finding that the finer the grains, the larger the mobility of the mass. Recent advances in analogue models of gas-fluidised granular currents have revealed the impact of aeration on current mobility, and how flow behaviour can control deposit architecture and morphology. However, these experiments have so far largely used only a single grain-size.

The impact of grain size variations on the mobility of aerated granular currents remains untested. Therefore, this project investigated the impact of grain size distribution on current velocity and run-out distance in a series of analogue experiments using an aerated flume.

The experiments demonstrate that the mobility of these dense granular currents is related to the proportion of fines within the current but is primarily controlled by the initial sorting of the current. The more well sorted currents have a lower velocity but a greater run-out distance than the poorly sorted currents. The proportion of fines is found to have very little control on current velocity, but does have some control on run-out distance and degree of non-uniformity in velocity. Deposition during the analogue experiments occurs by a combination of gradual and stepwise aggradation.

This work contributes our understanding of PDC mobility and how mobility can be interpreted from ignimbrites, with implications for numerical modelling and hazard mapping of PDCs.

Acknowledgements

Firstly, I would like to thank my supervisors Becky Williams, Pete Rowley and Natasha Dowey. Their knowledge has taught me so much over the past year and their support has always been there to push me to achieve the best that I can. I'm forever grateful for everything they have done.

This project would not have been possible without the lab work carried out at the University of Bristol. I would like to thank the School of Earth Sciences for letting me use their dry lab space, the technicians for helping set up the space and give me the required lab inductions, and all the other staff in the department for the chats with coffee.

I have been very lucky to join such a supportive community within the Catastrophic Flows Research Cluster and the wider volcanological community. I am grateful to Pete for introducing me to volcanology and PDCs at undergraduate and Becky for helping my interest grow while supervising my mapping dissertation.

I would like to thank Matt Johnson and Nemi Walding for their support throughout the project. Offering their thoughts on results, chatting about PDCs in general and especially Nemi for being my wobble buddy. I am also grateful to staff in the department, such as Eddie Dempsey, Anna Bird, Mike Widdowson, Lucy Campbell, Dave Bond and Bryony Caswell for taking the time to chat about my research and supporting me as I develop as an academic, allowing me to demonstrate in practicals and on field courses, and give a lecture. Extra thanks must go to Eddie Dempsey and Anna Bird for supporting me since I started my undergraduate degree at the University of Hull without you both I wouldn't be here now.

Thanks to all my friends who have supported me, kept me sane and been a constant source of entertainment, especially Matt, Charlotte, Rebecca, and Ben. I would also like to give special thanks to my partner, Jess, who has kept me sane and put up with me dragging her around ignimbrites on holiday. And, final thanks to my parents who have supported me in so many ways over the four years I've been in Hull.

Final thanks must go to my internal and external examiners, Anna Bird and Ralf Gertisser for taking the time to read this work. Their helpful feedback which has improved this manuscript greatly.

Contents

List of Figures

List of Tables

1 Introduction

Pyroclastic density currents (PDCs) are density-driven multiphase flows of hot mixtures of gas and volcanic particles generated during volcanic eruptions. These flows are initiated with little warning, can move at high velocities, have run-out distances ranging from hundreds of metres to more than a hundred kilometres, and can surmount topographic obstacles (Miller & Smith, 1977; Fisher et al., 1993; Bursik & Woods, 1996; Branney & Kokelaar, 2002; Loughlin et al., 2002). These characteristics are shown in the AD 186 Taupo eruption in New Zealand, where the flow had a minimum speed of 150 ms^{-1} and likely exceeded 300 ms^{-1} with run-out distances of approximately 80 km (Wilson, 1985).

PDCs can be generated from the collapse of eruptive columns (Fig. 1.1a-c), the collapse of lava domes (Fig. 1.1e), lateral blasts (Fig. 1.1d), and remobilisation of unstable agglutinates and lava autobreccias (Fig. 1.1f) (Druitt, 1998; Branney & Kokelaar, 2002). Examples of lava dome collapse inducing PDCs are the 1991 Unzen eruption (Yamasato et al., 1998), and the eruption of Soufrière Hills Volcano, Montserrat where in 2000, the collapse of 95% of the lava dome formed approximately 40 PDCs (Carn et al., 2004). A famous example of lateral blast induced PDCs is from the 1980 eruption of Mt St Helens where the initial lateral blast caused a widespread PDC prior to generation of the Plinian column (Kieffer, 1981; Criswell, 1987). In the 1991 eruption of Mt Pinatubo PDCs were generated by either the collapse of parts of a sustained Plinian column or the repeated collapse of the whole column (Newhall & Punongbayan, 1996).

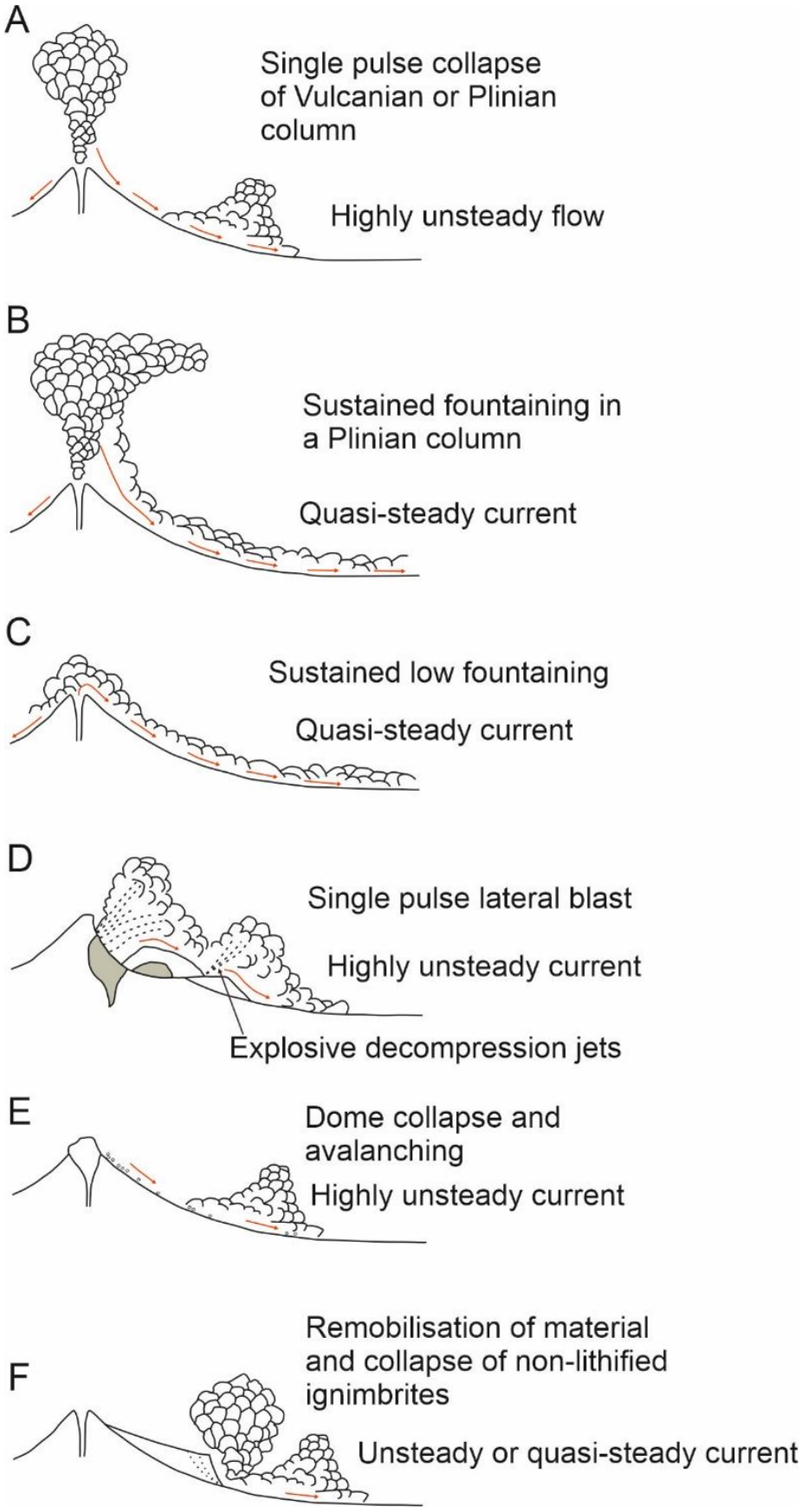

Figure 1.1: Sketches of different mechanisms for generating PDCs (Branney & Kokelaar, 2002)

Source conditions control the initial conditions of PDCs, their composition and behaviour. Changes in source conditions and interactions with the substrate can cause rapid flow transformation (Brand et al., 2014), as well as causing the volume, mass flux, grain-size, particle concentration and bulk density to vary over several orders of magnitude within a single PDC (Lube et al., 2007). This variation produces a range of endmembers which can be defined as either a fully dilute current or a granular-fluid current (Branney & Kokelaar, 2002; Breard & Lube, 2017; Smith et al., 2018). In granular flows motion is dominated by particle interactions (Calder et al., 2000), which means that if they are continuously fed at the source or favoured locally by steep slopes and topographic channels they can propagate for large distances through forced-convection mechanisms (Palladino & Giordano, 2019). Whereas, in dilute flows, gas is the dominant phase and transports particles in turbulent suspensions (Dade & Huppert, 1996; Lube et al., 2007). During transport, the density of the current can decrease due to the expansion of particles, deposition of particles and increasing ambient fluid. However, the current density can be increased by erosion of the substrate and entrainment of this material (Andrews & Manga, 2011).

The deposits from PDCs are broadly categorised as either ignimbrites or block-and-ash flow deposits (Sparks, 1976; Cas & Wright, 1987; Branney & Kokelaar, 2002). Ignimbrites are typically pumice- and ash-rich deposits that often appear massive but can contain sedimentary structures such as stratification and bedforms, soft sediment deformation, erosional surfaces, and grading (Sparks, 1976; Fisher & Schmincke, 1984). The usage of ignimbrite has varied over time with initial use to refer to welded tuffs, ash-dominated tuffs, and felsic pumice-and-ash flow deposits (Smith, 1960; Fisher, 1966; Sparks et al., 1973). While more recently ignimbrite has been used to refer to the deposit of pumice and ash through to scoria and ash-rich pyroclastic density currents. Irrespective of the composition, grain size, emplacement temperature, volume and relationship with topography (Giordano & Cas, 2021). In this thesis the more recent usage of ignimbrite following Giordano & Cas (2021) will be used.

Block-and-ash flow deposits are associated with collapse of lava domes and generally consist of dense, poorly to moderately vesiculated lava blocks with similar composition non-pumiceous ash (Cas & Wright, 1987; Branney & Kokelaar, 2002; Charbonnier & Gertisser, 2011). Studying these deposits helps develop our understanding of PDCs as they record temporal and spatial variations within the flow.

At least 600 million people live in areas potentially affected by volcanic hazards (Auker et al., 2013) and PDCs pose the largest threat to life of all volcanic hazards. Since 1600 AD, PDCs have caused 33% of all fatalities resulting from in volcanic activity (91,484 people; Auker et al., 2013). Due to this extreme risk to life, it is important to study PDCs to develop our understanding of the flow mechanics using field data (e.g. Walker, 1985; Branney & Kokelaar, 1992; Brown & Branney, 2013), analogue models (e.g. Savage & Lun, 1988; Vallance & Savage, 2000; Bareschino et al., 2008; Roche et al., 2008, 2010; Rowley, 2010; Rowley et al., 2014; Lube et al., 2015; Breard et al., 2016; Breard & Lube, 2017; Smith et al., 2018, 2020) and numerical models (e.g. Francis & Baker, 1977; Bursik & Woods, 1996; Druitt et al., 2007; Breard et al., 2019; Trolese et al., 2019; Esposti Ongaro et al., 2020; Deal et al., 2021). By using this understanding, it is possible to generate hazard assessments for areas near volcanoes.

One of the least understood characteristics of PDCs is their high mobility, yet this is what makes them so hazardous to communities even far from the volcanic vent.

1.1 Scope of thesis

This project aims to investigate the mobility of PDCs and the role that grain size distribution may have in controlling that mobility.

This aim will be achieved by answering three main research questions:

(1) how does the grain size distribution affect the run-out of PDCs?

(2) how does the grain size distribution affect the velocity of PDCs?

(3) how does the grain size distribution affect the deposits of PDCs and how can we use the depositional record to infer PDC mobility?

These research questions will be examined through a series of analogue flume experiments. First, by investigating the relationship between the range of grain sizes within an analogue PDC and current behaviours such as velocity and run-out distance in flume experiments. Second, by observing how these behaviours are recorded in the deposits from the analogue PDCs.

Chapter 2 reviews our present understanding of the mobility of pyroclastic density currents and how this can be investigated. Chapter 3 details the methods used in this thesis. Chapter 4 will answer the research questions about current mobility (1 and 2), both qualitatively describing and quantitatively defining changing current conditions with changing grain size distribution. Chapter 5 addresses research question 3, by interpreting bedforms within the deposits of the analogue experiments for common features and using these to interpret current behaviours, particularly in the flow boundary zone. Chapter 6 draws together the results from Chapter 4 and 5 to discuss the implications of this work on our understanding of PDC mobility, current behaviour and ignimbrite interpretation.

2 Literature Review

This chapter will provide an overview of the previous research carried out into pyroclastic density currents (PDCs). Initially this chapter will focus on PDC mobility, examining how mobility has been previously quantified and possible controls of the high mobility. After covering the mobility of PDCs this chapter will focus on sorting within PDCs, variation in grain sizes, PDC deposition and approaches to understanding PDCs. By examining the previous literature surrounding PDC behaviours and grain sizes within PDCs it will be possible to compare previous work to the results of this study in Chapter 6. The review of approaches to understanding PDCs will be used to create an experimental methodology (Chapter 3) that is best suited to answer the research questions.

2.1 Pyroclastic density current mobility

The mobility of a PDC can be thought of in terms of its run-out distance, area of run-out, velocity and ability to scale topographic barriers. For example, at Mt St Helens the May 1980 PDC overtopped the > 200 m Johnston Ridge (Criswell, 1987), PDCs that deposited the Campanian Ignimbrite overtopped the 685 – 1000 m high ridge of the Sorrento Peninsula, Italy (Fisher et al., 1993), and PDCs from the Fisher Caldera, Alaska, surmounted topographic barriers > 500 m high within the Tugamak Range (Miller & Smith, 1977).

Pyroclastic density currents are highly mobile, typically with larger run-outs than other types of gravity mass flows (Sparks, 1976), such as debris avalanches (Hayashi & Self, 1992). A notable difference between these flows is their material properties. Debris avalanches are mass movements of dry, unconsolidated, previously deposited rock material (Collins & Melosh, 2003) while PDCs are hot mixtures of gas and volcanic particles generated during volcanic eruptions (Dufek, 2016). Both PDCs and debris flows can be fluidised (Hayashi & Self, 1992). In debris flows this fluidisation is caused by acoustic fluidisation, where the shock of the impact briefly fluidises the debris flow (Gaffney & Melosh, 1982), which is in contrast to PDCs where fluidisation occurs over at least several minutes (Sparks, 1976), predominantly by excess gas pore pressure (Fenner, 1923; Wilson, 1980). Therefore, the difference in mobility may be attributed to material properties rather than flow mechanics (Hayashi and Self, 1992).

2.1.1 Quantifying mobility

There have been multiple attempts to quantify mobility using modelling and data from previous eruptive events. Mobility can be quantified as a ratio of height:run-out distance (H/L; Hayashi & Self 1992). This assumes that mobility is primarily controlled by eruption mechanics (using column height as a proxy). There is a correlation between increasing current volume and decreasing H/L ratio, which suggests that as current volume increases the run-out distance is expected to increase (Fig. 2.1). However, the relationship shown in the graph is limited by a lack of data for moderate to large ignimbrites, and in small scale ignimbrites eruption height can be underestimated (Druitt, 1998) which has resulted in large uncertainties.

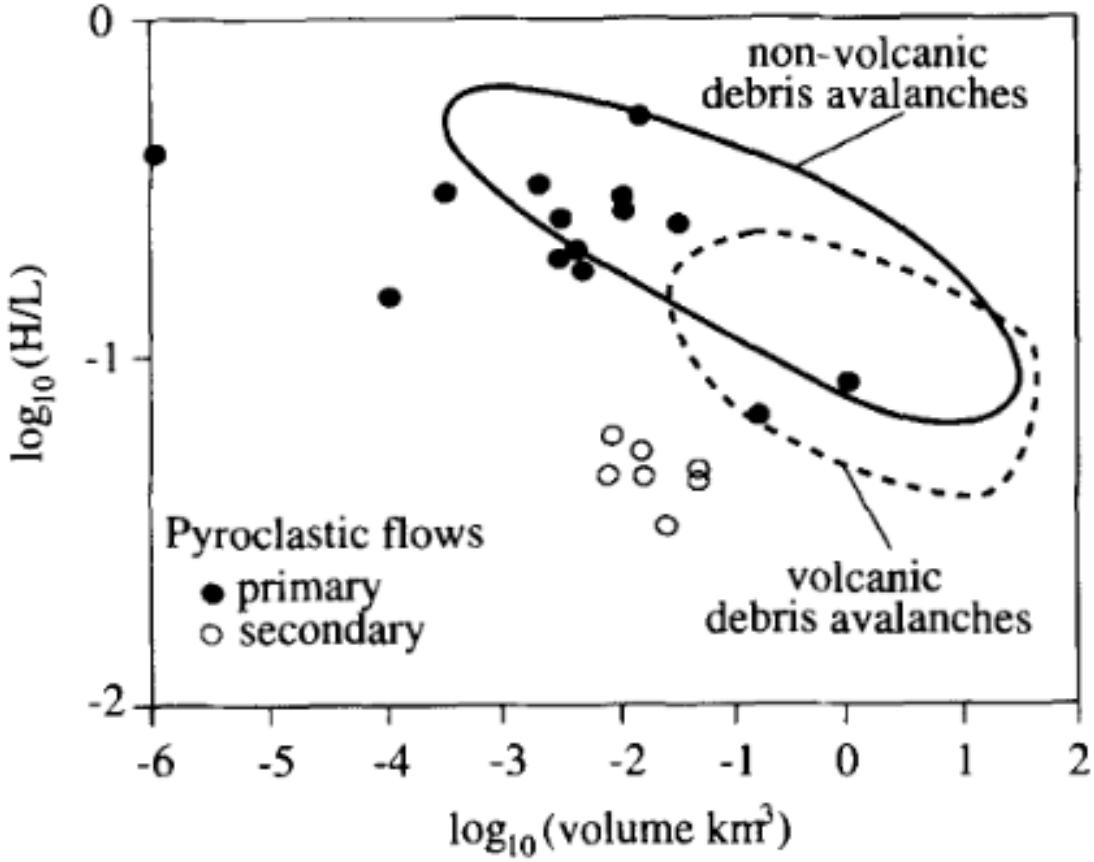

Figure 2.1: Plot of H/L (ratio of column height:run-out distance) against volume for PDCs with circles showing average values for debris avalanches (Druitt, 1998)

Based on field data from the Mt St Helens 1981 eruption, an energy cone model was created with equations for surge acceleration (equation 1), velocity (equation 2 & 3) and run-out time (equation 4) based on slope angle and slope distance:

$$a(i) = g(\sin\beta - \mu\cos\beta) \qquad \text{(eq. 1)}$$

$$v^2(i) = v_0^2 + 2a(i) \times s(i) \qquad \text{(eq. 2)}$$

$$v(i) = \sqrt{2g\Delta h(i)} \qquad \text{(eq.3)}$$

$$t(i) = 2s(i) \div (v_0 + v_i) \qquad \text{(eq. 4)}$$

where a(i) = surge acceleration, g = acceleration due to gravity, β = slope angle, μ is Heim coefficient (coefficient of constant kinetic friction), v(i) = velocity, v_0 = initial velocity, s(i) = slope distance, $\Delta h(i)$ = difference in elevation between energy surface and ground topography and t(i) = run-out time (Malin & Sheridan, 1982).

This model however only considers the whole flow, not individual parts of the flow, which means that it does not consider flow channelization (Clarke et al., 2020) which was observed in small volume flows in the deposits from the Soufrière Hills Volcano, Monserrat (Calder et al., 1999). Furthermore, this model does not consider how the flow changes temporally and spatially as it is calculated using an average slope angle (Clarke et al., 2020).

Initially it was suggested that the height of the eruption column at the time of collapse controls the mobility. For collapses of eruptive columns between 5-10 km high, the subsequent flows would be mobile enough to travel for the predicted run-out distance without the need for fluidisation (Sparks, 1976).

Based on analogue experiments, using non-fluidised, poly-disperse volcanic materials, the coefficient of friction, μ_A, has been calculated using equation 5:

$$\mu_A = \frac{h}{l} \qquad \text{(eq. 5)}$$

where h is the vertical drop of the granular material and l is the horizontal distance travelled (Dade & Huppert, 1996; Cagnoli & Romano, 2012). Cagnoli and Romano (2012) have suggested that mobility is the reciprocal of the coefficient of friction. This equation suggests that in granular flows an increase in eruptive column height with the same run-out distance would result in a less mobile current. Therefore the current mobility cannot be solely controlled by the height of the eruption column.

The most common value for flow mobility is based on the ratio between run-out distance and vertical height collapsed. However, this does not totally capture mobility as errors in the value for run-out distance increases with deposit volume; this produces low ratios suggesting greater mobility (Hayashi & Self, 1992). To account for this source of error an equation for mobility which is not affected by volume was created:

$$m_e = \frac{\Delta L}{H_i} = \frac{\alpha}{tan\delta - tan\theta} \qquad \text{(eq. 6)}$$

where ΔL is the run-out distance, H_i is the thickness of the granular mass on top of topography, α is the particle aspect ratio, δ is effective friction and θ is angle of topography (Lucas & Mangeney, 2007).

2.1.2 Controls over mobility

Broadly, there are a range of eruption mechanics that can control PDC mobility, which includes fluidisation, flow volume, discharge rate, eruptive column height and rheology (Cagnoli & Romano, 2012; Sulpizio et al., 2014; Palladino & Giordano, 2019). Mobility can be further modified by local environmental impacts such as topography, atmosphere and hydrosphere (Sulpizio et al., 2014; Palladino & Giordano, 2019). Here, some of these key variables are explored in more detail.

2.1.2.1 Fluidisation

One of the explanations for the high mobility of PDCs is the lubrication of flows by the fluidisation of fines, whereby the yield strength is removed and therefore any shear strength produces strain strength (Sparks, 1976).

The fluidisation of PDCs requires a gas supply capable of lasting for several minutes, with major sources of gas coming from the exsolution of gas from pyroclastic fragments and entrainment of air. Small quantities of pyroclastic fragments can generate large volumes of gas and gas velocities high enough to cause fluidisation. As finer particles in the flow fluidise there is lubrication of larger particles similar to how water reduces yield stress in a mudflow (Sparks, 1976).

Gas can be added to the flow during the duration of the current by continued entrainment of ambient air, gases from burnt vegetation, gas from fluids boiled by high temperature flows or gas released from clasts within the flow (Wilson, 1980; Branney & Kokelaar, 2002; Druitt et al., 2007; Roche et al., 2010). Therefore, degree of fluidisation of currents can vary temporally and spatially.

Currents can be categorised by the degree of fluidisation (Wilson 1980). The least fluid currents are homogenous with high yield strength, which restricts gravitational induced segregation and the formation of the basal layer. Slightly more fluidised flows are more heterogeneous and still have a yield strength while allowing for coarse tail grading, either as normal or reverse pumice grading and normal lithic grading, as well as forming a well-developed basal layer. And the most fluidised flows contain segregation structures of localised concentrations of denser material which are fines depleted. The deposits from these homogenous highly granular flows with limited fluidisation resemble lahar, landslide or rockfall deposits, while the more fluidised flows deposit as ignimbrites (Wilson, 1980).

The body of PDCs are almost fully fluidised provided that pore pressure diffusion is slow, and viscous gas-particle interactions are strong enough. These gas-particle interactions occur because of differential motion from particle settling, mixture contraction and auto-fluidisation between the solid and fluid phases (Roche et al., 2010).

The entrainment of air has an impact on the mobility of the current, especially run-out distance, as well as the co-ignimbrite plume buoyancy (Dufek, 2016). Variations in aeration (fluidisation) can influence the runout distance of a PDC; increased aeration leads to greater run-out distances, therefore in the flume greater gas flux is linked to greater runout distances, as this controls the current velocity (Smith et al., 2018).

2.1.2.2 Flow volume

Previous work on currents produced by slope failures has identified a relationship between current volume and the ratio of L/H. Dade and Huppert (1998) related these findings to other dense granular flows, such as PDCs, and suggested that as the volume of a PDC increases, the ratio of L/H increases (Fig. 2.2). This means that as the volume increases the run-out distance increases, for a constant plume height. Based on the equation for mobility generated by Lucas & Mangeney (2007) an increase in L/H corresponds to an increase in flow mobility.

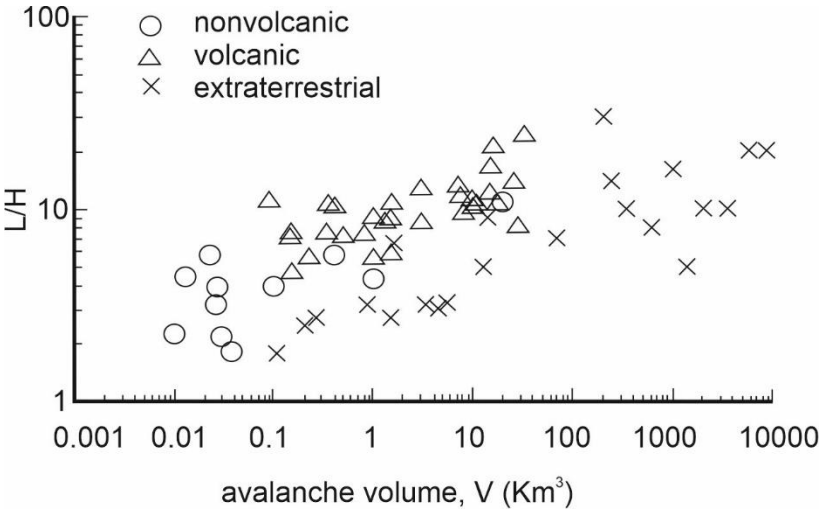

Figure 2.2: Graph showing L/H (ratio of flow length against plume height, representing current mobility) against flow volume for a variety of flow types. The data has been compiled from previous works (Dade & Huppert, 1998)

However, the relationship between volume and mobility for PDCs is not so clear cut (Sulpizio et al., 2014; Palladino & Giordano, 2019). For example, small and dense PDCs, fed by a single pulse, form a sliding regime; therefore in these currents the mobility and run-out distance is independent of volume (Staron & Lajeunesse, 2009). In medium to large volume dense PDCs that are continuously fed from a source with a high discharge rate, the flow regime starts proximally as sliding but more distally becomes spreading leading to accumulation of material down current (Palladino & Giordano, 2019). The flow regime occurring in a current controls mobility, as sliding is volume-dependent- therefore larger currents will have a greater run-out distance and are more mobile than smaller currents, while this trend does not exist during the spreading regime (Staron & Lajeunesse, 2009).

2.1.2.3 Rheology

The rheology of the flow can be considered as particular rheological controls and their impact on frictional forces (Sulpizio et al., 2014). For example, sorting of the particles affects the rheology of the flow and therefore may affect the mobility. Fig. 2.3 shows how a current may become inversely graded through percolation of smaller particles where larger particles move faster resulting in a resegregation regime shown in Fig. 2.3(b).

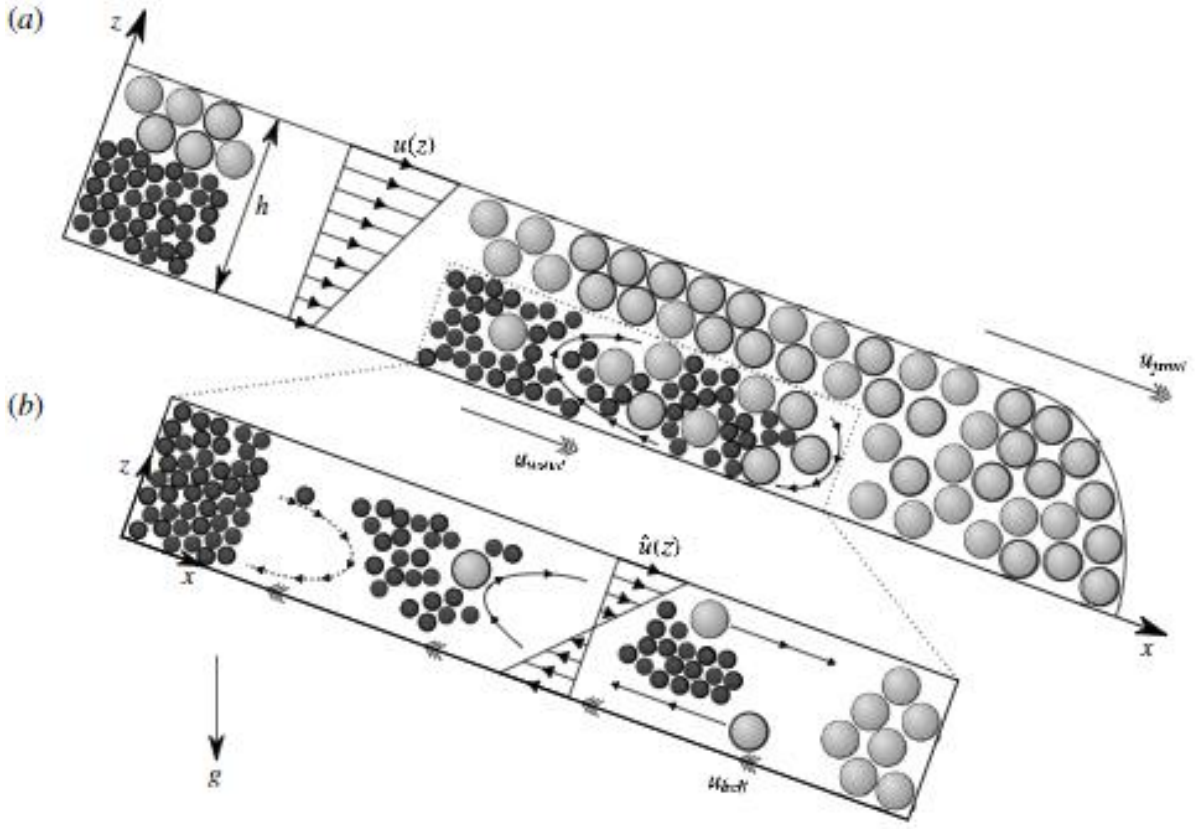

Figure 2.3: (a) Vertical section showing a steadily propagating current. (b) shows the proposed resegregation regime (Gajjar et al., 2016)

As percolation and sorting methods cause this inverse grading of the current, the larger grains rise to the faster flowing surface of the current which causes them to be transported to the front of the flow. If these large particles are overrun by the advancing flow, they can be recirculated into the current causing a resegregation mechanism to occur (Gajjar et al., 2016). A bouldery front, or current head, has a high proportion of large particles, with fine grains creating a more mobile interior of the flow. These fine grains then cause the larger grains to move from the head of the flow to the sides channelizing the flow, forming coarse grained levees (Kokelaar et al., 2014). The fine grains are then deposited in the channels which reduces friction on the base of the flow and therefore increases run-out distance (Kokelaar et al., 2014; Gajjar et al., 2016).

The friction within the flow also depends on the degree of fluidisation because as gas rises into the granular sediment, the drag force acts against the weight of the material, which reduces the inter-particle frictional forces (Druitt et al., 2007; Roche et al., 2008). The amount of fluidisation depends on the flow type and flow volume, as gas retention is favoured by fine-grained material. This means that coarse-grained materials degas much faster, resulting in shorter run-out distances than fine-grained flows in the same environment (Druitt et al., 2007).

Frictional forces are additionally modified by grain shape. During transport, aspherical grains and rough surfaces have greater resistance to shearing between the granular bed and flow than spherical grains. As shown in Fig. 2.4(c), this means that frictional resistance between

the bed and flow is increased as the aspherical grains slide rather than roll during transport (Deal et al., 2021). Based on the work by Gajjar et al. (2016) it is possible to infer that increased friction on the base of the flow results in reduced run-out distance.

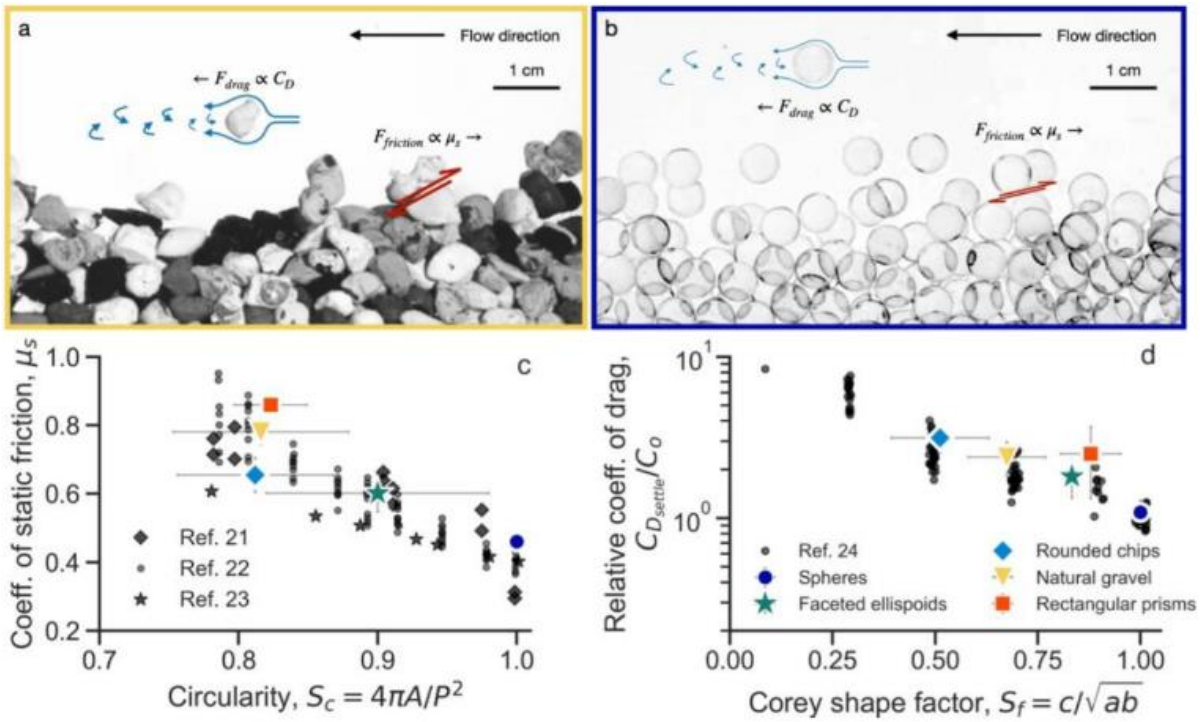

Figure 2.4: Effects of grain shape on bed load sediment transport. (a) Image of natural gravel undergoing bed load transport highlighting the forces due to fluid drag and grain-grain friction. (b) Same as (a) but with spheres. (c) Comparison of bulk coefficient of static friction with a measure of grain shape. (d) Comparison of the still-water-settling drag coefficient with a measure of grain shape (Deal et al., 2021)

2.1.2.4 Topography

During the initial generation of a PDC, steeper volcanic flanks allow flows to maintain energy, momentum and sediment carrying capacity. This means that flows can surpass topographic features easier and escape topographic boundaries such as valleys and other funnelled regions (Brand et al., 2014). On steeper slopes PDCs have higher current front velocities, which are sustained over a greater distance, and run-out distances can be increased by up to 50% (Smith et al., 2018). In experiments by Smith et al. (2018) slopes of 2° and 4° were used, indicating that small variations in slope angle can have large impacts on run-out distances.

Topography can influence flow dynamics by causing changes in fluid turbulence, particle concentration or by partially blocking the current (Sulpizio et al., 2014). When PDCs interact with topography the mobility of the flow can be affected by reduced kinetic energy and increased air entrainment. Kinetic energy is lost from flows traversing topography leading to a reduction in run-out distance. And, increased air entrainment results in reduced current density, changes in particle buoyancy and greater co-ignimbrite plume generation (Andrews & Manga, 2011).

The occurrence of PDC deposits on topographic highs have been previously used to infer the type and rheology of the currents that formed them. The Taupo and Campanian Ignimbrites

have been found high on topographic barriers (over 1000 m for both; (Wilson, 1985; Fisher et al., 1993)) showing that the PDCs that formed these deposits must have had high mobility to scale these significant topographic barriers. It has been suggested that these deposits must have been deposited from dilute PDCs (aka 'surges') because it was thought that dense granular currents could not travel up to these heights. This is because a dense current is unlikely to maintain the high velocity needed to deposit on topographic highs (Legros & Kelfoun, 2000). However, there is a lack of consensus about ignimbrites on topographic highs necessarily depositing from dilute PDCs. More recent work on the Peach Spring Tuff has indicated that high volume, low aspect ratio ignimbrites with deposition on topographic highs can be deposited from PDCs containing a dense basal section. In these currents an upper, more dilute zone may deposit on topographic highs (Roche et al., 2016). Furthermore, varying topography projects into the current differently based on elevation as each level of the current has varying characteristics, such as particle concentration, turbulence intensities and clast support mechanisms. As the topography projects further upwards into the current the lower flow boundary zone changes in regards to these characteristics which in turn affects mobility and deposition (Brown & Branney, 2013). Thus, any deposit on topographic barriers may only tell us about the portion of a potentially stratified current that is in contact with the ground.

The most common topographic feature surpassed by PDCs is a break in slope, where a reduction in the slope angle leads to deceleration of the current. This current deceleration will lead to increases in bed stress which enhances deposition and flow turbulence causing greater elutriation of fine-grained particles and co-ignimbrite lofting. If the bulk density is greater than the ambient fluid (atmosphere), the cloud will continue to propagate as a gravity-driven current, while if the bulk density is lower than the surrounding ambient fluid there will be greater convective lofting and stopping of the current (Sulpizio et al., 2014). When a PDC reaches an increase in slope angle, if the resistance and momentum forces are nearly equal there will be greater deposition and current stopping. Flow deceleration reduces the turbulence of the flow which can lead to the development of density stratification in the fully turbulent homogenous upper zone of the flow. Flow deceleration may also lead to particles moving towards the base of the flow causing enhanced deposition.

The effect of topography on PDC mobility is shown in Fig. 2.5, where experimental data by Andrews & Manga (2011) suggest a non-linear relationship between flow height and obstacle height. For currents that encounter topographic barriers that are less than 1.5 times the height of the flow, there is little correlation between run-out distance and barrier height. While for currents that encounter topographic barriers that are equal to or greater than 1.5 times the height of the flow there is a topographic block preventing further flow of the current (Andrews & Manga, 2011).

The most important and complex topography to understand the impacts of on PDC mobility is that of built environments, which have an irregular morphology affecting the flow mechanics and run-out distance of PDCs. This is because in built environments, collisions between the flow and structures can reduce kinetic energy of the flow, and the assemblage of roads and buildings can cause surface roughness which can increase flow pressure and

turbulence, as well as creating vortices that reduce the flow temperature (Sulpizio et al., 2014).

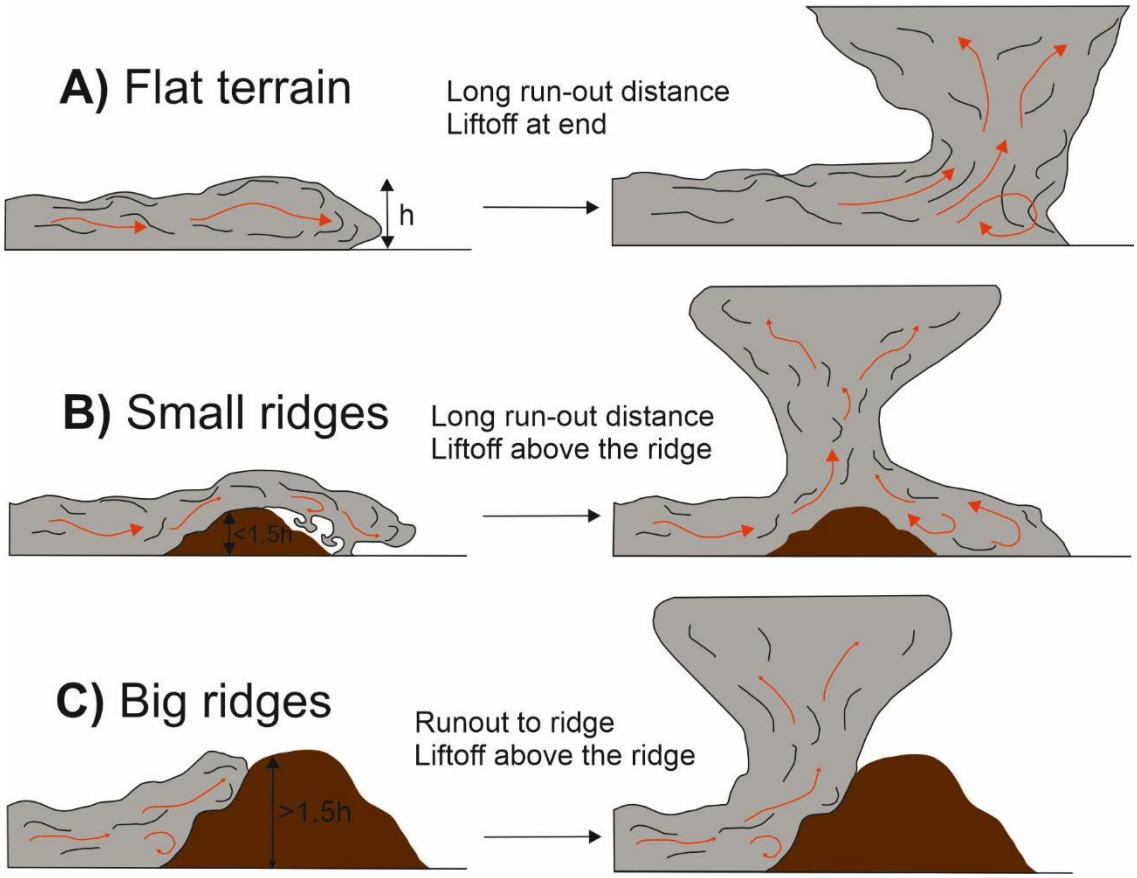

Figure 2.5: Diagram showing how topography affects the flow of the current with thickness, h. Where the topographic ridge height is < 1.5h the current continues after the ridge with a co-ignimbrite plume forming; while if the topographic ridge height is > 1.5 the current ceases to run out and a co-ignimbrite flume forms (Andrews & Manga, 2011)

As a current deposits material, the topography changes which means that later parts of the current overpass a different topography causing temporal variation of mobility at the same location. Topography can also exert a major influence on the depositional mechanism of gravity driven currents. As initial deposition occurs later parts of the flow have lower rates of deposition, as initial deposition infills valleys causing a reduction in accommodation space and relief (Brown & Branney, 2013). Also, as deposition occurs the new topography generated by these deposits causes a change in slope which leads to localised deceleration forming a depletive flow that deposits material. Over time these deposits continually change the topography causing the depositional zone to move more proximal to the vent (Brown & Branney, 2013).

2.2 Sorting within pyroclastic density currents

In granular flows clasts are sorted depending on the clast size, density, shape, degree of fragmentation, flow turbulence and flow duration (Cas & Wright, 1987; Branney & Kokelaar, 2002). Size is an important factor in current sorting as larger clasts are more likely to grade (Sparks, 1976) with coarse low-density particles rising towards the top of the sheared layer.

This is followed downwards by fine low-density particles then coarse high-density particles, with fine high-density particles settling to the base of the flow (Savage & Lun, 1988). Coarse tail grading occurs in high concentration flows and causes only the coarsest particles to be sorted while no lateral or vertical grading of finer particles occurs (Sparks, 1976).

In PDCs inverse sorting is commonly observed in both field and lab deposits, however there are multiple methods for this sorting. The methods of segregation of granular material are well researched already with multiple mechanisms identified, including: percolation, kinetic sieving, gravitational settling and diffusive mixing (Vallance & Savage, 2000; Lube et al., 2007).

Percolation is a size dependent, gravity driven process where particles move downwards into spaces below. This means that small particles percolate more frequently than large particles which leads to inverse grading in the deposits. However, as percolation is not density dependent it does not explain the increasing proportion of low-density clasts with distance (Vallance & Savage, 2000; Lube et al., 2007). Multiple methods for percolation have been suggested, one is that because of the movement of particles voids are created which are then more easily filled by small particles. Then compression of smaller particles causes greater friction between the different sized particles, allowing these smaller particles stay in place below larger particles. The other method suggested is based on probability, because for a space large enough for a larger particle several small particles would have to moved simultaneously, but to create a space for a small particle only one small particle would have to be moved. This suggests that it is therefore more likely for space for small particles to form causing upwards migration of large particles (Vallance & Savage, 2000).

The increasing proportion of low-density clasts with distance is explained by kinetic sieving where the squeeze-out of particles occurs. This causes the migration of smaller particles to the base of the current by falling into inter-granular voids (Sulpizio et al., 2014). Squeeze-out occurs when there are imbalances in contact forces between particles, such as when particles of the same size but different densities are in contact, and causes denser particles to push downwards (Lube et al., 2007). However, if the density of the particles and the fluid are equal kinetic sieving cannot occur resulting in percolation of particles (Thornton et al., 2006).

Gravitational settling of a liquid-particle mixture causes normal segregation of granular flows. Gravitational settling occurs when the concentration of solids, fluid viscosity and fluid strength are insufficient to support larger and denser particles which rapidly migrate towards the bed. Multiple factors are necessary for gravitational settling to occur. The fluid must be viscous enough for particles to reach terminal velocity; there must be low inter-particle interactions, otherwise percolation will occur; and the flow cannot move as a rigid plug, otherwise no sorting can occur until the waning stage where minor sorting occurs (Vallance & Savage, 2000).

Diffusion is the tendency of particles to become more evenly dispersed. In slow granular flows, the particles undergo less agitation which means that diffusive processes are weaker than percolation. Whereas in dry cohesionless granular flows there are more collisional interactions between particles which means that diffusive processes are stronger than percolation (Vallance & Savage, 2000).

Sorting in the deposit can occur due to the surface-roughness effect where in a flow a denser clast, such as a lithic fragment, or a small low-density clast is deposited easier than a large low-density clast (Fig. 2.6; (Walker, 1985). However experimental data shows that clast size is more important than clast density and shape, unless the clasts are highly non-spherical (Branney & Kokelaar, 2002).

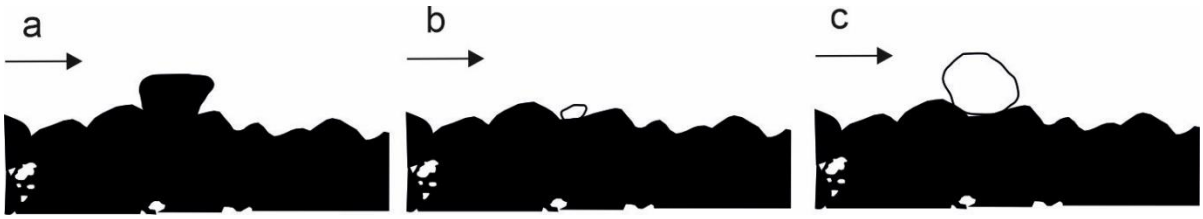

Figure 2.6: Diagram showing surface roughness effect with arrow to show flow direction. (a) shows a dense lithic fragment, (b) shows a small low-density pumice fragment, and (c) shows a large low-density pumice fragment adapted from (Walker, 1985) in (Branney & Kokelaar, 2002)

As shown by Fig. 2.6c, larger particles do not fit into gaps in the surface layer easily which can cause overpassing. This overpassing can occur because: large clasts are more exposed to the shearing flow, meaning that they experience more drag from the flow; larger clasts have greater momentum in debris falls, meaning that they travel further before the energy is low enough to allow for deposition; or large clasts are less likely to be deposited from the flow, due to surface roughness as they slide over gaps in the deposited sediment (Branney & Kokelaar, 2002).

2.3 Grain size variation within pyroclastic density currents

The grain size of PDC deposits (especially dilute PDCs) depends on the initial fragmentation of magma at the time of eruption and the ability for flows to carry material (Walker, 1985; Cas & Wright, 1987). This suggests that within the flow the grain size depends on initial fragmentation (Dufek & Manga, 2008) as well as initial energy to carry material and not cause deposition as a lag breccia within the deflation zone prior to transport as a PDC (Walker, 1985).

PDCs encompass a range of particle concentrations and sizes (from fine ash to large blocks) (Murai, 1961), Fig. 2.7 shows that fine ash ($\phi = 3$) to medium-coarse lapilli ($\phi = -3$) are the most common grain sizes which come from both the initial fragmentation of material and later reworking and modification during transport (Dufek & Manga, 2008).

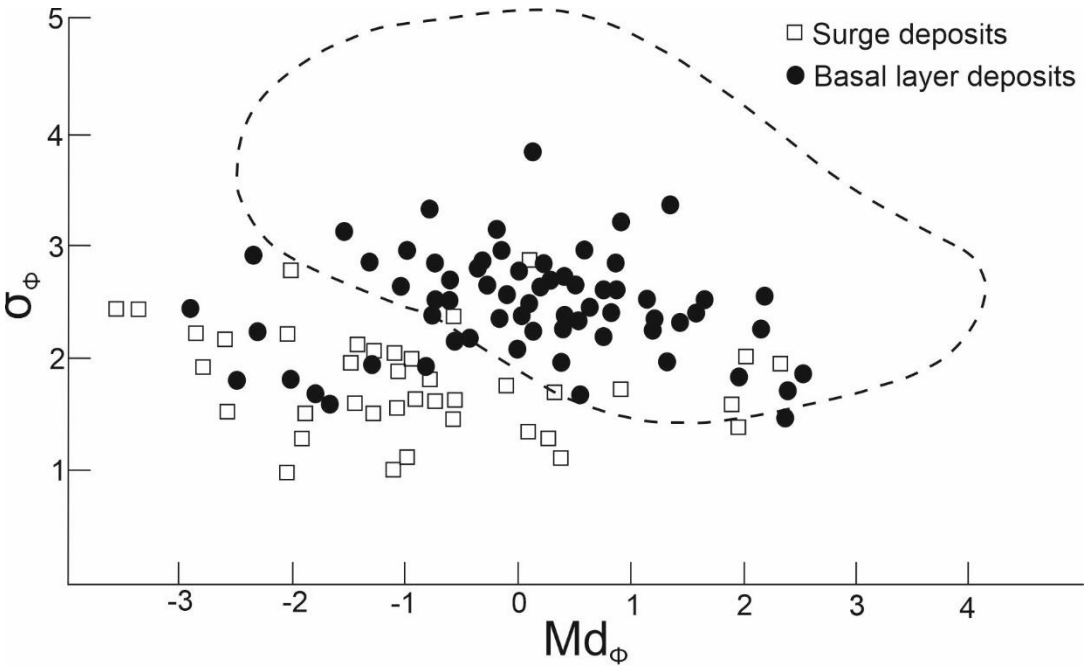

Figure 2.7: Graph showing median grain size against dispersion, the dashed line shows the area in which 95% of ignimbrites plot (Sparks, 1976)

Ash is formed by two main mechanisms: magmatic fragmentation and hydrovolcanic fragmentation. During magmatic fragmentation, exsolution and expansion of gases within the magma contribute to ash production, along with the production of pumice and vesicles. During hydrovolcanic fragmentation, ash is produced through physical contact and mixing of water with magma (Wohletz et al., 1989).

As seen in the sorting methods, particles within PDCs collide and slide past each other during the current. These collisions lead to mechanical abrasion (Walker, 1981) and in highly energetic collisions, such as after a break in slope, shattering of clasts (Schwarzkopf et al., 2006). These two mechanisms will change the rounding of clasts with abrasion causing rounding, and shattering causing an increase in angularity. The clast abrasion rate varies depending on the amount of abrasion and the clast properties. For example, the rate of abrasion decreases as the clast abrades; and a crystal rich clast abrades slower than a crystal poor pumice clast, due to the strength from the crystals (Manga et al., 2011). Pumice shows that abrasion happens during the flow as initially angular pumice is rounded in ignimbrites. This initial angularity is observed in ash fall tephra deposits where pumice fragments often remain angular due to the absence of abrasion (Dufek & Manga, 2008).

The initial production of ash can affect run-out distance, internal pore pressure, sorting and volume of atmospheric ash (Dufek & Manga, 2008). More fine particles in a current lead to more particles in the suspended load region of the flow where turbulence and interparticle interactions cause suspension of fines (Dufek & Bergantz, 2007). This suspended layer is highly mobile and can detach from the basal layer to surmount topographic barriers (Miller & Smith, 1977; Calder et al., 1999; Dufek & Manga, 2008).

Flows with finer grain sizes tend to be more mobile with greater acceleration than coarse flows (Sparks, 1976). In flows with finer grained particles, the number of particles is greater

than in a flow with large grained particle of the same volume. This means that agitational forces between the flow and underlying surface are lower and therefore less energy is dissipated resulting in greater run-out distances (Cagnoli & Romano, 2010).

2.4 The flow boundary zone

Deposition from PDCs can occur in both steady and unsteady conditions, such as during current waning, quasi-steadiness, and waxing. Deposition occurs within a PDC when clasts pass through the lower flow boundary of the current. Flow boundary zones show variations in velocity and concentrations, meaning that shear and concentration varies throughout the flow boundary zone (FBZ). The FBZ can be characterized by the dominant mechanisms based on the variations in shear, concentration and deposition rate (Branney & Kokelaar, 2002).

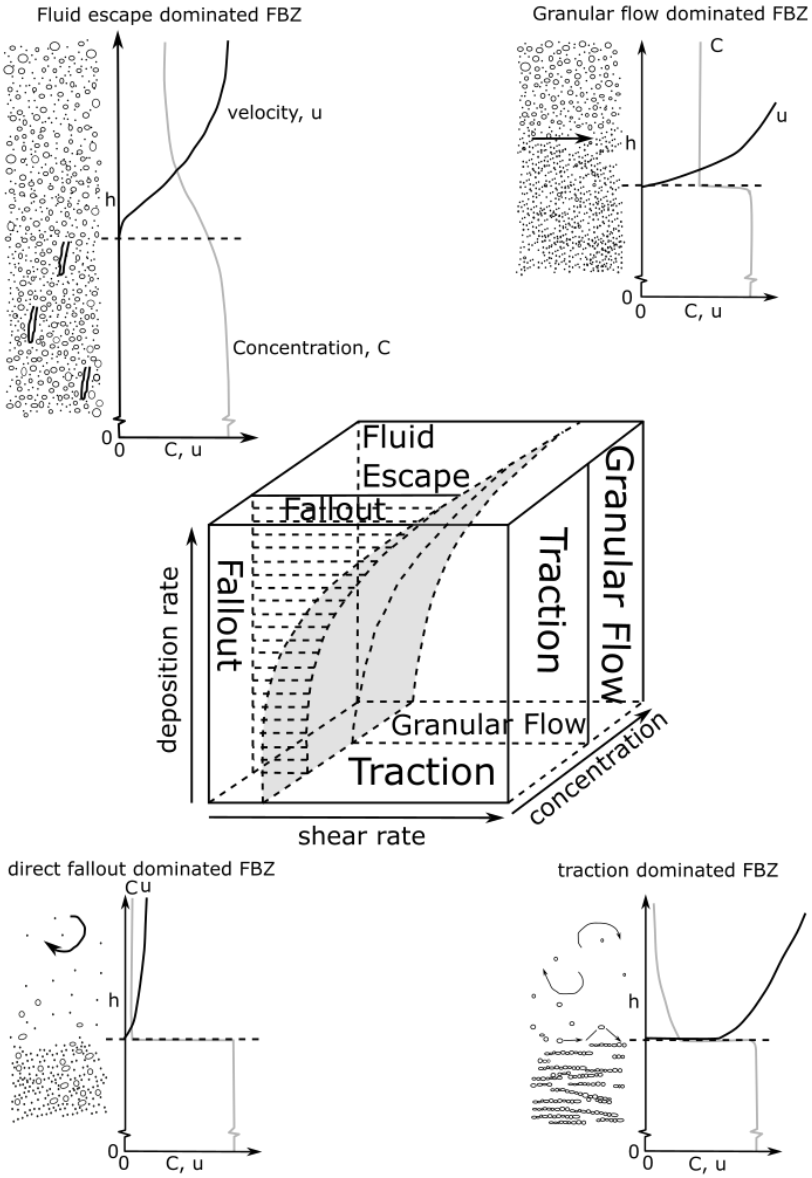

Figure 2.8: conceptual image of the four types of flow boundary zone with schematic concentration and velocity profiles (Branney & Kokelaar, 2002)

In a fluid escape dominated FBZ (Fig. 2.8a) clast support is predominantly a result of fluid escaping upwards from the underlying deposit. This requires low shear to prevent granular

effects and high concentration to limit the permeability of the sedimenting dispersion. Within the FBZ the clast concentration, yield strength and viscosity increase downward while shear rate decreases downwards. This happens either due to a downward decrease in the upward escape of gas and the clast support from the gas, due to dispersive pressure causing a downward decrease in dilation, or due to density stratification of the poly-disperse bedload. The deposits accumulate rapidly and are poorly compacted with elutriation pipes forming when gas expulsion is high. Deposit concentration increases with depth as the rate of compaction and fluid expulsion decreases (Branney & Kokelaar, 2002).

In a granular flow dominated FBZ (Fig. 2.8b) the concentration and shear rate allow for inter-particle interactions to dominate clast support. In steady deposition, frictional interlocking of the current and substrate causes gradual aggradation of a massive deposit. The interlocking of particles prevents segregation of particles at the flow boundary, however, segregation of the overriding current in a granular flow is likely. This results in fine particles entering the flow boundary zone preferentially (Branney & Kokelaar, 2002).

The direct fallout dominated FBZ (Fig. 2.8c) occurs in a dilute lower current. This results in minimal inter-clast interactions or fluid escape effects, with negligible saltation or rolling causing the clasts to deposit directly. The FBZ is dominated by direct fallout when the rate of deposition is so rapid that as soon as the clasts touch the underlying surface they are buried, preventing transport by saltation or rolling. Or when the clasts are sticky from moisture or heat which results in clasts sticking to the underlying surface unable to transport (Branney & Kokelaar, 2002).

In the traction dominated FBZ (Fig. 2.8d) the higher rate of shear results in clasts transporting by saltation, rolling, or sliding through fluid lifting, however the low concentration results in few inter-particle interactions. Interactions between the current and underlying substrate causes localised non-conformities with development of various bedforms, such as moderate to well sorted stratified and cross-stratified deposits (Branney & Kokelaar, 2002). These deposits are comparable to the pyroclastic surge deposits described by Cas and Wright (1987).

In unsteady currents the FBZ can change with time which results in varying deposition conditions forming differing grading and bedforms over time. On the small scale, this unsteadiness can produce waves or turbulent eddies which can produce thin laminations (Branney & Kokelaar, 2002).

2.5 Deposits from pyroclastic density currents

Deposits of PDCs can be classified based on lithology and sedimentary structures as ignimbrites, pyroclastic ‘surge’ deposits and block and ash flow deposits. Typically, ignimbrites are poorly sorted deposits, which are pumice and ash rich with lithic lapilli supported in the matrix. Ignimbrites often appear massive but can contain a wide range of stratification types, erosional surfaces, elutriation pipes, soft sediment deformation and grading patterns (Cas & Wright, 1987; Branney & Kokelaar, 2002).

Deposits of dilute PDCs (previously known as pyroclastic surges) are more sorted than ignimbrites with distinct stratification (Branney & Kokelaar, 2002), these individual laminae

are often well sorted while deposits of multiple laminae can be poorly sorted. Surge deposits mantle topography forming thicker deposits in topographic lows while also depositing on topographic highs. Due to the stratified nature of the deposits, dunes are common in these deposits with elutriation pipes forming (Cas & Wright, 1987).

Block and ash flow deposits are typically a smaller volume mono-lithological deposit containing a large proportion of dense, poorly to moderately vesicular juvenile (lava) blocks with non-pumiceous ash (Branney & Kokelaar, 2002). Levees, steep flow fronts and, grading and rare elutriation pipes occur in these deposits (Cas & Wright, 1987).

2.5.1 Bedforms

In subaqueous systems, dune growth is limited by the shear velocity which defines the transition from predominantly bedload transport to predominantly suspension transport. This shear velocity is grain-size dependent with potential bedform sizes being greater in coarse sediments than fine sediments (Flemming, 2000).

Within the deposits of PDCs sedimentary structures are commonly observed and reflect the depositional conditions and conditions within the flow (Smith et al., 2020). Various types of cross bedding are present in PDC deposits and previously were thought to be related to dilute, high velocity PDCs (Cas & Wright, 1987; Cole, 1991; Douillet et al., 2013). While more massive deposits, lacking sedimentary structures, were thought to be related to dense granular flow PDCs (Sparks, 1976; Branney & Kokelaar, 2002; Cas et al., 2011). However more recent work has suggested that dense granular flows within PDCs can form deposits containing bedforms, such as cross stratification (Smith et al., 2020).

A system of dividing bedforms into five categories was created by Schmincke et al. (1973) based on fieldwork at Laacher See, Germany. Type 1 dunes (Fig. 2.9a) have steeply dipping coarse grained stoss side deposits and shallower angled, thinner, and more finely grained parallel beds on the lee side of the dune. Type 2 dunes (Fig. 2.9b) are generally finer grained dunes with shallower stoss side deposits than type 1 dunes and greater deposition on the lee side of the dune. Type 3 dunes (Fig. 2.9c) are more symmetrical dunes with finer grained material, the majority of deposition in these dunes is on the lee side of the deposit with minor stoss side deposition. Type 4 dunes (Fig. 2.9d) are similar to Type 3 dunes but consist of coarser material (medium to coarse sand) and are more well sorted, the shape of these dunes is slightly asymmetrical with greater deposition on the stoss side which is angled slightly steeper than the lee side. Type 5 dunes (Fig. 2.9e) are massive dunes of fine-grained material, typically these dunes are lensoids of silt and fine sand with a high wavelength and low amplitude (Schmincke et al., 1973).

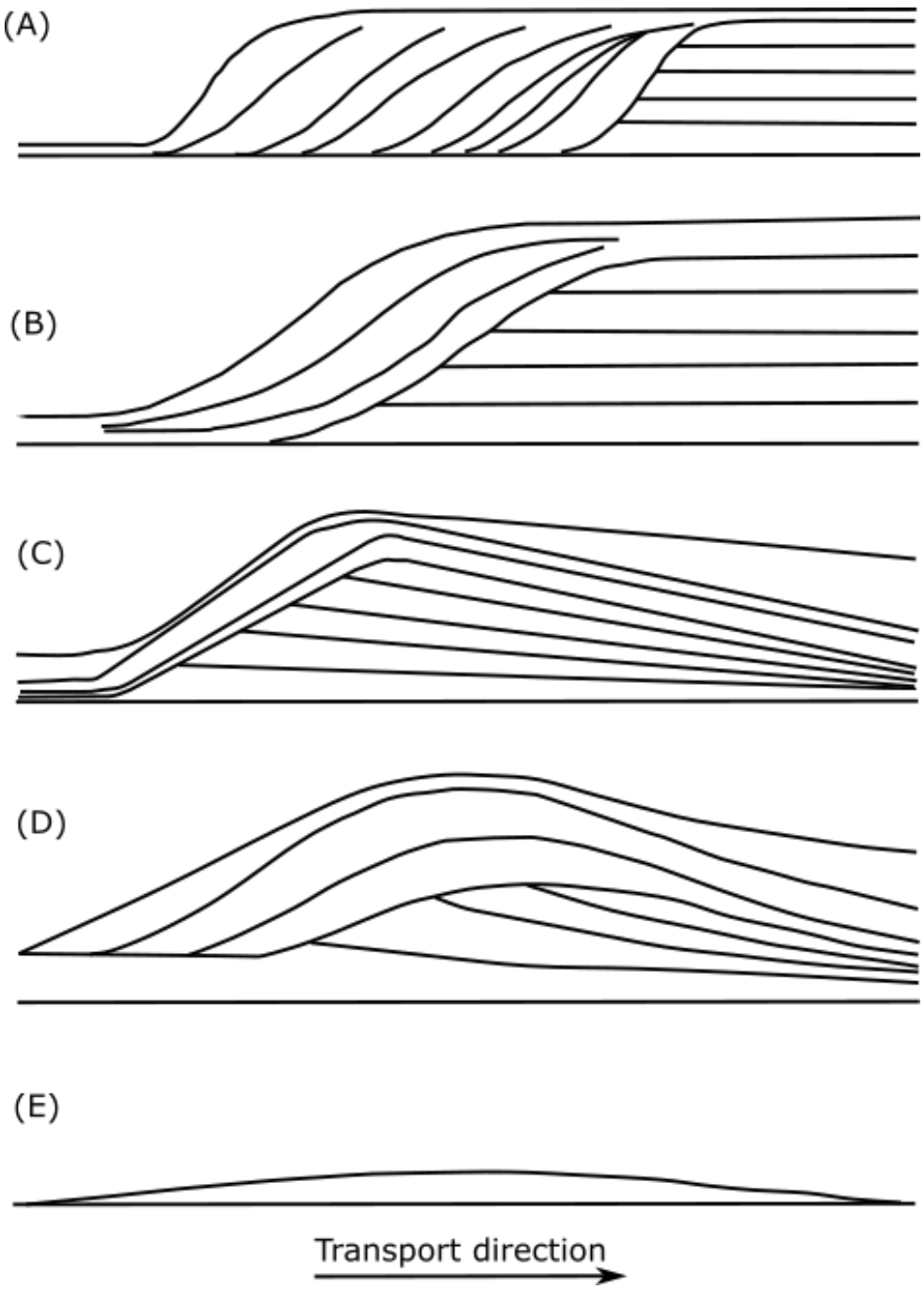

Figure 2.9: Schematic representation of the five major bedforms identified at Laacher See (Schmincke et al., 1973)

Other previous fieldwork on Roccamonfina volcano (southern Italy) and Sugarloaf Mountain (Arizona, United States) by Cole (1991) divided the bed structures into five deposit types with varying depositional environments. Type A dunes (Fig. 2.10a) consist of progressively steepening lee side beds which have built up against previously deposited planar beds; these beds can be stationary, progressive, or regressive bedforms indicated by the bed thickness on the stoss and lee side of the dune. Type B dunes (Fig. 2.10b) consist of progressively steepening lee side beds progressing from planar beds, these beds are progressive bedforms and therefore have thicker deposits on the lee side of the dune. Type C dunes (Fig. 2.10c) consist of beds similar to type B but the beds here are thicker and contain distinct coarse- and

fine-grained beds; these beds are progressive bedforms and therefore have thicker deposits on the lee side of the dune. Type D dunes (Fig. 2.10d) consist of steeply dipping stoss side beds with thin lee side planar beds, these dunes migrate towards the flow source making these a regressive bedform. Type E dunes (Fig. 2.10e) consist of stoss side beds which have deposited against previously deposited lee side beds, as these dunes migrate towards the flow source making these a regressive bedform (Cole, 1991).

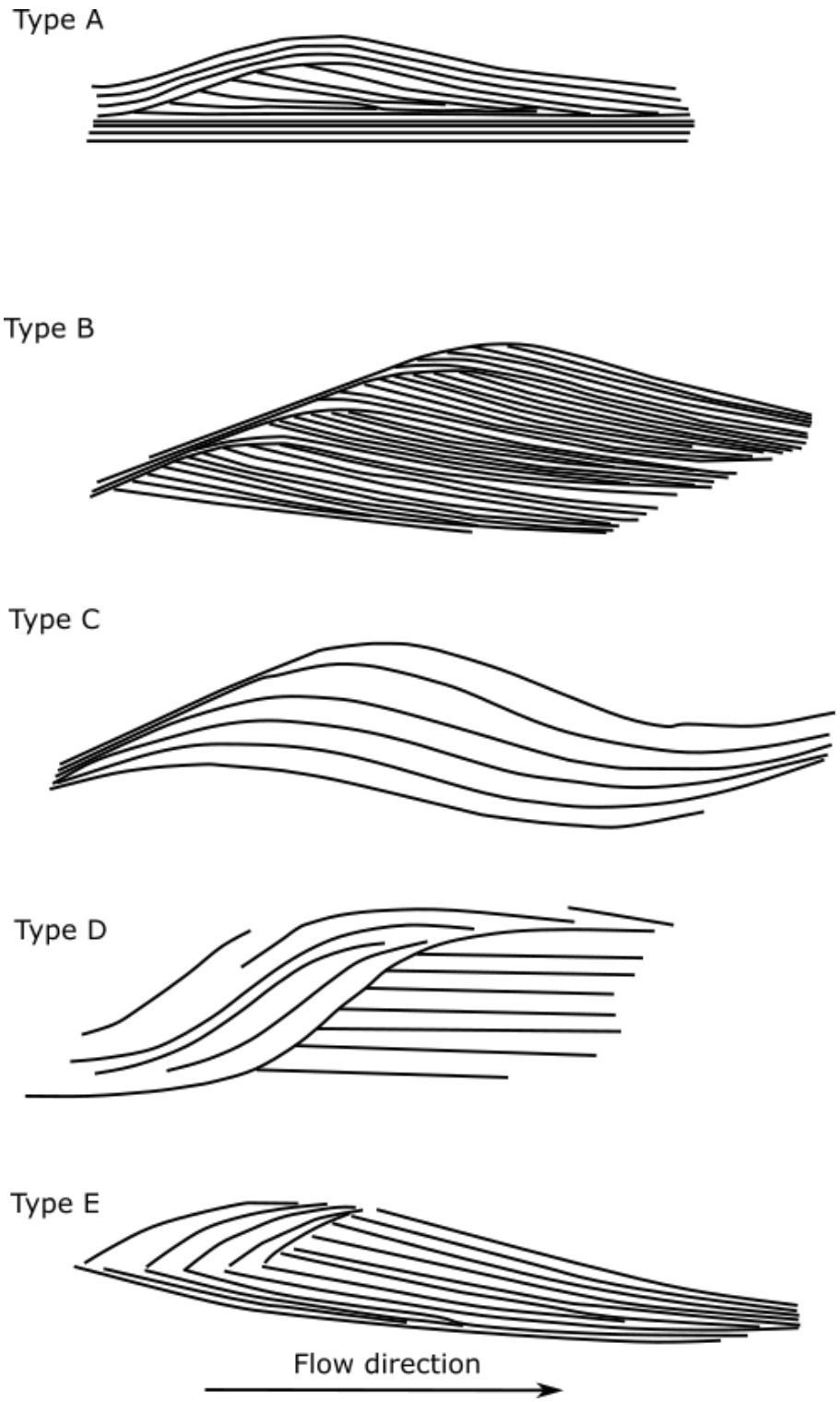

Figure 2.10: Sketches of the five bedform classifications based on fieldwork at Roccamonifina and Sugarloaf Mountain, Arizona (Cole, 1991)

Douillet et al. (2013) classified dune bedforms into four types: elongate, transverse, lunate and two-dimensional dunes based on deposits at Tungurahua volcano, Ecuador. Elongate dunes are low angle, high ripple index dunes where the lee side is slightly shallower than the stoss side. These bedforms are interpreted to be deposited by dense granular currents that are able to carry the blocks present in these dunes (Douillet et al., 2013).

Transverse dunes have a low ripple index and contain crests perpendicular to the flow direction. They contain beds which are steeper on the stoss side than the lee side, with internal cross stratification forming due to laminations within the ash. As these dunes form from fine laminations of ash they are interpreted as forming in turbulent, fully dilute currents, with beds forming from pulses within a single current and the internal laminations forming from turbulent eddies within these pulses (Douillet et al., 2013).

Lunate dunes have a ripple index similar to transverse dunes but have longer beds on the lee side deposit creating an asymmetrical shape. As these dunes have a similar shape to transverse dunes they are interpreted as depositing within a turbulent, fully dilute current with topographic boundaries promoting stoss side aggradation, leading to the generation of the asymmetrical shape (Douillet et al., 2013).

Two-dimensional dunes crest in a similar way to the transverse dunes, while in 2D dunes the dune width is greater than the dune length. These dunes are almost symmetrical and there is repetition in the direction of flow. These dunes suggest that the flow was unconstrained at the time of deposition allowing for lateral spreading (Douillet et al., 2013).

These three methods of defining bedforms have slight similarities and differences based on bedforms observed at each deposit, shown in Table 2.1. The Type 2, 3, and 4 bedforms of Schmincke et al., 1976 can be related to the Type D, B, and A bedforms of Cole, 1991 respectively. By combining these methods, it is possible to accurately describe PDC bedforms in a way that is comparable across global deposits.

Table 2.1: Table comparing the three systems of describing bedforms

Schmincke et al., 1976 bedform	Similar bedform Cole, 1991	Similar bedform Douillet et al., 2013
Type 1	-	-
Type 2	Type D	-
Type 3	Type B	Transverse
Type 4	Type A	-
Type 5	-	Elongate

2.5.2 Ripple index

Ripple index (RI) is a method created to classify ripples in a dimensionless manner based on the height and length of the ripple, the equations from Tanner (1967) allow for characterisation of dunes based on dune bedform shape (Douillet et al., 2013).

$$RI = \frac{s}{h} \qquad \text{(eq. 7)}$$

$$RI = \frac{s}{2a} \qquad \text{(eq. 8)}$$

Where s = crest spacing or the wavelength of the dune, h = wave height, and a = amplitude of the wave. In sedimentology it is taken that an RI greater than 15 represents wind type ripple and a RI less than 15 represents a water type ripple (Tanner, 1967). However, as in analogue deposits and natural PDCs the full wavelength of a deposit is rarely observed this cannot necessarily be used to classify PDC deposits.

2.5.3 Experimental bedforms

In previous experimental work by Smith et al. (2020) using gas-fluidised granular material, planar beds, with an angle <2 °. Shallow backset beds, where the stoss side is lower angle than the dynamic angle of repose; and steep backset beds, where the stoss side has a higher angle than the angle of repose were observed. These planar deposits are deposited at velocities > 0.8 ms^{-1}, the shallow backset bedforms are deposited at lower velocities, and the steep backset bedforms are deposited at lower velocities between 0.3-0.6 ms^{-1}. With increasing current thickness, higher velocities are required to maintain deposition of the planar deposits and shallow backset bedforms. Therefore, it is possible for bedforms to change characteristics without requiring a change in flow velocity (Smith, 2020).

Deposition in analogue experiments is triggered by the rapid de-aeration of the current as it enters a flume chamber with reduced or absent basal gas flux, leading to an increase in inter-particle frictional forces. This process of rapid deaeration simulates the rapid degassing of natural PDCs, which is hypothesised to occur due to a decrease in the proportion of fines, decrease in temperature, reduction in flow thickness or entrainment of coarser material (Smith et al., 2020).

2.6 Approaches to understanding pyroclastic density currents

Previous work has used field data (e.g. Walker, 1985; Branney & Kokelaar, 1992; Brown & Branney, 2013), analogue models (e.g. Savage & Lun, 1988; Vallance & Savage, 2000; Bareschino et al., 2008; Roche et al., 2008, 2010; Rowley, 2010; Rowley et al., 2014; Lube et al., 2015; Breard et al., 2016; Breard & Lube, 2017; Smith et al., 2018, 2020) and numerical models (e.g. Francis & Baker, 1977; Bursik & Woods, 1996; Druitt et al., 2007; Breard et al., 2019; Trolese et al., 2019; Esposti Ongaro et al., 2020; Deal et al., 2021) to understand the behaviours of PDCs. This section will examine some of these methods in greater detail to design the methodology of this study (Chapter 3).

2.6.1 Analogue modelling

Various analogue experiments have been carried out on fluidised granular flows using the same basic set up whereby material is dropped from a hopper and into a constrained tank (Fig. 2.11; Roche et al., 2008; Rowley et al., 2014; Smith et al., 2018, 2020) however, different fluidisation methods have been used. Roche et al. (2004) used material that was fluidised in a reservoir prior to being released down the flume. This allowed for investigation into how flows de-fluidise as they propagate and the influence of initial fluidisation on flow dynamics. Rowley et al. (2014) and Smith et al. (2018, 2020) used a gas flux fed from the base of the flume, this allowed for simulation of high gas pore pressures characteristic of thick PDCs. The basal gas supply allowed for investigation into how sustained aeration of the

flow and variable aeration in different sections of the flow affect flow behaviour and deposition.

These experiments by Roche (2004), Rowley (2010), Rowley et al. (2014), and Smith et al. (2018, 2020) all used silica glass ballotini beads which produce more expanded flows that are not able to produce all the internal features of PDCs. This is because glass beads have a greater co-efficient of restitution than the natural material in PDCs, which results in glass beads being more agitated throughout the flow (Cagnoli & Manga, 2005; Cagnoli & Romano, 2010).

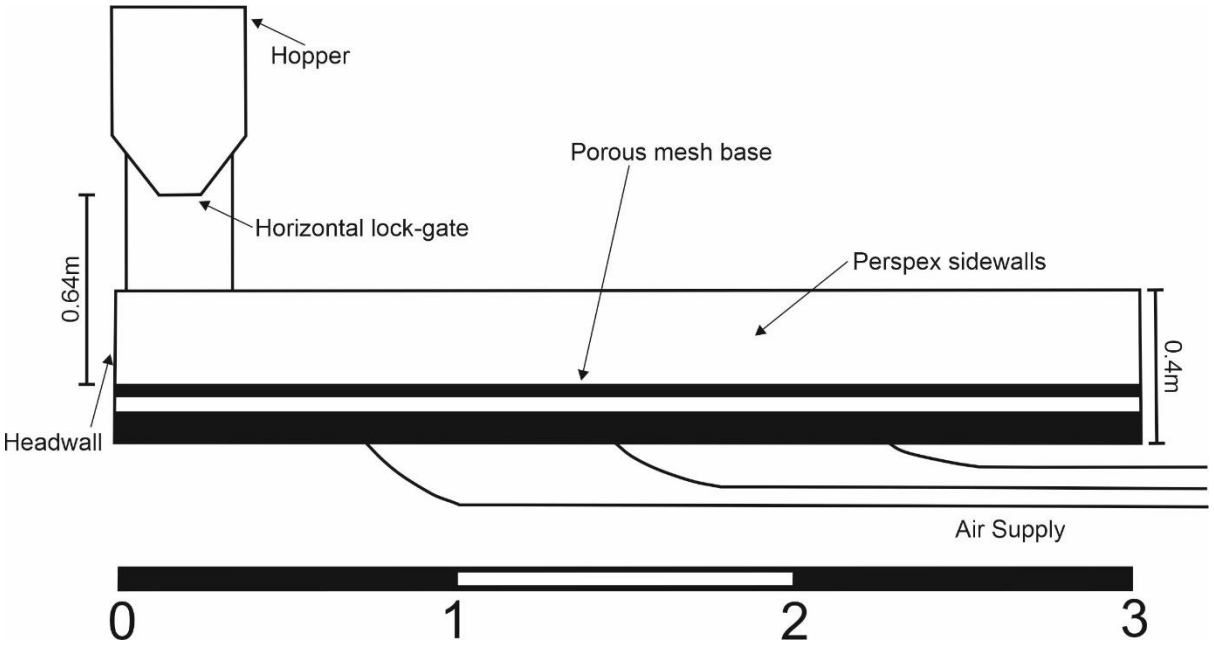

Figure 2.11: Experimental flume set up (Smith et al., 2018)

Digital photography and high-speed videos have been used to record data from these experimental flows by Roche et al. (2004), Rowley (2010), Cagnoli & Romano (2010, 2012), Rowley et al. (2014), and Smith et al. (2018, 2020). These photos and videos can be analysed with particle image velocimetry (PIV) analysis as in Cagnoli and Romano (2010, 2012).

As well as these small-scale analogue models there have been large-scale analogue models produced. Such as Lube et al. (2015) with the PELE set up, Dellino et al. (2020) and the USGS' debris flow flume at H.J. Andrews Experimental Forest (Iverson et al., 1992).

The PELE set-up from Lube et al. (2015) involves a 13 m-high structure where an eruptive column collapse is reproduced by releasing material from a hopper. This falling material then collapses down into a 12 m long chute with varying slope angles, before flowing along a 25 m long section leading outside. To make the flume more like a natural PDC the hopper contains a heating system and an aeration unit, with material from the Taupo ignimbrite were used (Lube et al., 2015). This removed the errors identified by Cagnoli & Manga (2005, 2010) in using glass beads, meaning that the behaviour in Lube et al. (2015) is more comparable to natural PDCs. In this set up the flows were analysed using PIVlab, a PIV algorithm using 3 high-speed cameras, 2 fast cameras and 2 normal-speed cameras to record flow evolution and analyse gas-particle transport and sedimentation processes. On

top of these cameras, pressure transducers and load cells were used to measure basal pore pressure and current mass; and infrared sensors were used to measure density stratification and temporal changes in density (Lube et al., 2015).

In the setup of Dellino et al. (2020) material collected from the Mercato eruption at Vesuvius and the Agnano-Monte Spina eruption at Campi Flegrei were launched out of a gas-particle jet which simulated a column collapse. However, this setup did not consider particle re-fragmentation or the effects of topography (Dellino et al., 2020).

The debris flume set up by the USGS is one of the largest analogue modelling flumes. Built into the hillside it is 95 m long, 2 m wide and 1.2 m deep. In this flume either 20 m^3 of sediment can be released down the slopes at an angle of 31° or a sloping mass can be watered until failure causes a collapse and debris flow. This set up allows for direct observations to be made through glass windows. And there are eighteen data collection ports on the base on the flume allowing for collection of data, such as the force of particles sliding and colliding at the base of the flow. The scale of this flume allows for testing numerical models of debris flows and the development of technology to mitigate the impacts of debris flows (Iverson et al., 1992).

2.6.2 Numerical modelling

As well as modelling these flows with analogue experiments, there have been attempts to numerically model PDC flow dynamics and quantify mobility of flows (Malin & Sheridan, 1982; Bursik & Woods, 1996; Dade & Huppert, 1998; Lucas & Mangeney, 2007; Cagnoli & Romano, 2012). Bursik & Woods (1996) created equations to quantify dynamics (density, pressure, momentum), entrainment, sedimentation, and initial temperature for radially spreading flows as well as sedimentation and run-out distance for subcritical ash flows. These equations were based on previous analogue models by Bursik & Woods (1994) and supported by field observations. This shows that numerical modelling alone is not enough to develop our understanding of PDCs, especially their mobility, as it is necessary to identify the parameters which need to be quantified. And then these equations must be validated by comparisons with analogue experiments and field observations.

Modelling by Malin & Sheridan (1982) created a series of equations to quantify surge acceleration, velocity and run-out time based on the slope angle and slope distance. There are issues with this numerical model as it does not consider the temporal and spatial changes within the flow nor flow channelization (Clarke et al., 2020) as observed in the Soufrière Hills Volcano, Monserrat (Calder et al., 1999). This shows how numerical modelling requires simplifications of these complex PDC systems to create a basic method of quantifying flow dynamics, which do not always match observed dynamics without the equations becoming overly complex.

Other numerical methods for quantifying mobility have been developed over time as Hayashi & Self (1992) detailed why the classical equation ($mobility = \frac{run\text{-}out\ distance}{verticle\ height\ change}$) for larger volume flows with greater run-out distances were less accurate due to errors in field observations. These errors were corrected by Lucas & Mangeney (2007) where they

created an equation based on this original equation that removed the influence of flow volume.

2.6.3 Fieldwork

Parameters for collection in field data have been identified along with the methods required to collect the data required to interpret the flow and deposit, shown in Table 2.2. Direct field observations of the dense basal portion of PDCs are hard to make due to the overlying dilute co-ignimbrite cloud obscuring observations (Delannay et al., 2017).

Also, due to the unpredictable nature and destructive force of PDCs, direct measurements are difficult to make as they can easily damage equipment (Delannay et al., 2017). However, direct observations have been made (Arattano & Marchi, 2008; McCoy et al., 2013) and PDCs have been investigated using acoustic and seismic data (Ripepe et al., 2009; Hibert et al., 2011; Levy et al., 2015).

Table 2.2: Parameters for PDC flow and deposit observations, and the method to make these observations (Delannay et al., 2017)

	Parameter	Method
Flow	Mean and surface flow velocity and flow direction	Ultrasonic sensors, geophones, pressure sensors, infrasound sensors, seismometers, Doppler speedometers, video recordings
	Flow depth	Radar sensors, wire sensors, ultrasonic sensors, laser
	Granulometry, particle concentration	Direct sampling
	Erosion	Scour sensors, buried radars
	Basal (normal or shear) and impact force	Load cells, piezoelectric sensors, seismometers
	Pore fluid pressure	Pressure sensors
	Ground vibration and sound	Seismometers, geophones (velocimeters, accelerometers)
	Particle collisions	Geophone
Deposit	Granulometry, particle density	Sampling
	Area, volume, flow runout, morphology	Aerial and satellite images, stereo-photogrammetry, GPS, theodolite, LiDAR, sidescan sonar

In ignimbrites deposited from a sustained current, the vertical succession of lithofacies records temporal changes in conditions and depositional processes, while lateral variations in lithofacies record spatial variations at a single period of time (Brown & Branney, 2013). This means that field work can be used to gather data to develop our understanding of how PDCs deposited, caused variations in topography and how this affected mobility as in Brown & Branney (2013).

Wilson (1985) used field work to collect data from the AD 186 Taupo ignimbrite; grain size and bed thickness data was collected along with field descriptions of bedforms and structures. Using these field observations, it was possible to make interpretations about the turbulence of the flow. Fluidisation processes were identified to be important for the PDC mobility but to evaluate these interpretations analogue lab experiments were required. This fieldwork was used to create a method for quantifying mobility by Dade & Huppert (1996) which suggests that a combination of approaches is important to create valid interpretations for PDC behaviours.

3 Methodology

This chapter will describe the methods used for the experiments and subsequent analysis. For the experimental methods, details will be provided for the analogue flume set-up, the materials that were released down the flume, the experimental design (detailing the control variables) and the methods in which the data was collected. The subsequent data analysis methods will detail how the collected data was used to calculate values to quantify mobility, as well as, how the video was analysed to describe the flow quantifiably and qualitatively.

3.1 Experimental design

This study investigates how grain size distribution affects the flow mobility by carrying out multiple runs using bidisperse and polydisperse materials. Previous work has primarily focused on monodisperse and bidisperse currents with investigations into polydisperse currents focusing on the flow behaviours using 2D analogue flumes. In monodisperse currents it is not possible to observe sedimentary structures such as reverse grading, which limits the ability to relate behaviours with sedimentary structures; and work on polydisperse currents has not investigated the deposit formation from these currents. Mixes of particles of varying grainsizes, in varying proportions, were created (details in Table 3.1, grain size distribution graphs in Figure 3.1).

Previous work by Sparks (1976) has shown that the majority of grain sizes in ignimbrites are <0 ϕ which suggests that the deposits are dominated by ash and fine material. The ash in natural PDCs relates to Group A of the Geldart classification (Druitt et al., 2004, 2007) therefore to simulate these natural material properties the dominant material in each current in this study will display Group A properties. Previous work by Roche et al. (2004) and Girolami et al. (2008) shows that experiments using natural material and silica glass ballotini show similar behaviours, therefore the silica glass ballotini will accurately simulate natural PDCs. By limiting the amount of Group B and D materials in each current, more sustained aeration is possible with less rapid degassing allowing for greater modelling of natural PDCs and observations to be made of beds.

The independent variables identified include:

- Material grain size. These grain sizes, shown in Fig. 3.1, were chosen because the range of grain sizes allows interpretations of the impacts of the grain size on flow mobility while still enabling gas fluidisation to occur of the largest particles. The proportions were chosen, based on pilot experiments, to allow for homogenous fluidisation of the material, as in currents where the majority of the materials display Group A behaviours fluidisation will occur at the same U_{mf} and bubbling will be prevented.

These mixes were oven dried to minimise cohesion from ambient moisture, which would result in clumping of material (primarily of the 45-90 µm particles) which would simulate anomalously large grainsizes, triggering lower mobility. Experiments using each mix were repeated multiple times with different camera set ups (Experimental set-up, including camera set up and mix details shown in Appendix I) to allow for a data to be collected along the entire flume and at intervals along the flume. This grain size variation within the mixes is not totally

accurate to natural PDCs, covers an order of magnitude of variation to best simulate the range of grain sizes in natural materials.

Table 3.1: Proportion of each material for each experimental mix

Mix number	Description	% 45-90µm	% 125-355µm	% 355-500µm	% 500-710µm
1	Quad-disperse	85	5	5	5
2	Fine bidisperse	90	10	0	0
3	Coarse bidisperse	90	0	10	0
4	Fine tri-disperse	90	5	5	0
5	Coarse tri-disperse	80	10	10	0

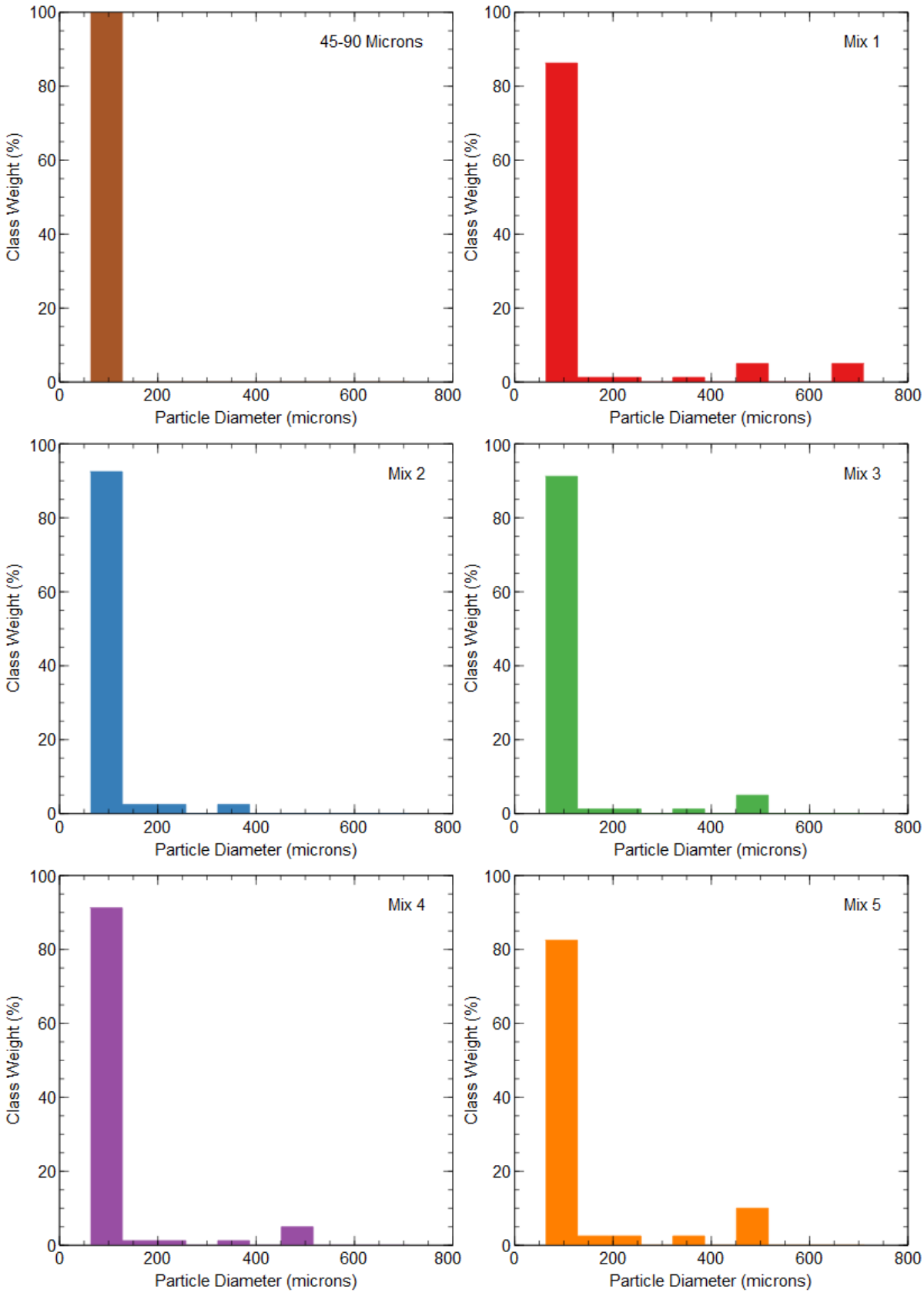

Figure 3.1: Grain size distribution of each mix used in this study.

The control variables for these experiments:

1. Gas supply: maintained at 53.33 cm/s in the 1st chamber and 40 cm/s in the 2nd and 3rd chambers; this is because the gas supplied affects the fluidisation so by keeping the gas supply constant it is possible to interpret the effects of grain size on mobility without having to consider the effects of varying gas flux. By using a gas flux of 80 L/s it is possible to fully aerate and fluidise the Group A and B materials while not fully fluidising the Group D materials, which prevents the generation of major bubbles especially of the Group A materials which would no longer flow as a current but separate entirely, thereby not simulating the grain size variations observed in natural PDCs;
2. Particle density: materials of consistent density (2500 kg/m^3) were used to remove the impact of density on flow mobility and particle behaviours, such as density-driven sorting;
3. Mass of particles being released: maintained at 10 kg to remove the impact of flow volume on mobility. Based on previous work by Rowley et al. (2014) and Smith et al. (2018; 2020) a 10 kg charge was chosen as it would supply enough material down the flume to allow for the formation of bedforms;
4. Flume angle: 1° to encourage the material to propagate along the flume, while the base plate of the flume is not completely flat with a variation of ± 1° this is as close as possible to making the impact of topography on the flow negligible

3.2 Experimental methods

3.2.1 Analogue flume set-up

The analogue flume is a small-scale experimental set up, where dense granular material was released down a 3 m long chute with aeration through the base. The goal of this set up is to experimentally simulate the natural behaviours of PDCs to allow for observations of behaviours and processes to be made.

Particles were supplied from a hopper into a 0.15 m wide, 3.0 m long flume from a lock gate release mechanism with a variable aperture (Fig. 3.2). The flume has an initial impingement ramp angled at 46°, to direct the material to travel down the flume. The currents then propagated along a flat channel, which for these experiments was angled at 1° downslope.

The porous base allows for compressed air to be supplied to the bottom of the current, enabling aeration of the material. In thin, rapidly degassing laboratory currents this allows for mimicking of the slow pore-pressure diffusion and long-lived mobility observed in natural PDCs (Rowley et al., 2014). The flume base is divided into three chambers, each 1 m long, with independent compressed air supplies to allow a variation in aeration along the flume. By having multiple chambers, it is possible to control the degree of aeration along the flume which in turn allows control over the degree of fluidisation, this allows gradual degassing of the current which occurs in natural PDCs and prevents the current from flowing out of the flume.

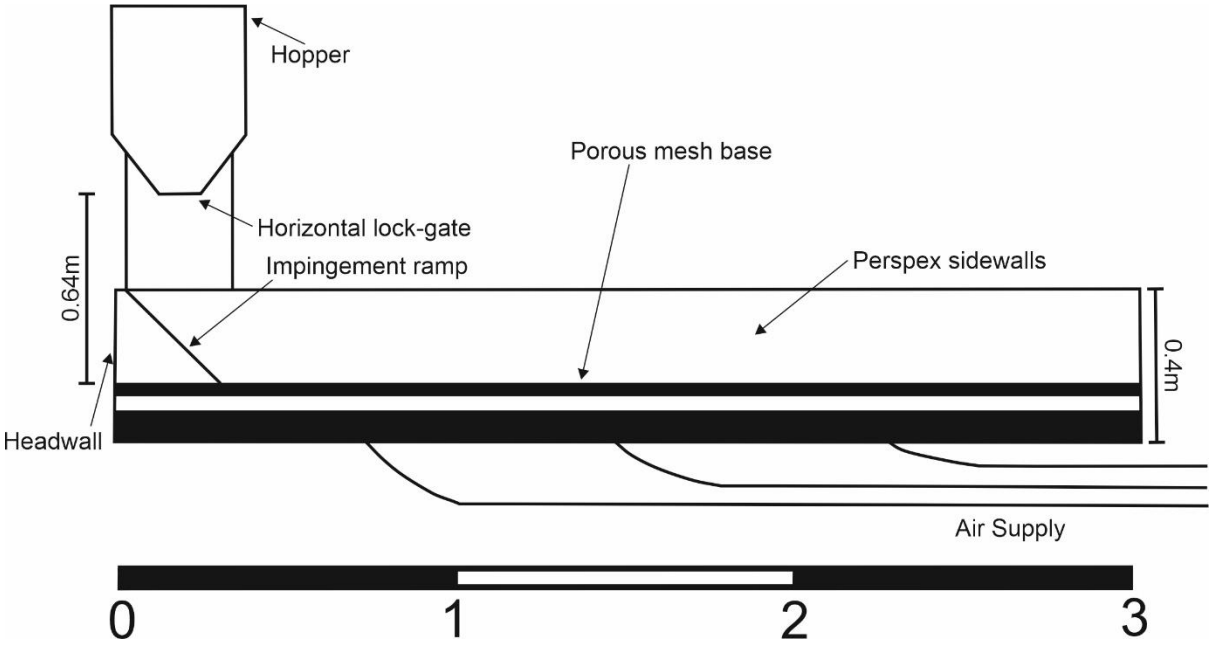

Figure 3.2: Section view of the experimental flume set up

3.2.2 Materials

Spherical soda lime ballotini beads were used with grain sizes from 45 µm to 710 µm, and a particle density of 2500 kg/m^3 (Table 3.2).

Table 3.2: Grain size and density of each particle used in the experiments

	Material	Size range (µm)	Median diameter (µm)	Particle density (kg/m^3)	Colour	Classification	
						Geldart, 1973	Yang, 2007
1	Glass	45 – 90	67.5	2500	White	A	A
2	Glass	125 – 355	230	2500	Orange	B	A/B
3	Glass	355 – 500	417.5	2500	Green	B	B
4	Glass	500 – 710	605	2500	Purple	B/D	B/D

Solid particles when fluidised can be characterised by their behaviour which is controlled by the mean particle size and the density difference between the material and fluidising gas. Using experimental data to quantify these behaviours, particles have been grouped based on shared properties when gas fluidised (Geldart, 1973).

Group A materials will rapidly mix due to circulation of particles similar to convection currents, and the beds will expand before bubbling commences (where bubbles of gas form and rise through the particles and the gas is released from the current) and slowly collapse when the gas supply is cut off. Group B materials will have naturally occurring bubbles form at or slightly above the minimum fluidisation velocity (U_{mf}) with little bed expansion, rapidly collapsing when gas supply is removed. Group D materials display a different method of gas exchange and bypassing to Group A or B materials, where gas bubbles rise more slowly than interstitial fluidising gas, resulting in gas flowing through these bubbles and releasing from the current. The presence of the Group D material is important as in flows containing these materials the flow regime around particles can be turbulent with rapid elutriation of fines (Geldart, 1973).

Using more experimental data including at increased pressure and temperature the Group A/B boundary was more clearly defined by Yang, 2007. With this more refined boundary, the majority of the ballotini are expected to follow Group A behaviours. This suggests that more of the materials will homogenously expand after the U_{mf} is reached and prior to the minimum bubbling velocity; and the beds will collapse more slowly and maintain aeration for longer after the gas supply is removed (Yang, 2007).

Using Group A materials in these experiments is important as beds of this material will expand and fluidise homogenously (Geldart, 1973). These particles will also have long pore diffusion timescales and experience negligible cohesion (Schellart, 2000; Gilbertson & Eames, 2003; Rowley et al., 2014) this allows for simulation of the sustained aeration of natural PDCs. However, as these lab flows are thinner they will de-fluidise more rapidly than natural currents. While for Groups B and D bubbles will form at U_{mf} which will promote particle circulation and gas-solid mixing in the fluidised bed (Wang et al., 2015) this circulation and mixing will allow for behaviours proposed to occur in natural PDCs (Gajjar et al., 2016).

Previous work by Roche, 2004 has identified the U_{mf} of materials with a grain size of 45-90 µm as 0.83 cm s^{-1}, materials with a grain size of 106-212 µm as 2.16 cm s^{-1}, and materials with a grain size of 600-800 µm as 27 cm s^{-1}. However, in bidisperse and polydisperse currents due to the variation in U_{mf} of different materials not all of the particles will fluidise at $U_{mf\ 1}$ (Gilbertson, 2019). This means that initially in currents where there are particles with different U_{mf} values the fluidisation will not be homogenous, therefore in these experiments the gas flux is high enough to ensure all the materials are fluidised.

3.2.3 Data collection

The experiments were recorded using a high-speed video camera at 500 frames per second at a resolution of 1632 x 1200 pixels. This high sample rate enables frame-by-frame analysis of the current to make quantitative observations of the flow head and qualitative observations of details of the flow body and deposit. The high resolution allows for PIV analysis and particle tracking of the flow to understand flow conditions in the basal flow and overriding cloud.

The high-speed camera was positioned to record segments along the flume with different runs showing different segments. The video footage was used to calculate current velocity and acceleration, record qualitative observations and analyse the internal dynamics of the current. The experiments were also recorded by a wide-angle GoPro camera which covered 2 m of the flume at a lower resolution, to allow for flow head velocity calculations for the entire current, and to confirm timings on wider current processes with respect to the narrower high-resolution video frame.

Once each flow had stopped propagating forwards the gas supply was cut off to prevent remobilisation of the deposit and elutriation of fines. Still photographs were taken of the deposit through the side wall and along the top of the flume. These images allow for bedforms to be identified within the deposit as well as any lateral segregation of the flow recorded in the deposit surface. These still photographs were linked with frames from the high-speed videos to get a 3D sense of the deposits.

3.3 Analytical methods

3.3.1 Velocity analysis

Flow head velocity was calculated by measuring the final run-out distance of each experiment and the total flow duration as recorded on the GoPro video. ImageJ software (Schneider et al., 2012) was used for frame-by-frame analysis of the high-speed videos. From this it was possible to accurately measure the distance travelled by the current between frames, and by using the frame number and frame rate it was possible to calculate the time between frames. Using these two values it was then possible to calculate velocity at varying intervals along the flume, and with time through the experiment, and from this acceleration.

These interval lengths, shown in Table 3.3, were chosen to allow for enough data points to show trends without producing too many data points which confuse trends in velocity along the flume. For the shorter flume sections, due to the high image quality, it was possible to do very detailed analysis of the current as the flow head could be picked out with greater precision.

Table 3.3: Table showing the length of the intervals used for velocity profile calculations for the corresponding length of the section of flume in that analysis

Length of flume section shown (cm)	Interval length (cm)
120	20
70	10
60	10
40	10
40	5
25	2
20	1
10	1

3.3.2 Sorting parameter

Sorting parameter is the primary method for quantifying sorting of sediments. By using the Method of Moments analysis, it is possible to calculate the mean, mode(s), sorting (standard deviation), skewness, kurtosis, D_{10}, D_{50}, D_{90}, D_{90}/D_{10}, D_{90}-D_{10}, D_{75}/D_{25} and D_{75}-D_{25}. Eqn. 7 was then used by the 'Gradistat' software to calculate the standard deviation of the grain size using the logarithmic methods of moment method (Blott & Pye, 2001). Using this value for standard deviation as the value for sorting, it is possible to compare each material mix in a quantitative manner.

$$\sigma_\phi = \sqrt{\frac{\sum f(m_\phi - \bar{x}_\phi)^2}{100}} \qquad \text{(eqn. 7)}$$

These sorting values could then be classified using the values in Table 3.4.

Table 3.4: Sorting Values for Gradistat (Blott & Pye, 2001)

Sorting Description	Standard Deviation value
Very well sorted	< 0.35
Well sorted	0.35 – 0.50
Moderately well sorted	0.50 – 0.70
Moderately sorted	0.70 – 1.00
Poorly sorted	1.00 – 2.00
Very poorly sorted	2.00 – 4.00
Extremely poorly sorted	> 4.00

3.3.3 Bedform analysis

Bedforms were qualitatively analysed using a bedform classification system (Chapter 5) based on the work of Cole (1991), Douillet et al. (2013), Schmincke et al. (1973) and Smith et al. (2020) which are described in Chapter 2. By describing the bedforms compared to natural PDC deposits it is possible to make interpretations of the conditions which formed these deposits in the flume. Then, by comparing these interpretations with the flow behaviours described in Chapter 4 it is possible to analyse if these correlate with interpretations of field deposits which in turn will improve future field interpretations based on the new understanding of PDC mobility in this thesis.

4 Current Behaviours

The mobility of PDCs is controlled by eruption mechanics, environmental conditions and material properties (Sulpizio et al., 2014; Palladino & Giordano, 2019) (see Chapter 2). This chapter will discuss the behaviours of currents generated during flume experiments, examining how variations in grain size and grain size proportions affect mobility. The experimental currents are compared both qualitatively and quantitively to see how different mixes affect current behaviours, run-out distance and velocity, with a focus on the polydisperse mixes (described in Chapter 3).

Qualitative analysis of the experimental currents is undertaken to identify rheological behaviours that impact mobility. Calculations using high-speed video footage allow for quantitative analysis of current run-out distance, velocity and acceleration. The data used in these calculations can be found in Appendix IV. Interpretations of how grain size variations affect run-out distance and flow velocity developed from this analysis are then discussed with application to natural PDCs. The material used in the flume has been shown to be a suitable analogue for natural PDC material (Chapter 3), but these experiments do not contain the range of grain sizes observed in the real world, therefore limitations are also considered.

4.1 Rheological behaviours

High-speed video footage of the analogue currents was used to observe current behaviours with respect to changing grain size distribution. This video footage is available on YouTube (Appendix III) and detailed descriptions of each current are available in Appendix II. In this section, qualitative and quantitative descriptions of each current are made and interpreted, to understand the way in which current behaviours vary. Monodisperse currents will be discussed first, before progressing onto the more complex bidisperse and polydisperse currents. Comparison with the observations of the monodisperse currents are key to understanding which behaviours are linked to changes in particle size and distribution.

In this section, time stamps reflect the time after the hopper was opened and are given as representative examples of observed behaviours. Unsteadiness refers to current behaviour where the flow conditions were variable, and it is possible to see features such as waves in the current.

4.1.1 Monodisperse currents

The use of monodisperse currents allows for improved identification of variations in current behaviours for bidisperse and polydisperse currents, through identifying which behaviours are generated by the 45-90 µm particles and which behaviours are generated through interactions between the 45-90 µm particles and coarser particles. These monodisperse experiments are Experiment 9 and Experiment 13 on the YouTube playlist (Appendix III).

Current Description

In the monodisperse currents, typically the initial flow head (Experiment 9: 0.21 cm thick; Experiment 13: 0.12 cm thick) is very stable (Experiment 9: travelling at 1.28 ms^{-1}; E13: travelling at 1.82 ms^{-1}) with an overriding plume generated as the material impinged on the baseplate (Experiment 13: 0.140 seconds; Fig 4.1). Following elutriation of fines into the

overriding cloud, there was the generation of waves (Experiment 13: 0.654 seconds, 45 cm along the flume, travelling at 1.45 ms^{-1}) and a pulse (Experiment 9: 0.654 seconds, 46 cm along the flume, 0.755 cm thick, travelling at 1.50 ms^{-1}; Experiment 13: 0.700 seconds, 1.06 cm thick, travelling at 1.40 ms^{-1}) (Fig 4.1) showing that the current became unsteady.

Initial deposition starts as progressive aggradation at the base of the ramp underneath the flowing current (Experiment 9: 1.15 seconds; Experiment 13: 0.696 seconds) which was followed by rapid deposition through regressive aggradation. There was reworking of the deposit where remobilisation occurred (Experiment 9: 1.226 second, between 60 and 80 cm along the flume; Experiment 13: 0.844 seconds compared to 4.00 seconds shown in Fig 4.2).

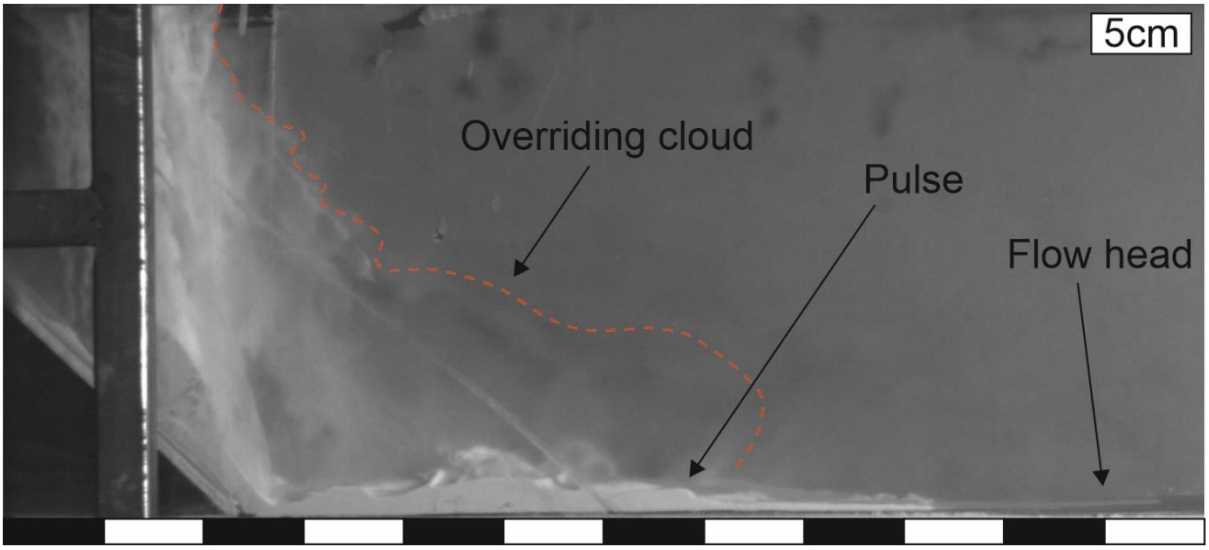

Figure 4.1: Annotated shot of Experiment 13 flow at 1.154 seconds showing the overriding cloud of fines, thin flow head and generation of a pulse near the flow front.

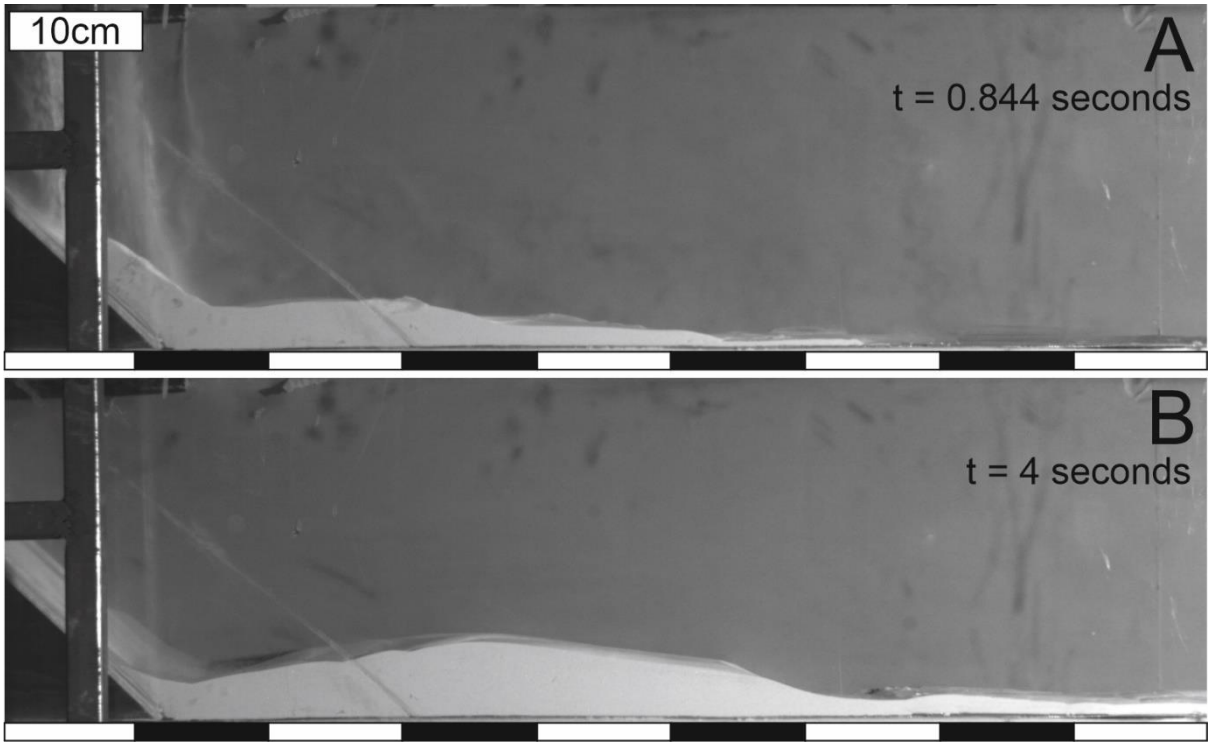

Figure 4.2: Images of the Experiment 13 deposit at A, 0.844 seconds, and B, 4 seconds, showing how deposit thickness changed through time, with initial thickness at the base of the ramp and later thickness in the mid-section.

Interpretation

The change in deposit thickness at the base of the ramp between 0.844 seconds and 4 seconds suggests that either this part of the deposit undergoes remobilisation during this time, or that a thick slow-moving flow at 0.844 seconds makes the deposit appear thicker than it actually is.

4.1.2 Quad-disperse

The currents are polydisperse (45-90, 125-355, 355-500 and 500-710 µm), the proportions of these mixes are detailed in Chapter 3, and shown in Fig. 3.1. The use of this mix allows interpretations of behaviours which originate in polydisperse currents due to the range of grain sizes present. This variation while not totally accurate to natural PDCs, as experimental designs are limited by grains which fluidise in an analogue flume, covers an order of magnitude of variation to best simulate the range of grain sizes in natural materials. These experiments were carried out as previous work has not covered polydisperse currents and these are best suited to simulating the grain size variations observed in natural PDCs. These experiments are Experiment 22, Experiment 23, Experiment 24 and Experiment 25 on the YouTube playlist (Appendix III).

Description

The initial flow head is thin (Experiment 22: 0.153 cm, travelling at 1.07 ms^{-1}; Experiment 23: 0.341, travelling at 1.10 ms^{-1}; Experiment 24: 0.327 cm, travelling at 1.78 ms^{-1}; Experiment 25: 0.243 cm, traveling at 1.57 ms^{-1}), steady but slightly unstable with fines separating and

elutriating into the overriding cloud and coarse grains saltating through the main flow, and entrains some of these coarser materials. This flow is fines rich showing lateral and vertical normal grading, and above the main flow body, the overriding cloud becomes larger and turbulent.

Preceding the main flow head, the transport of coarse grains was entirely by saltation and there was an overriding cloud of fine particles (45-90 μm). There were multiple grain sizes within the saltating particles where the coarser particles (500-710 μm) (Experiment 22: vertical offset of 24 mm) and finer particles (125-335 μm) (Experiment 22 vertical offset of at least 58.5 mm).

Following the initial unsteadiness in the current there was the generation of a 2nd pulse of material which is unsteady and mainly consists of coarser materials (Experiment 23 initially the pulse is richer in fines until saltating particles are entrained), with the fine particles travelling faster than the coarser particles (Experiment 22: 0.364 seconds, 0.848 cm thick, travelling at 1.62 ms^{-1}; Experiment 23: 0.43 seconds, 0.365 cm thick, travelling at 1.24 ms^{-1}; Experiment 24: 0.554 seconds, 0.617 cm thick, travelling at 1.43 ms^{-1}, Fig 4.5; Experiment 25: 0.406 seconds, 0.376 cm thick, travelling at 1.31 ms^{-1}). There was a 3rd pulse present (Experiment 23: 0.458 seconds, 0.644 cm thick, travelling at 1.44 ms^{-1}; Experiment 25: 0.546 seconds, 0.686 cm thick, travelling at 1.32 ms^{-1}), this is unstable and shows vertical stratification (fine base, coarse surface) and recirculation of coarse particles, with an overriding cloud ahead of the pulse that has the same shape as the flow. The flow then progressively aggrades before a 4th pulse is generated with lateral and vertical segregation, possibly fines-rich due to fall out from overriding cloud (Experiment 23: 1.156 seconds, 0.609 cm thick, travelling at 0.625 ms^{-1}; Experiment 25: 0.592 seconds, 1.06 cm thick, travelling at 0.552 ms^{-1}). As the flow propagates, fine particles fell out of suspension and were incorporated into the current, as shown by Fig. 4.4 where the overriding cloud can be seen being entrained by the breaking waves (Experiment 23: travelling at 0.802 ms^{-1}; Experiment 25: travelling at 1.43 ms^{-1}).

Deposition varied during the flow with initial deposition occurring as progradation before becoming reterogradation. While the deposit develops backset beds there is fallout from the suspended cloud producing fine beds.

Interpretation

The normal grading in the unsteady flow following the saltating particles is due to coarse material at flow head and base being entrained from saltation. While in the 2nd pulse of material there is lateral segregation of the flow causing a fines rich flow head due to the fine particles travelling faster than coarser particles.

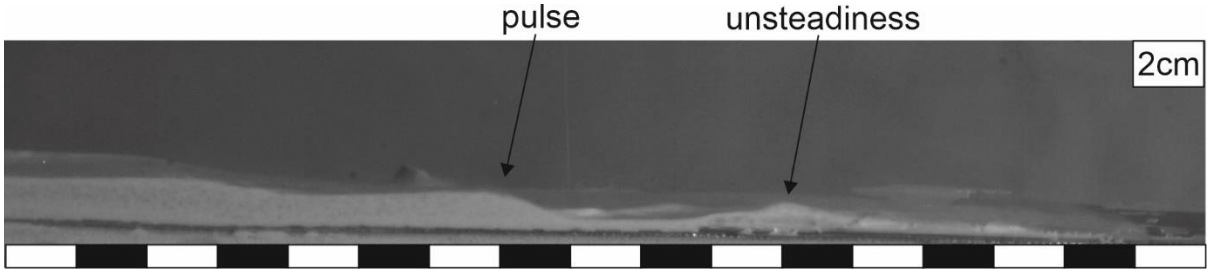

Figure 4.3: Annotated photograph of the Experiment 22 current at 0.464 seconds.

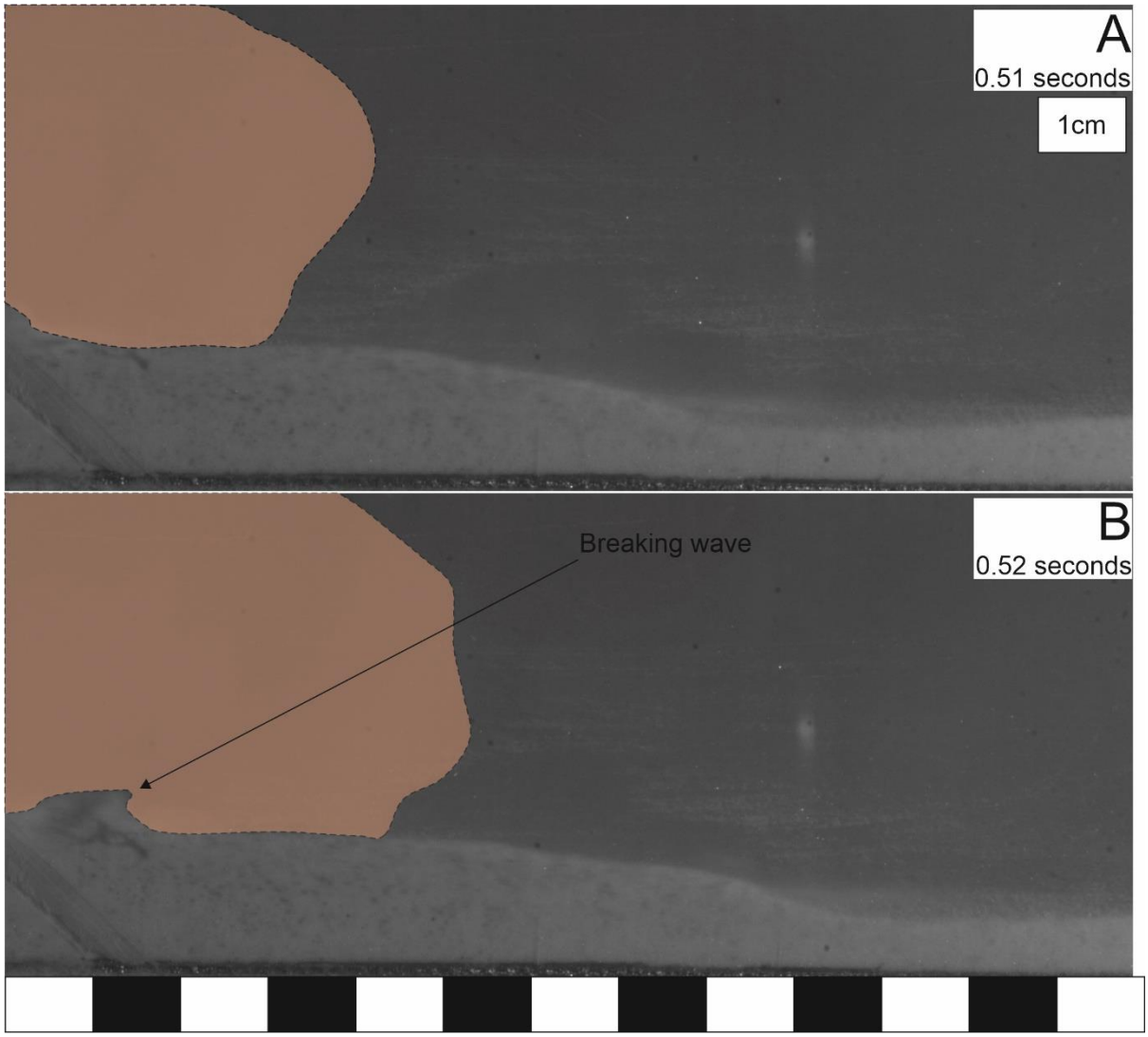

Figure 4.4: Images of Experiment 23 showing a breaking wave in the current and overriding cloud (brown) fall out at (A) 0.51 seconds and (B) 0.52 seconds.

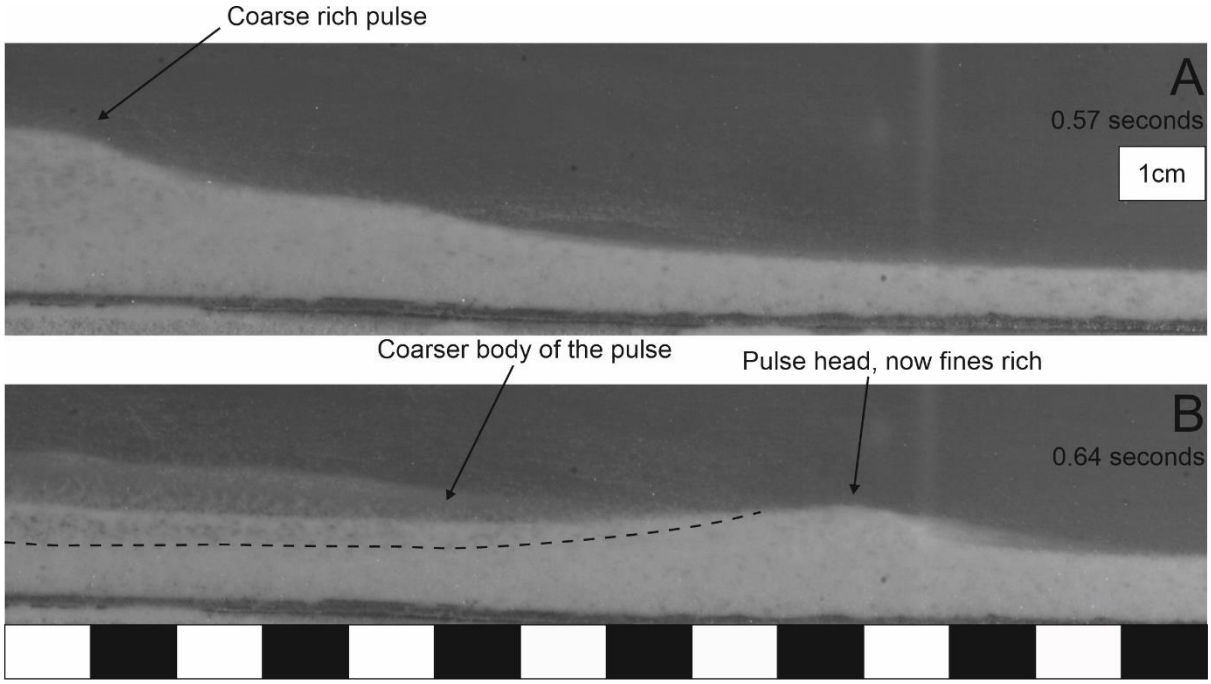

Figure 4.5: Photographs of the current in Experiment 24 showing lateral grading within the pulse (A) 0.57 seconds (B) 0.64 seconds.

4.1.3 Fine bi-disperse

The currents are bidisperse currents (45-90 and 125-355 µm) the proportions of these mixes are detailed in Chapter 3, shown in Fig. 3.1. The use of this mix allows interpretations of behaviours which originate from the interactions between 45-90 µm and 125-355 µm particles. By comparing the two bi-disperse currents it is possible to identify variations in behaviours that come from interactions between the grain sizes present in the current and interactions between the number of grain size ranges within the current. These experiments are Experiment 6 and Experiment 8 on the YouTube playlist (Appendix III).

Current Description

In this current the overriding cloud generated very rapidly as the material impinged on the baseplate (Experiment 8: flow thickness is 1cm and cloud height is 15cm).

The initial flow head was a few millimetres thick overtaken by a thicker pulse (Experiment 6: 0.200 seconds; Experiment 8: 0.332 seconds, 60cm along the flume). Following this overtaking the current and flow head became unsteady, the flow head then became laminar (Experiment 8: 0.44 seconds, 75cm along the flume), at the same time later unsteadiness in the flow results in a second pulse (Experiment 6: 0.390 seconds, 0.894 cm thick, travelling at 1.33 ms^{-1}; Experiment 8: 0.518 seconds, 0.940 cm thick, travelling at 1.43 ms^{-1}). The continuing unsteadiness is followed by a 3rd pulse forming (Experiment 6: 0.516 seconds, 0.353 cm thick, travelling at 1.10 ms^{-1}; Experiment 8: 0.538 seconds, 1.012 cm thick, travelling at 1.473 ms^{-1}).

Deposition varied between different runs of the fine bi-disperse material, as in experiment 6 the initial deposition consists of reterogradation which becomes progradation (after 0.76 seconds); with later deposition is mainly from fall out from overriding cloud forming shallow backset beds. While for Experiment 8, progressive aggradation is the most common method

of deposition, with regressive aggradation beginning to occur (at 1.08 seconds) just after hopper at approximately 40cm along the flume.

Interpretation

The short-lived 3rd pulse suggests either mixing between the pulses occurred due to sorting within the flow of the two pulses or that unsteadiness of the 2nd pulse resulted in a long wavelength giving the appearance of a 3rd pulse.

4.1.4 Coarse bi-disperse

The currents are bidisperse currents (45-90 and 355-500 µm) the proportions of these mixes are detailed in Chapter 3. The use of this mix allows interpretations of behaviours which originate from the interactions between 45-90 µm and 355-500 µm particles. These experiments are Experiment 10, Experiment 11 and Experiment 12 on the YouTube playlist (Appendix III).

Current Description

In this current the initial flow head is steady, followed by an unsteady pulse of coarser particles (Experiment 10: 0.534 seconds, 0.393 cm thick, travelling at 1.76 ms^{-1}; Experiment 11: 0.432 seconds, 0.711 cm thick, travelling at 1.74 ms^{-1}; Experiment 12: 0.390 seconds, 0.602 cm thick, traveling at 1.29 ms^{-1}) which forms a breaking wave as it overtakes the original flow head (Experiment 10: 0.584 seconds, traveling at 0.97 ms^{-1}; Fig. 4.6) and mixes with this previous flow head (Experiment 11: 0.516 seconds). The continued unsteadiness results in the generation of a 2nd pulse (Experiment 10: 0.604 seconds, 0.821 cm thick, traveling at 1.65 ms^{-1}; Experiment 11: 0.826 seconds, 0.711 cm thick, traveling at 1.78 ms^{-1}; Experiment 12: 0.516 seconds, 0.492 cm thick, traveling at 1.17 ms^{-1}) which shows breaking waves and a 3rd pulse (Experiment 10: 0.680 seconds, 0.763 cm thick, traveling at 1.49 ms^{-1}). Above the main body of the flow is an overriding cloud with fines elutriating from the flow and shows turbulence.

Deposition starts as progressive aggradation (Experiment 10: 0.774 seconds; Experiment 12: 0.750 seconds) with further deposition from fallout of suspended particles. After deposition from progressive aggradation, the deposition is dominated by reterogradation (Experiment 10: 1.39 seconds).

Interpretation

As most of the material is transported by suspension within the overriding cloud the majority of deposition is through progressive aggradation as particles fall out of suspension.

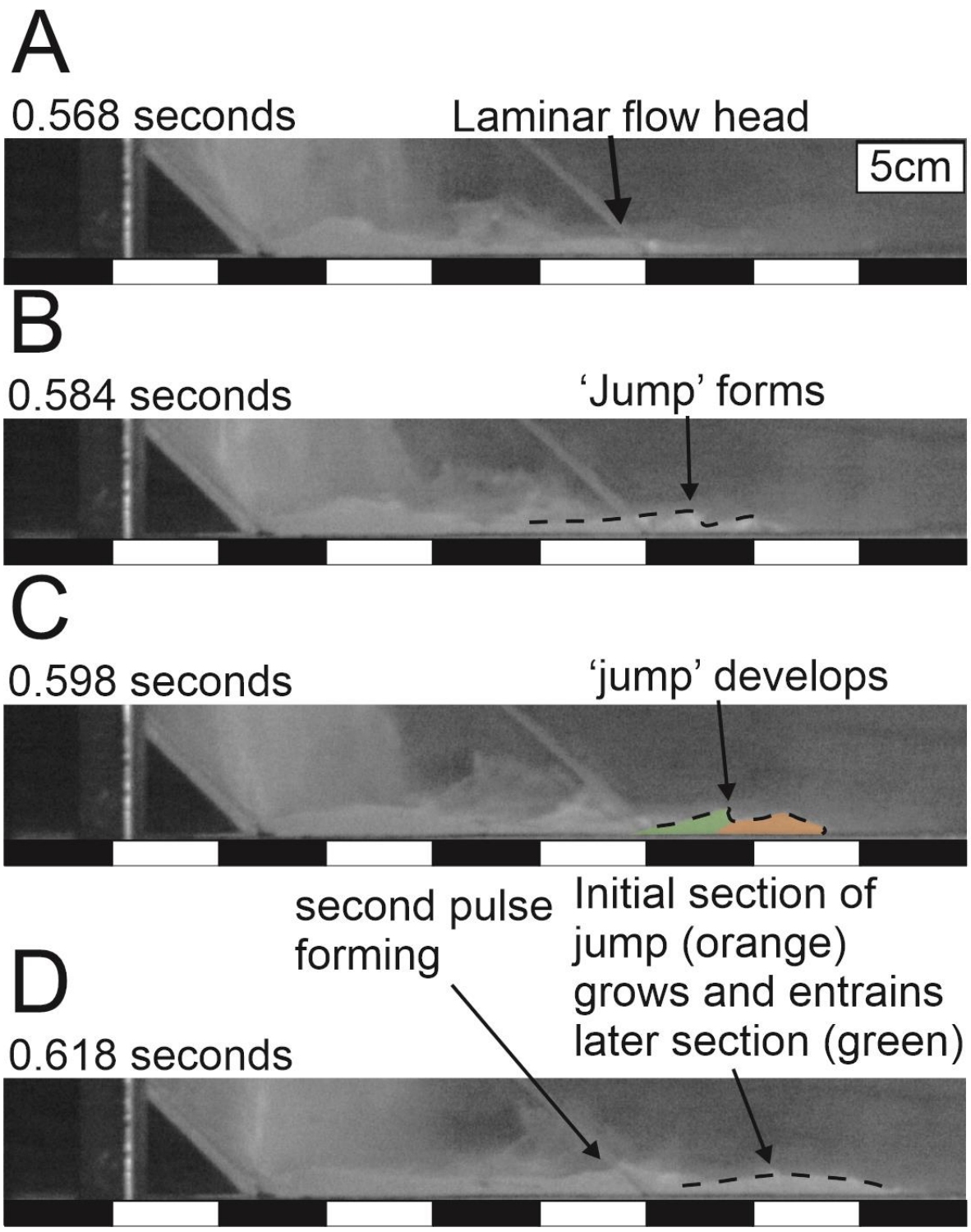

Figure 4.6: Annotated photographs showing the progression of the 'jump' as it reincorporates into the flow and the generation of the second pulse in Experiment 10. A = 0.568 seconds, B = 0.584 seconds, C = 0.598 seconds, D = 0.618 seconds.

4.1.5 Fine tri-disperse

The currents are polydisperse (45-90, 125-355 and 355-500 µm), the proportions of these mixes are detailed in Chapter 3. The use of this mix allows interpretations of behaviours caused by the 125-355 µm and 355-500 µm particles, including how these grain sizes interact with each other and by comparing to the quad-disperse currents, behaviours which originate

in the coarsest grains (500-710 µm) can be interpreted. These experiments are Experiment 14, Experiment 15, Experiment 16 and Experiment 17 on the YouTube playlist (Appendix III).

Current Description

In this current the overriding cloud precedes the basal flow head. The initial flow head is steady and consists of fine material a few millimetres thick (Experiment 14: 0.112 cm; Experiment 15: 0.138 cm; Experiment 17: 0.184 cm); with a thicker unsteady flow unit catching up with the flow head (Experiment 14: 0.366 seconds, 1.10 cm thick, travelling at 1.59 ms^{-1}; Experiment 15: 0.312 seconds, 0.401 cm thick, travelling at 1.00 ms^{-1}; Experiment 16: 0.358 seconds, 0.725 cm thick, traveling at 1.68 ms^{-1}). In this unsteady thicker pulse, the fine particles travel faster than the coarse particles causing both vertical and lateral grading where initially the current is stratified (Experiment 14: Fig. 4.7; Experiment 15: Fig 4.8a, b; Experiment 17: Fig. 4.9). The presence of this stratification is prevented by the generation of a pulse (Experiment 15: 0.354 seconds, 0.850 cm thick, travelling at 1.63 ms^{-1}) which mixes within the flow head and leads to deposition of fines (Fig. 4.8). When the current is unsteady there are breaking waves and fines elutriating into the overriding cloud throughout the current (Experiment 17: 0.468 seconds).

Deposition occurred in all runs as progressive aggradation, generating backset beds or regressive features. However, in some cases (Experiment 14, Experiment 16) the coarse particles deposited first with a less coarse mix flowing over the top (Fig. 4.7 e and f); while in others (Experiment 15, Experiment 17) the fine particles deposited first.

Interpretation

Here the flow behaviour displays similar characteristics to a resegregation regime, which suggests that percolation is occurring within the flow allowing for larger grains to rise to the surface of the current before being recirculated and overran by later particles within the current (Gajjar et al., 2016).

In experiment 15 the deposition seems to occur under steady conditions while showing reverse grading.

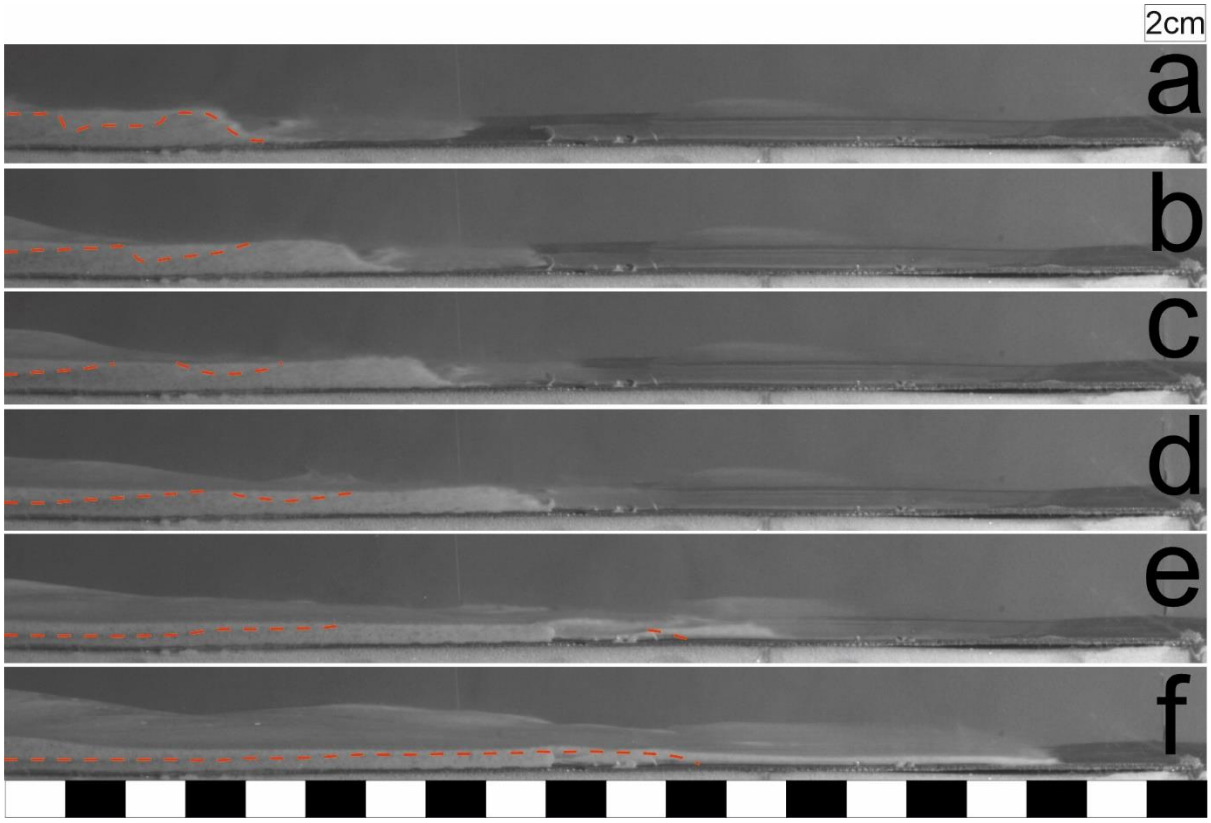

Figure 4.7: Annotated high-speed photographs of Experiment 14 showing the vertical and lateral grading observed, scale shows every 2 cm. a – 0.418 seconds, b – 0.442 seconds, c – 0.458 seconds, d – 0.48 seconds, e – 0.534 seconds, f – 0.6 seconds

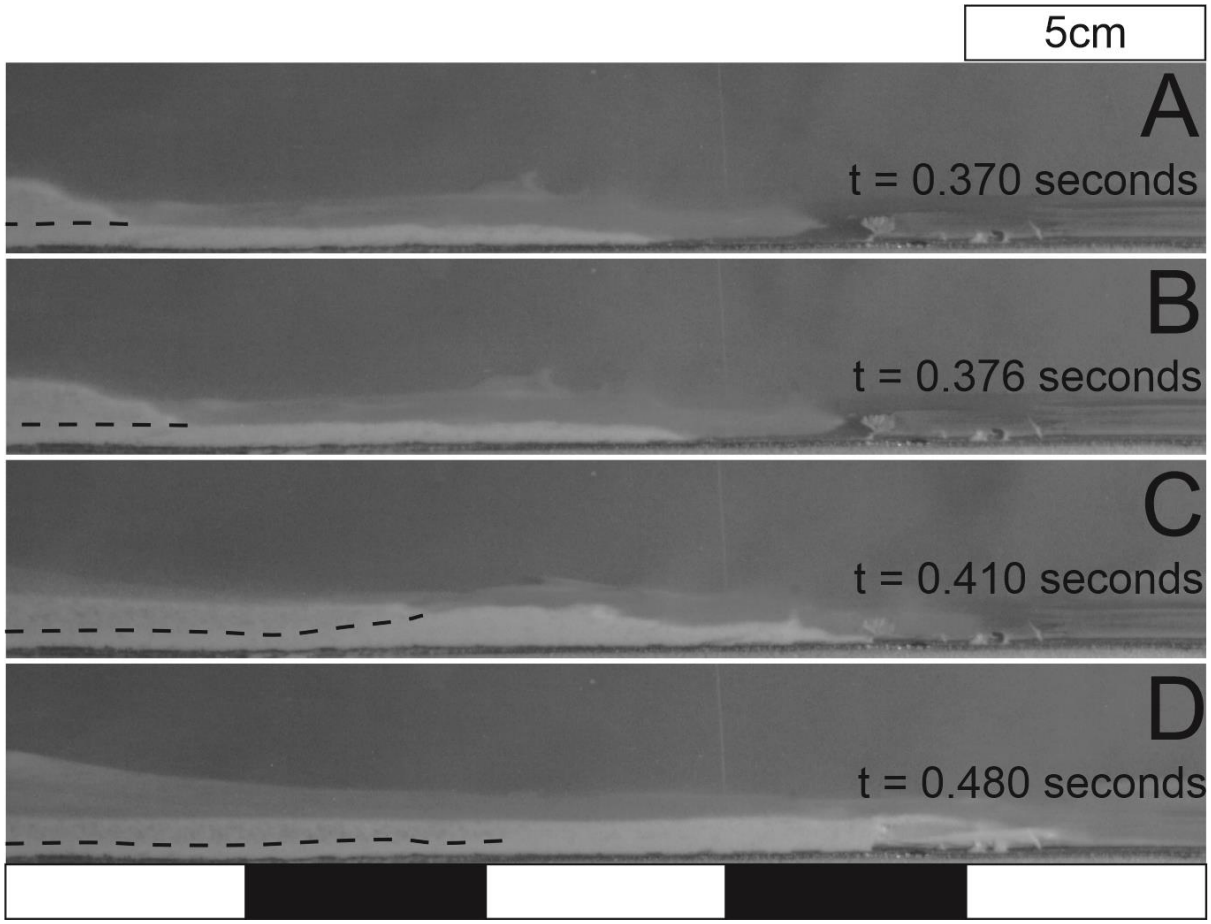

Figure 4.8: Annotated photograph of Experiment 15 showing initial segregation then mixing. a – 0.370 seconds, b – 0.376 seconds, c – 0.410 seconds, d – 0.480 seconds

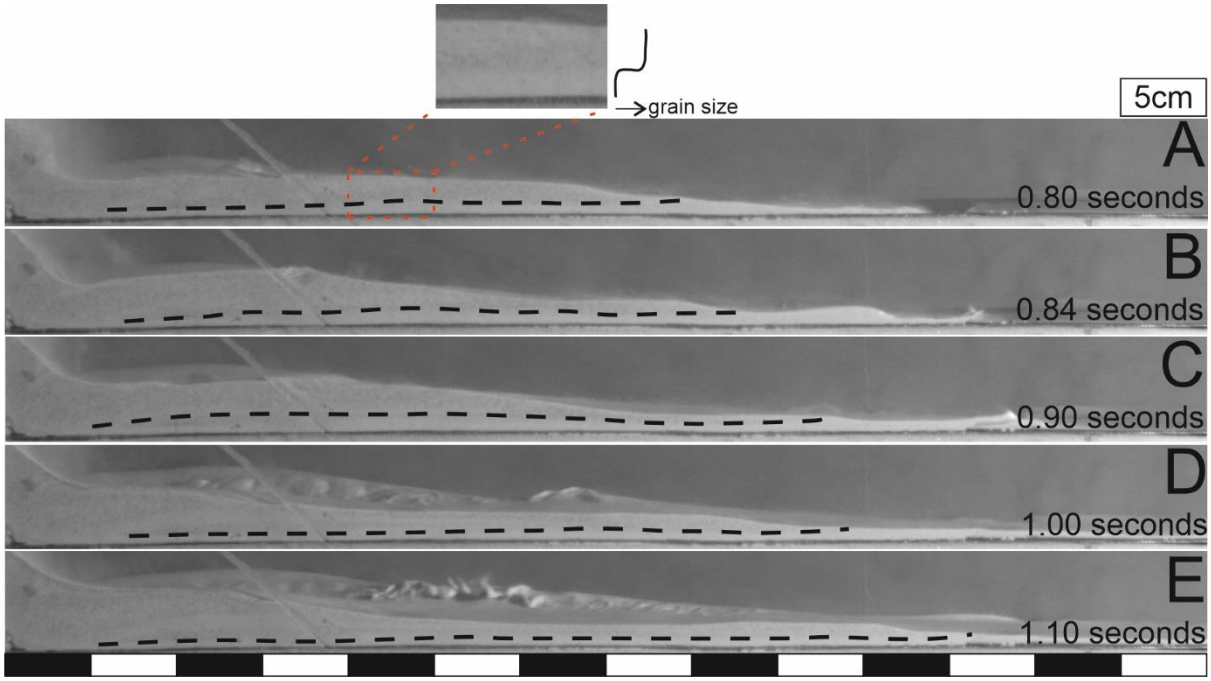

Figure 4.9: Annotated photographs of Experiment 17 showing stratified current at A 0.80 seconds, B 0.84 seconds, C 0.90 seconds, D 1.00 seconds, E 1.10 seconds.

4.1.6 Coarse tri-disperse

The currents are polydisperse (45-90, 125-355, 355-500 µm), the proportions of these mixes are detailed in Chapter 3. The use of this mix allows interpretations of behaviours caused by the 125-355 µm and 355-500 µm particles, by comparing to the fine tri-disperse currents it is possible to interpret the impacts the proportion of 45-90 µm particles have on current behaviours. These experiments are Experiment 18, Experiment 19, Experiment 20 and Experiment 21 on the YouTube playlist (Appendix III).

Current Description

In the current, the initial flow head (Experiment 19: 0.172 seconds, 0.303 cm thick; Experiment 20: 0.172 seconds, 0.264 cm thick; Experiment 21: 0.617 cm thick), is steady to quasi-steady and shows as the flow propagates lateral and vertical normal grading occur. This flow head is preceded by saltating particles (>355 µm) (8.21 cm ahead of flow head) and a cloud of fine particles (45-90 µm) (6.59 cm ahead of flow head) (Experiment 21: 0.104 seconds).

The flow then varies with the generation of a pulse of coarse material (Experiment 18: 0.646 seconds, 0.650 cm thick, travelling at 1.240 ms^{-1}; Experiment 19: 0.516 seconds, 0.924 cm thick, travelling at 1.20 ms^{-1}; Experiment 20: 0.240 seconds, 0.567 cm thick, travelling at 1.477 ms^{-1}; Experiment 21: 0.320 seconds, 0.595 cm thick, traveling at 1.118 ms^{-1}), this was followed by another pulse of coarse material (Experiment 18: 0.684 seconds, 0.425 cm thick, traveling at 0.880 ms^{-1}; Experiment 20: 0.378 seconds, 0.475 cm thick, travelling at 1.230 ms^{-1}) and a third pulse of coarse material (Experiment 20: 0.528 seconds, 0.633 cm thick, traveling at 1.126 ms^{-1}). These pulses entrain previously deposited fines (Experiment 21: 0.320 seconds), and laterally grade as they propagate with a fines rich flow head with the coarser particles depositing first. When these pulses overtake the previous flow head waves generate and become breaking waves at the point of overtaking (Experiment 20: 0.420 seconds, traveling at 1.352 ms^{-1}; Fig. 4.10)

Deposition initially begins with fines from the flow head, before deposition is dominated by progressive aggradation from the coarse particles within the pulses. Between the pulses deposition is dominated by fallout from the suspended fines in the overriding cloud, which results in a reverse graded deposit when the pulses overrun these fines entraining some particles and depositing the coarser material. Once the energy within the basal layer is lower than the energy needed to transport material (Experiment 19: 1.650 seconds) transport and deposition is dominated by the overriding cloud of fines (45-90 µm) which forms massive deposits.

Interpretation

Within the pulses the entrainment of fine particles at the surface of the deposit suggests that turbulent eddies were generated which caused reworking of the loose deposit. And, the deposition of coarse particles shows that the current was waxing and there was unsteadiness due to the saltating coarser particles (Branney & Kokelaar, 2002). The reverse grading of the deposit suggests that percolation was the dominant sorting method whereby due to the greater friction between the coarse and fine particles, the finer particles stay in place below

the coarser particles (Vallance & Savage, 2000) and form a fine deposit overran by coarser particles.

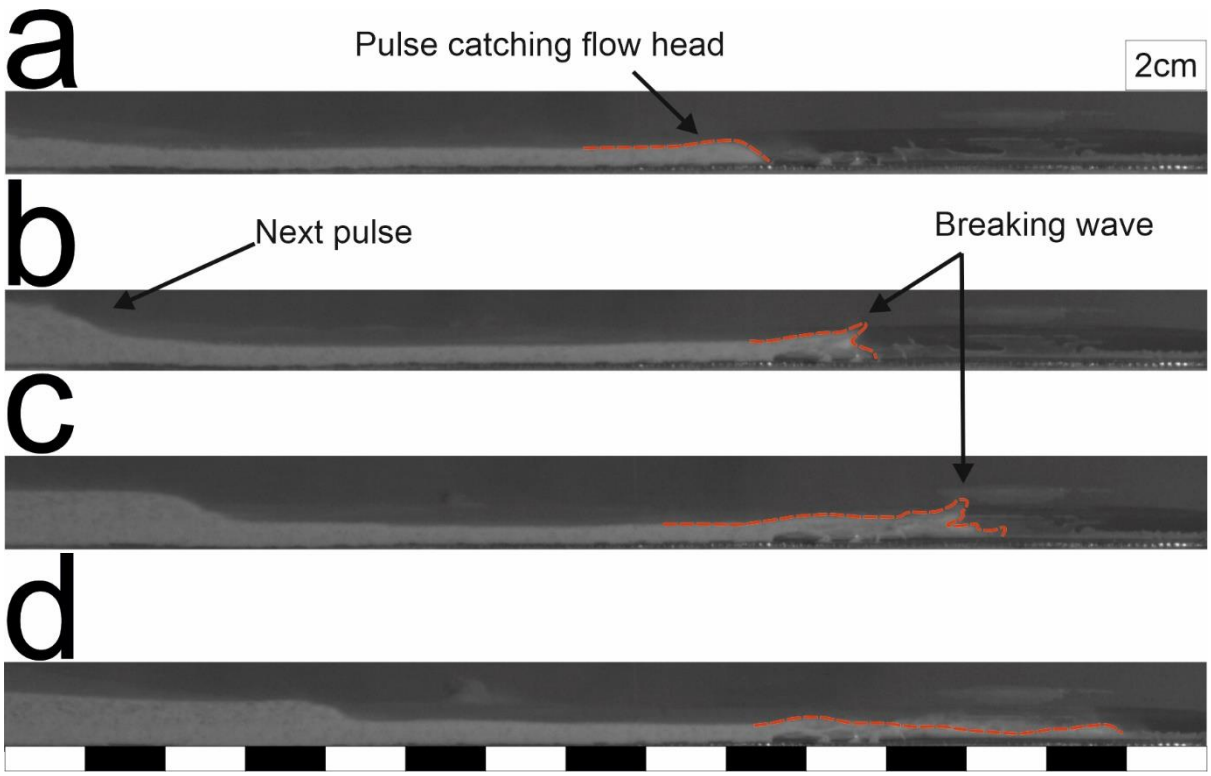

Figure 4.10: Annotated high-speed photographs of the flume showing the pulse 'jumping' over the flow head in Experiment 20 as described above, scale 2cm. a – 0.38 seconds, b – 0.4 seconds, c – 0.422 seconds, d – 0.45 seconds

4.1.7 Discussion

By comparing behaviours in the currents, it is possible to make interpretations about rheological behaviours. Table 4.1 shows the behaviours present in each run for the current, there are variations for each current due to camera location impacting which features were visible.

Table 4.1: Table showing behaviours common to the currents

	2 Pulses	3 pulses	4 pulses	Saltation	Overriding cloud	Stratified Current
Mono-disperse		✓			✓	
		✓			✓	
Fine bi-disperse	✓				✓	
		✓			✓	Prior to pulses
Coarse bi-disperse		✓			✓	
		✓			✓	
		✓			✓	Prior to pulses
Fine tri-disperse					✓	✓
					✓	✓
					✓	
					✓	✓
Coarse tri-disperse		✓			✓	
	✓				✓	
		✓			✓	
			✓	✓	✓	
Quad-disperse	✓				✓	Prior to pulses
			✓	✓	✓	
	✓			✓	✓	
	✓				✓	

The experiments that used 100% 45-90µm particles consisted of a steady initial flow head, with later unsteadiness as the thicker main flow unit caught up with the head of the flow. This unsteadiness led to 2 pulses within the flow.

In general, the quad-disperse currents had a consistent behaviour. In this series of experiments the flow consisted of saltating particles ahead of flow, where the initial flow head was steady with later unsteadiness being generated from entrainment of saltating particles. There were 4 pulses in each run, which consisted of coarse particles showing both vertical and lateral grading.

The series of experiments using fine and coarse bi-disperse currents showed similar behaviours. Both bi-disperse currents consisted of a steady initial flow head, with later unsteadiness as the thicker main flow unit caught up with the head of the flow. There were 3 pulses in each run with a turbulent overriding cloud.

The experiments comprised of fine and coarse bi-disperse currents have similar behaviours, which suggests that the proportions of fines are a dominant factor in controlling current mobility. As these fine particles are more mobile these currents have similar behaviours dominated by the behaviour of these finest particles.

The series of experiments using fine tri-disperse currents consisted of a steady initial flow head, with later unsteadiness as the thicker main flow unit caught up with the head of the flow; this unsteadiness after the initial flow head led to pulses of coarse material. In these experiments the deposition varies in some cases fine particles deposited first in others the coarse particles deposited first.

The series of experiments using coarse tri-disperse currents consisted of saltating particles ahead of the flow, where the initial flow head was steady with later unsteadiness being generated as the thicker body of the flow overtook the original flow head. There were 4 pulses in each run with a turbulent overriding cloud generating from the beginning of the flow.

These currents have shown some common behaviours regardless of proportion of fines, and some variable behaviours depending on material proportions. The most common behaviour to all the currents is that the flow is initially stable with unsteadiness being generated as the current propagates along the flume, with lateral grading occurring during current propagation as fine particles travel faster than coarse particles. In the currents which contain more coarse particles, saltation occurs more commonly. In these currents the saltating particles cause the flow to break up into smaller packages of material which flow as a smaller unit which leads to unsteadiness in the flow.

Fig 4.11 shows that the number of pulses in the current is independent of the proportion of fines and current sorting. The data for some of the currents makes trends difficult to see as the high-speed camera only showed a portion of the flume which prevents some pulses from being visible.

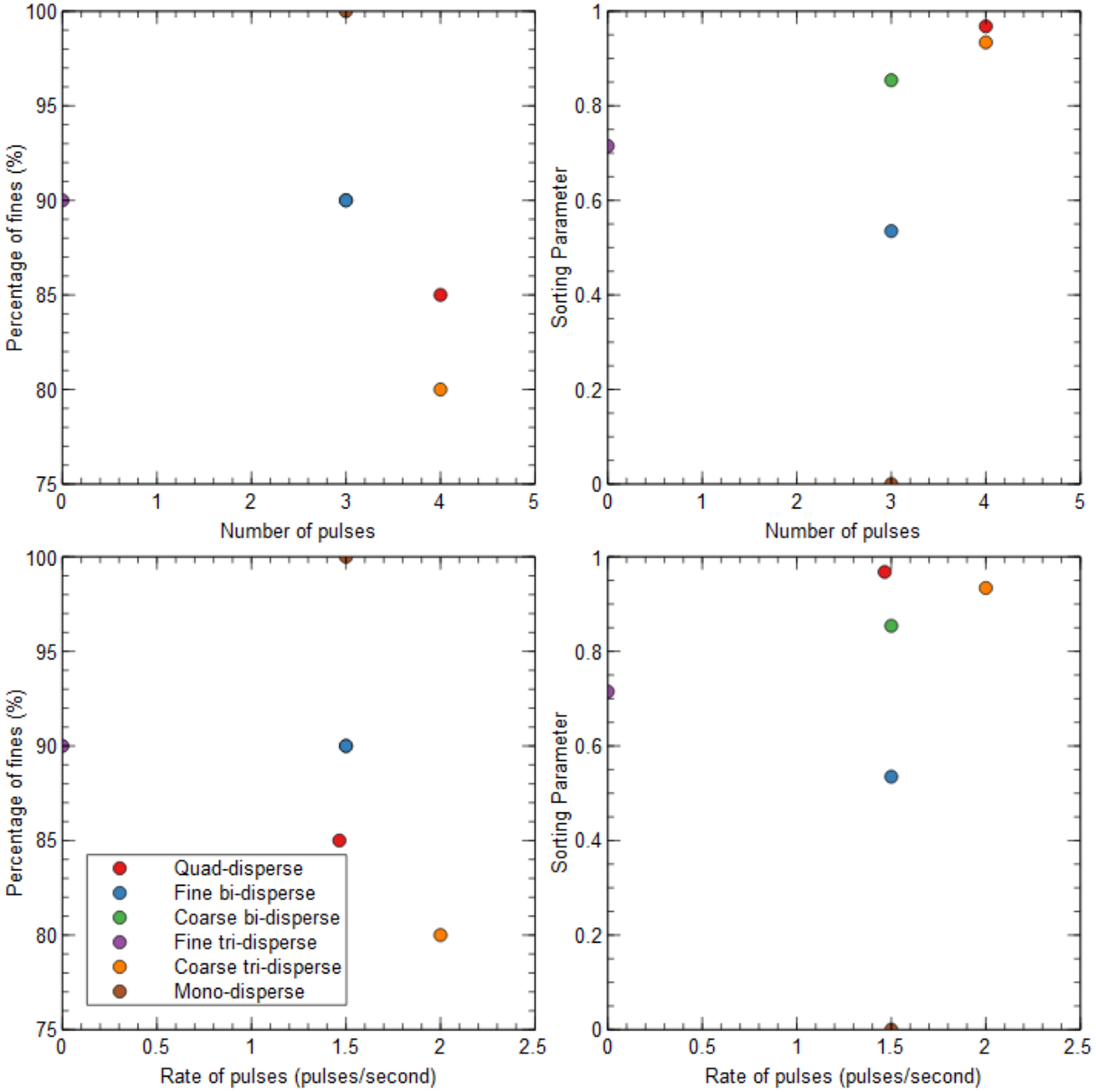

Figure 4.11: Graphs showing the relationship between the pulses and the proportion of fines within the currents

In currents where there are no pulses the current is stratified, and then some currents are initially stratified but then pulses form which prevent stratification. The absence of stratification in the bi-disperse currents is due to the process of resegregation, where percolation caused coarse particles to migrate upwards and travel to the flow head whereby they are reincorporated into the current (Gajjar et al., 2016). This constant cycle of percolation and recirculation prevents the formation of stratification in the current. However, in the quad-disperse and coarse tri-disperse currents the absence of stratification is likely due to the 500-710 µm particles traveling by saltation; this transport will create voids that allow for percolation and particle mixing. Stratified currents consist of two non-mixing layers where coarse particles override the flowing finer particles, suggesting that in the stratified currents percolation was dominant causing finer particles to move downwards into pore spaces below (Vallance & Savage, 2000). In the stratified fine tri-disperse currents

recirculation was prevented by the larger particles (355-500 µm) travelling at slower velocities than the finer particles, which means that the coarse upper layer was unable to overtake the fine lower layer and recirculate.

4.2 Current run-out distances

In this section the run-out distance has been quantified allowing for interpretations of relationships. Quantification was done by using the high-speed video and wide-angle video, along with measurements taken along the flume when the experiments were carried out.

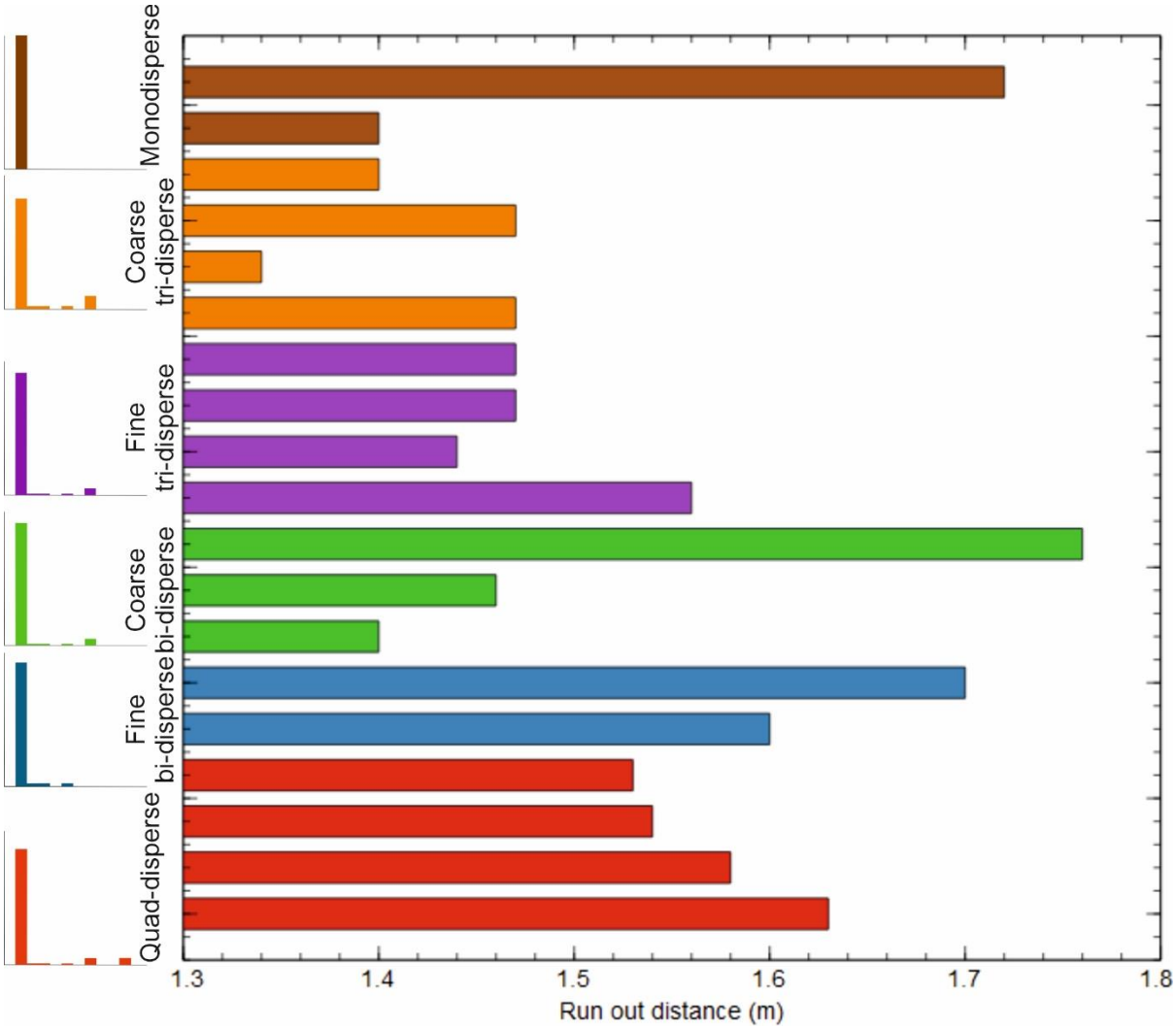

Figure 4.12: Graph comparing the run-out distance of each run by material mix. Mini plots indicate grain size distribution of mixes (colour coordinated to results), shown in full in Fig 3.1.

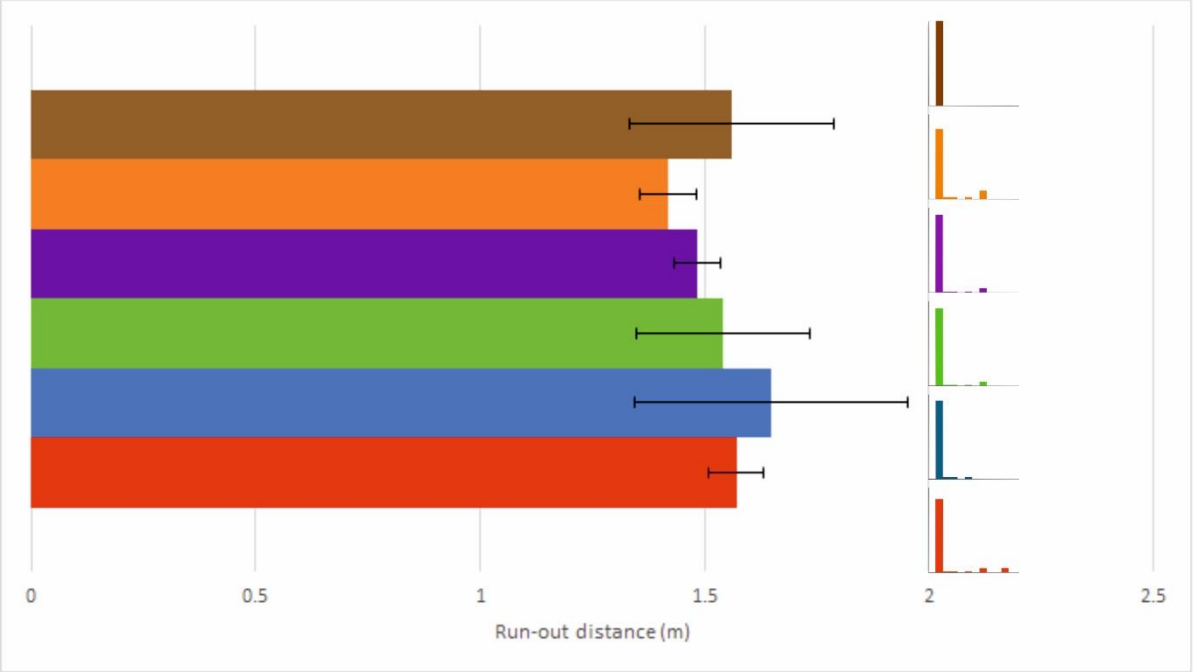

Figure 4.13: Graph showing the average run-out distance for each material mix. Error bars report n-1 standard deviation. Mini plots indicate grain size distribution of mixes (colour coordinated to results), shown in full in Fig 3.1.

Figs 4.12 and 4.13 show that in these experiments, a greater proportion of fines within the current leads to a greater run-out distance. The average run-out (Fig 4.13) for a current containing only 45-90µm is possibly being impacted by moisture in the air causing the material to be more cohesive resulting in non-homogenous fluidisation which would reduce mobility and therefore run-out.

Fig. 4.13 suggests that the average run-out distance for coarse bi-disperse currents may be increased by an anomalous value, in this case the average run-out distance of fine tri-disperse currents would be greater than for coarse bi-disperse currents which suggests that by increasing the proportion of coarser material within the current, the run-out distance is decreased.

The standard deviation was calculated using the n-1 method, using the equation:

$$\sigma = \sqrt{\frac{\sum(x-\bar{x})^2}{(n-1)}} \qquad \text{(eq. 8)}$$

The values shown in Fig 4.13 suggests that the run-out distance trends for quad-disperse, fine tri-disperse and coarse tri-disperse are significant. This supports the general trend that as the proportion of fines decreases the run-out distance decreases. The large standard deviation for fine bi-disperse currents suggests that the trends are less significant and therefore not as useful for making conclusions.

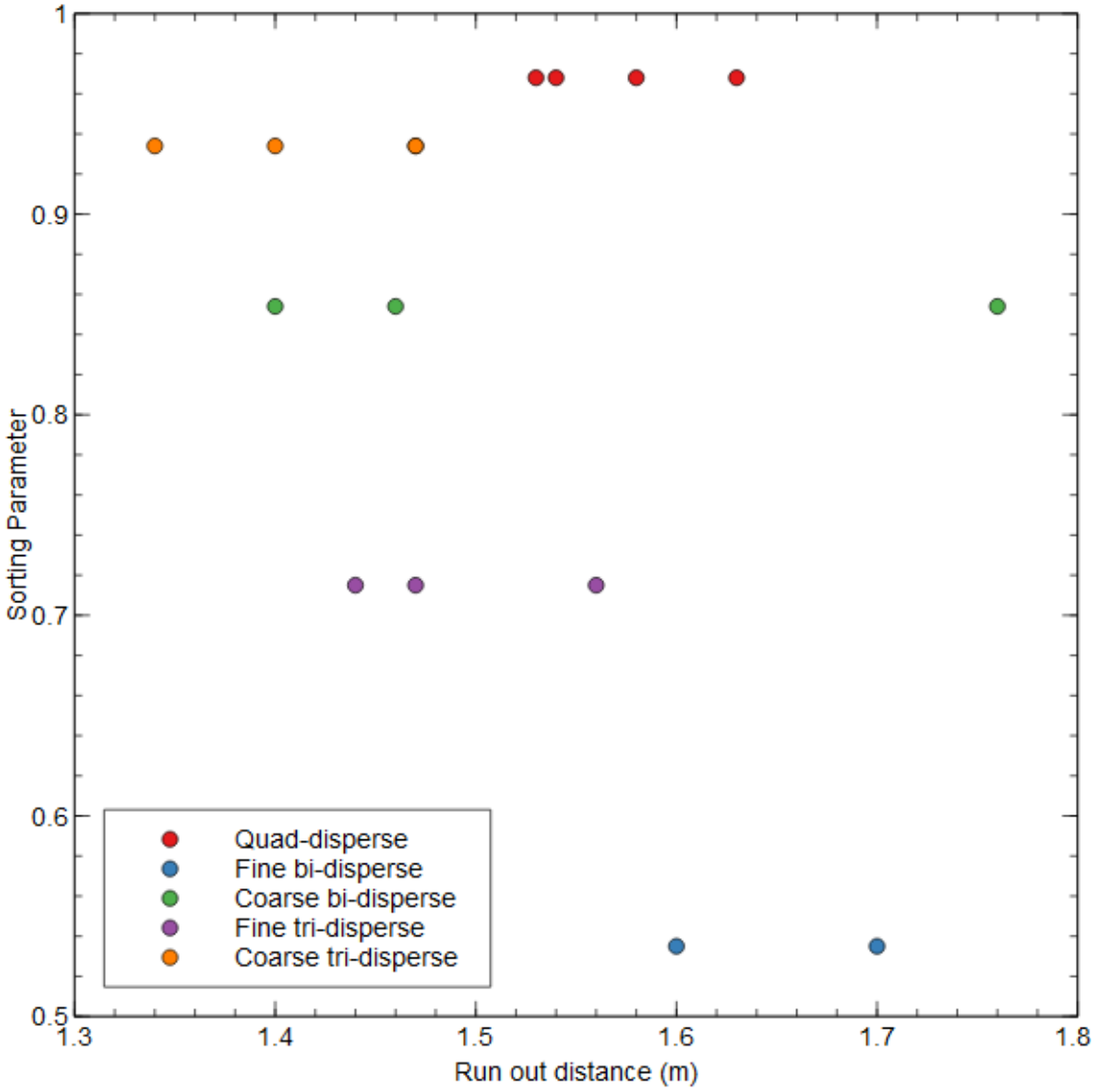

Figure 4.14: Graph showing the relationship between current sorting and run-out distance

Fig. 4.14 suggests that as the current becomes more poorly sorted the run-out distance decreased. The sorting parameter shows more clearly that while the proportion of particles that are 45-90 µm is a major controller of mobility, the size of the other particles within the current and therefore the degree of particle sorting determines the run-out distance for currents with an equal proportion of particles sized 45-90 µm.

The most poorly sorted current has greater run-out distances than some of the more well sorted currents which is suggests that sorting isn't a key factor in controlling current run-out. It is possible for poorly sorted poly-disperse currents the variations in grain size allows for more particle interactions which generate unsteadiness and cause the flow to propagate further.

By reducing the proportion of 355-510 µm even when replacing with 500-710 µm increases run-out distance, this suggests that the coarsest particles create an internally graded current which reduces friction on the finest particles allowing for a longer run out distance.

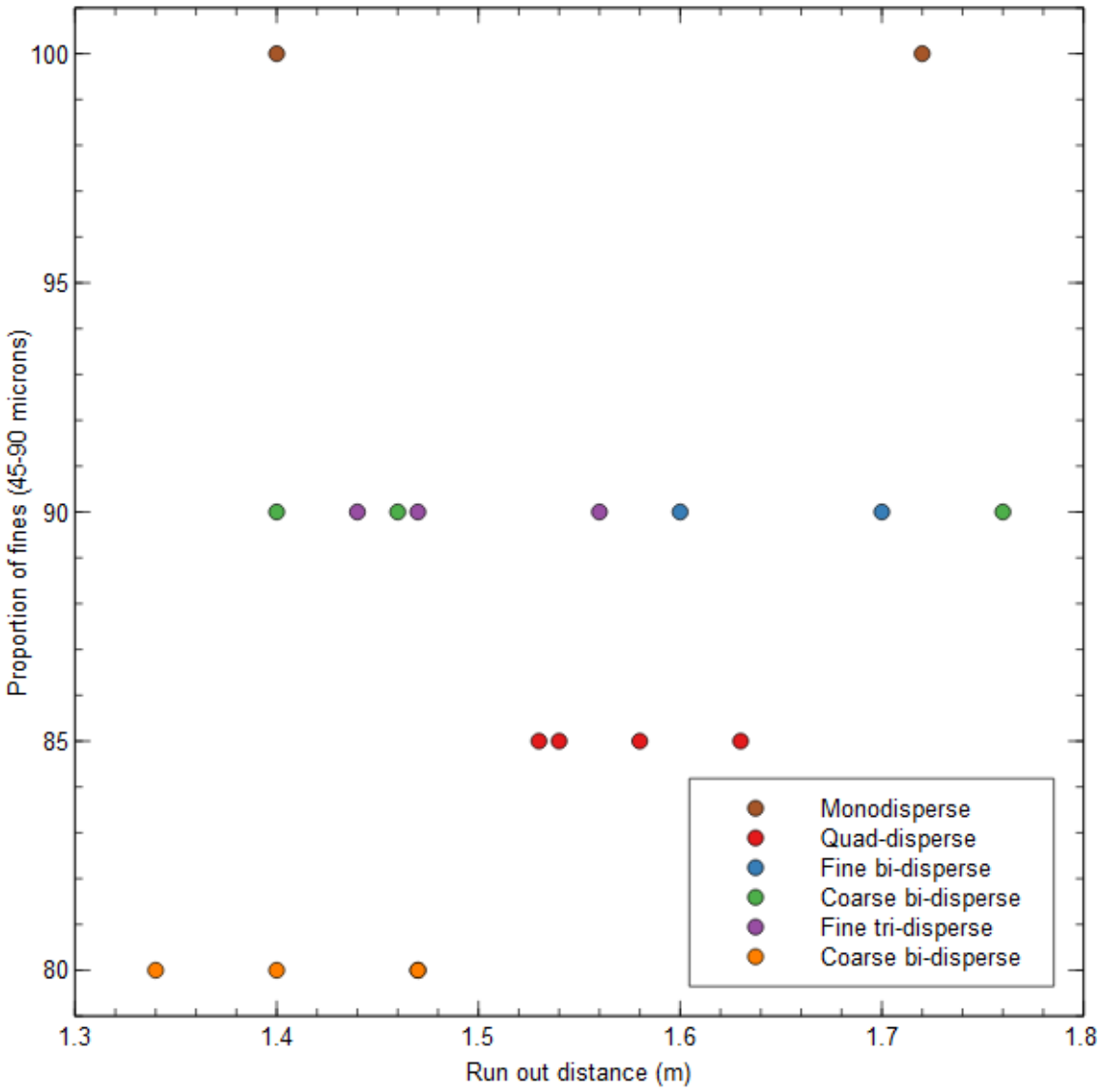

Figure 4.15: Relationship between run-out distance and percentage of fines within the experimental currents

Fig 4.15 shows that in general as the proportion of fines increases the run-out distance increases. However, the currents of 100% fines have a lower run-out than the 90% fines flows which suggests that increasing the percentage of fines alone doesn't increase run-out distance.

The decrease in run-out distance for the 100% 45-90 µm currents suggests that some coarser particles are required to cause the high mobility observed in natural PDCs. The graph in Fig. 4.15 follows a similar trend to Kokelaar et al. (2014), which suggests that the coarse particles within each current create levees which constrain the flow forcing forward propagation, like in experiments using coarser grained materials.

4.3 Flow velocities

4.3.1 Bulk velocity

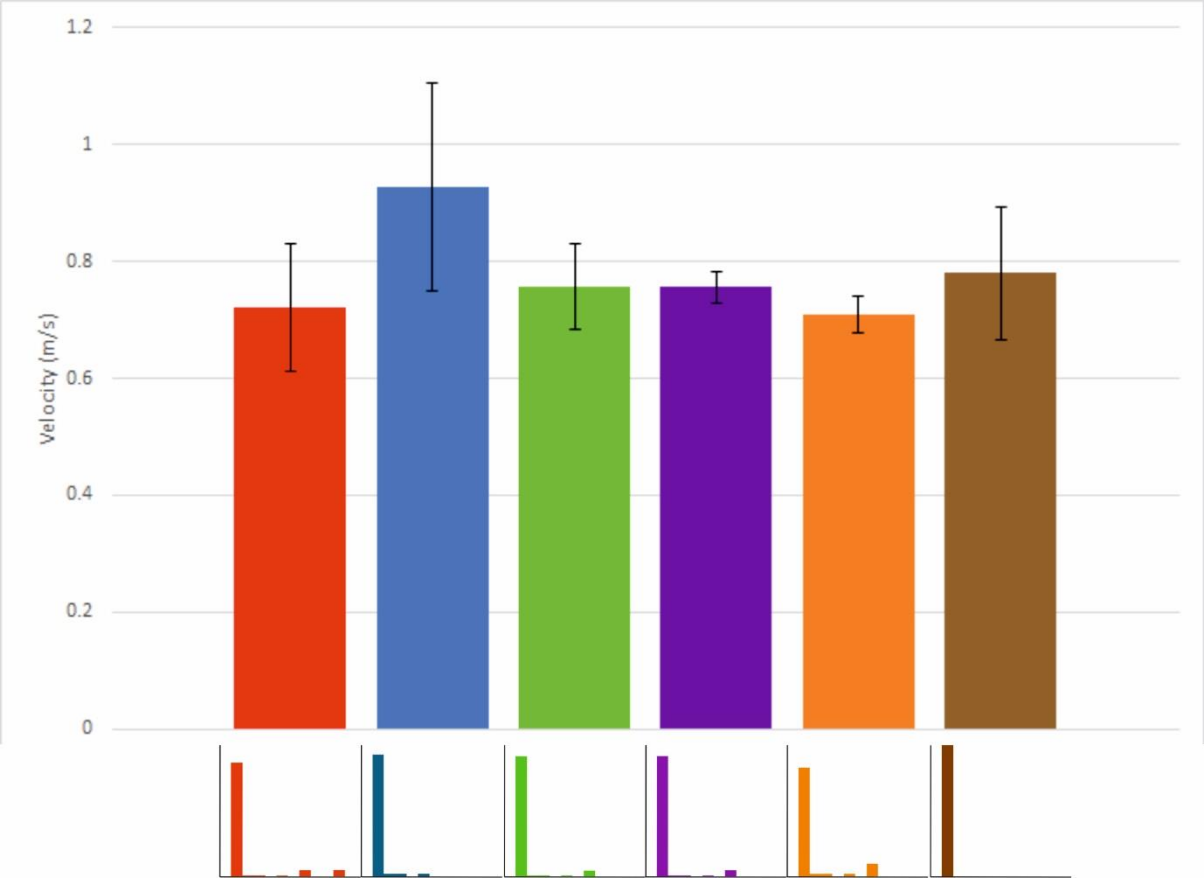

Figure 4.16: Graph showing the average velocity for each material mix with error bars for the standard deviation of the velocity for each mix. Mini plots indicate grain size distribution of mixes (colour coordinated to results), shown in full in Fig 3.1.

Figure 4.16 shows that for the average velocity of the currents by material mix, there is very little variation in bulk velocity. The high standard deviations for most of the mixes suggests that the variations in velocity observed are unreliable to make detailed observations about.

As the proportion of mid-grain sized particles increases the fine particles fill the pore spaces preventing current behaviours like percolation from occurring which then causes the velocity to reduce (Staudt et al., 2017). This suggests that the lower velocities of quad-disperse and coarse tri-disperse currents are due to the lower proportion of 45-90 µm particles which prevents the rheological controls of mobility, such as percolation and resegregation, identified in Chapter 2.

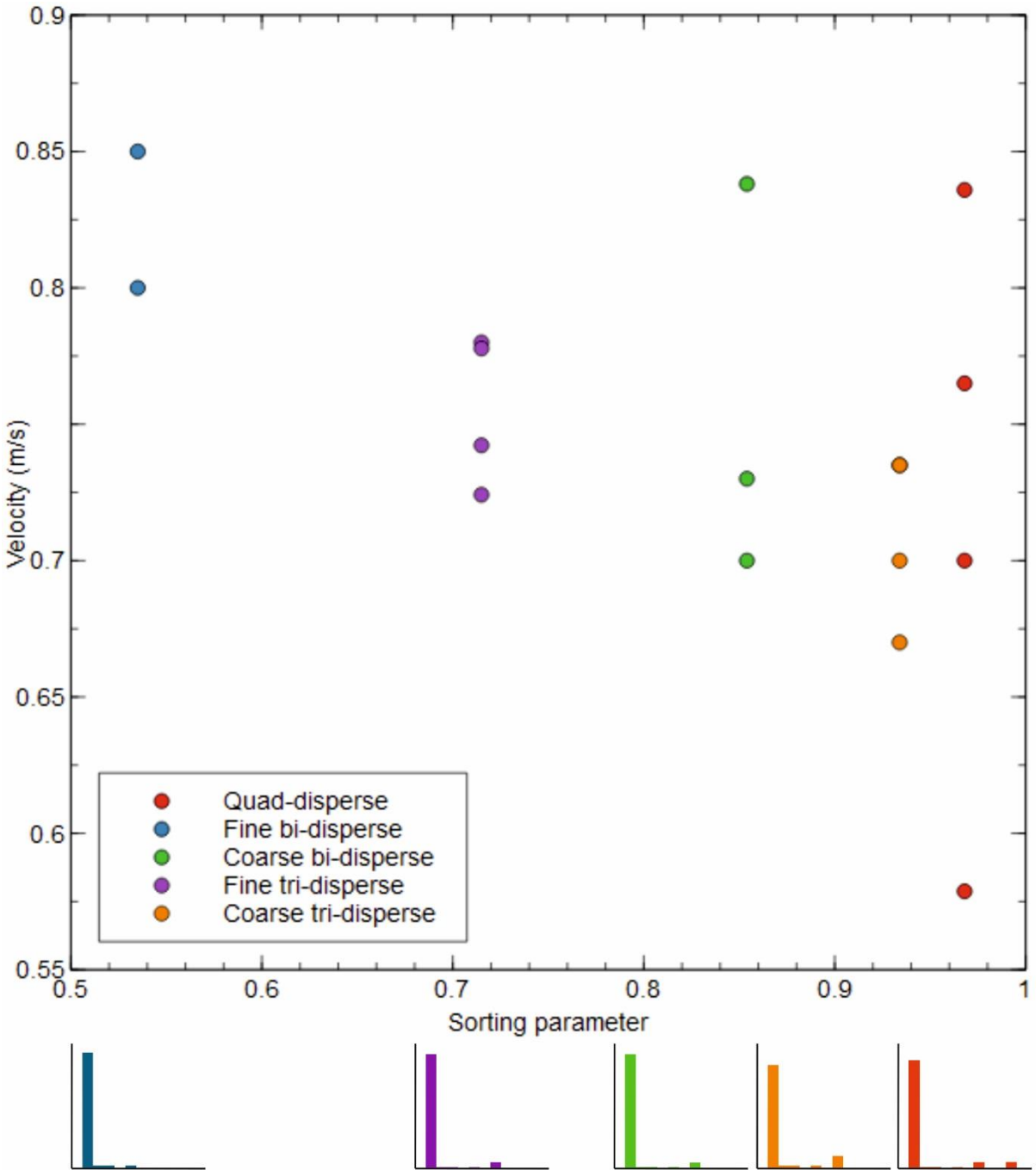

Figure 4.17: Graph showing the relationship between sorting and velocity

If we consider the highest velocity for the coarse bi-disperse currents to be anomalous a trend begins to show that as the current becomes more poorly sorted, the bulk flow velocity decreases. However, this dataset is quite unreliable as the standard deviation as shown in Fig. 4.16 is high, which means that these trends are not as robust.

Using Eqn. 3 (Chapter 2) does not answer the questions as the change in height is constant for all currents which means that the values for velocity would be constant. This equation shows that the initial fall velocity is equal and suggests that the variations in velocity occur once the material impinges on the ramp and base.

4.3.2 Velocity maps

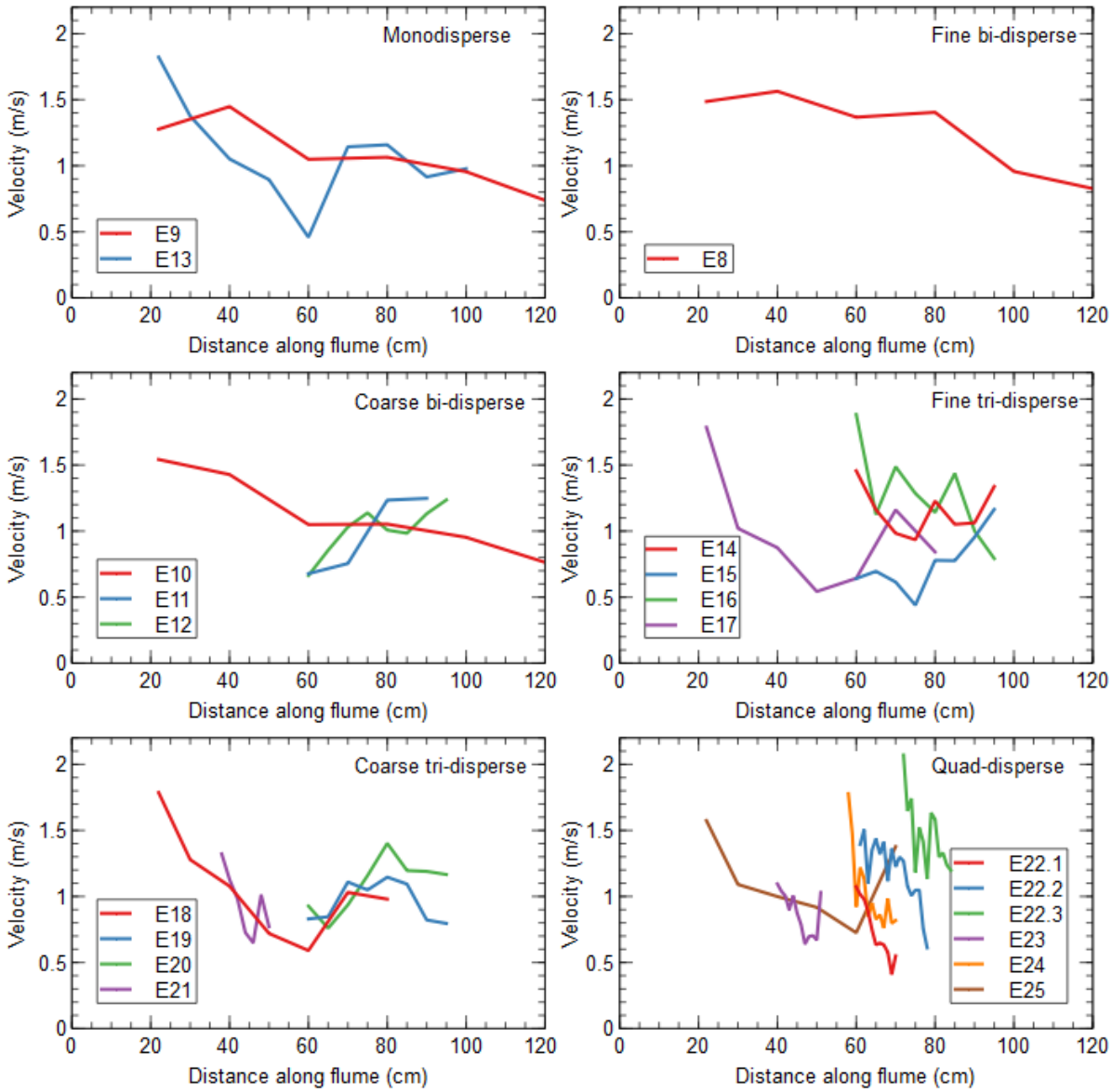

Figure 4.18: Series of graphs showing velocity against distance along the flume to create a velocity map for each current.

In the series of experiments the range of velocities for each current is consistent, which suggests that the range of velocities is controlled by the mass of the charge.

In the polydisperse currents multiple spikes in velocity are observed, this is likely caused by pulses of material which overtake the decelerating initial flow head. As the proportion of fines within the current decreases the variation in velocities along the flume increases, this suggests that increasing particle collisions and flow unsteadiness reduces the energy of the particles at the flow head leading to these drops in velocity and more energetic pulses of material overtaking the initial flow head.

The pulses observed in experiment 22 contained more coarse material within the flow, the velocity here is possibly higher due to fines filling the gaps between the coarser particles

which then reduces the angularity of the surface and therefore the impact of the surface roughness effect on the flow.

4.3.3 Flow front acceleration

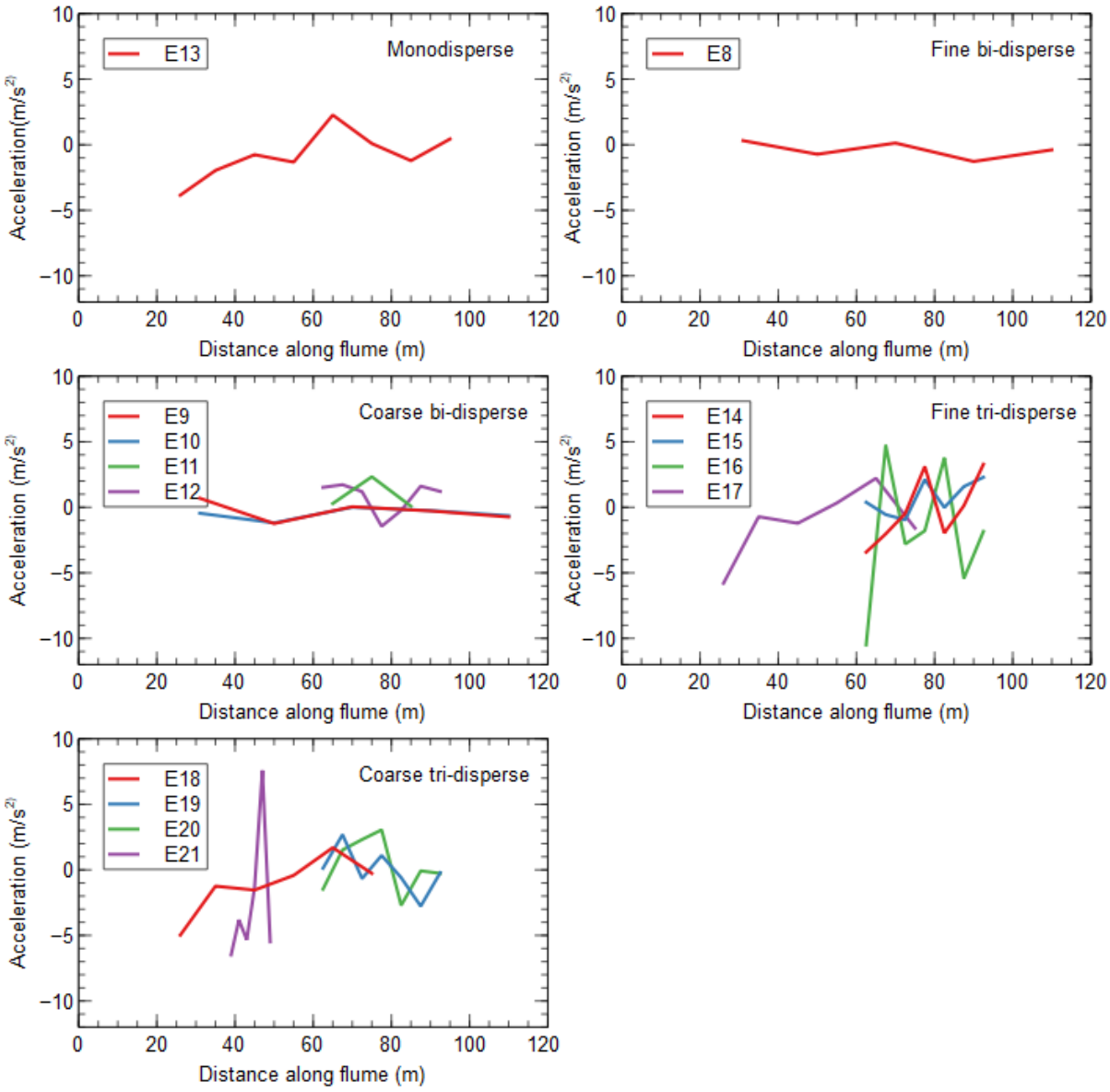

Figure 4.19: Series of graphs showing the acceleration against distance along the flume to create an acceleration map for each current. Each graph is labelled with the composition of each current as a ratio of particle sizes (45-90 µm:125-335 µm:335-500 µm:500-710 µm)

The graphs show that initially as the flow impinges on the ramp and baseplate there is a rapid deceleration. This change from fall to flow results in rapid deceleration, possibly due to interparticle collisions dominating rather than particle-air collisions which previously dominated.

In currents containing 90% 45-90 µm and 10% 125-335 µm there is very little change in acceleration, which suggests that this is a more stable current. As the range of particles sizes in a current increases, the current becomes more unstable. The monodisperse current

containing 100% 45-90 µm could have greater variations in acceleration due to a lack of coarser particles to create levees. These levees force forward propagation and prevent lateral spreading of the flow. By preventing this lateral spreading less energy is lost to lateral transport which causes forward velocity to be more consistent.

The currents with a greater range of grain sizes show greater variations in acceleration, which indicates more flow instability. This instability is possibly linked to greater collisions between different particles sizes and current sorting through percolation during the flow. This percolation leads to resegregation of the flow and an internal eddy system which could cause instability.

Cagnoli and Romano (2010) have found that in granular flows as the grain size decreases the mobility increases. Mobility increases because in fine dominated flows the number of particles contacting the surface is greater, which prevents frictional forces acting deeper into the flow allowing for the interior of the flow to travel further (Cagnoli & Romano, 2010). Finer particles also formed plugs in these experiments, which allowed for greater mobility; these can be compared to the small packages of fine material observed in the flows.

Rapid acceleration with each pulse suggests that as the previous flow head was losing energy, a new pulse of material began to overrun the flow tail. This overriding pulse incorporated material from below which increases the material percolating and allowing for a more mobile flow (Gajjar et al., 2016).

The larger variations in acceleration represent large pulses of material which allows for greater flow propagation. This suggests that the long run out distance of PDCs is caused by the instability which generates flow pulses and therefore acceleration changes.

When the deposit bed contains approximately 17% of the finest material within a current, the effect of the surface roughness effect on the overriding current is reduced. This allows for the current to accelerate as it overpasses this deposit (Staudt et al., 2017). This suggests that in flows where the initial flow head is rich in fines, the overriding pulses have a rapid acceleration due to the reduction in surface roughness effect.

5 Current Deposits

Deposits from PDCs reflect conditions at the flow boundary zone (Branney & Kokelaar, 2002), with dense granular flows able to generate bedforms (Smith et al., 2020) (see Chapter 2). This chapter will identify bedform features observed in the deposits and make interpretations about the flow boundary zone conditions during deposition. The deposits for the currents that consist entirely of 45-90 μm particles could not be used in this chapter due to the lack of visible bedforms in monodisperse deposits. Previous work has shown that monodisperse currents produce a range of shallow angled, high angle and planar bedforms similar to in this study (Smith et al., 2020). Smith et al. (2020) used dyed ballotini beads to make these observations possible.

The purpose of this chapter is to understand which behaviours in the flow boundary zone caused the deposits observed in the flume in order to relate to natural PDC deposits which then allows for better understanding of the behaviours in the flow boundary zone of natural PDCs. Using an understanding of the flow boundary zone conditions in each of the currents it is possible to interpret if variations in the range of grain sizes produced any variations in flow boundary zone conditions. Examples of each bedform have been provided within this chapter and photographs of each of the deposits can be found in Appendix V.

5.1 Bedform characterisation

The deposit from each experiment was photographed and analysed. The internal architecture of the deposit pile was assessed and classified into either massive, or four bedform types – elongate, lunate, cross stratified and asymmetrical cross stratified (Fig 5.1). This classification scheme has been developed following Schmincke et al. (1973), Cole (1991), Douillet et al. (2013) and Smith et al. (2020) and has been designed to capture the range of bedforms observed in this study.

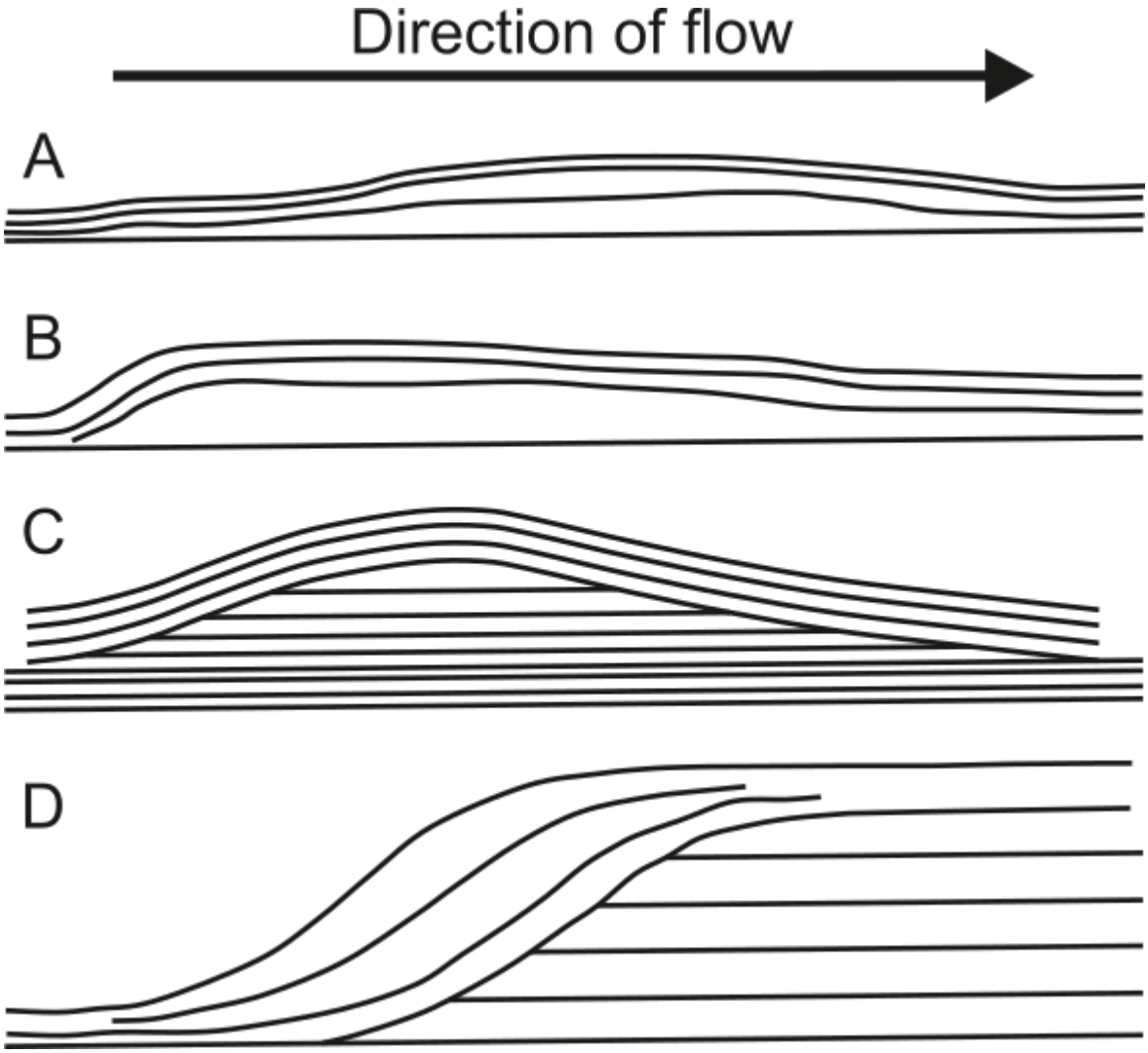

Figure 5.1: Sketches of bedforms identified in these deposits. A – Elongate, B – lunate, C – cross stratified, D – asymmetrical cross stratified

Elongate beds are sub-parallel deposits which have a very shallow lee side and slightly steeper stoss side (Fig. 5.1a), lunate beds (Fig. 5.1b) are similar to elongate beds but with a steeper stoss side deposit, cross stratified beds consist of a steepening lee side layer overlying planar deposits (Fig. 5.1c), and asymmetrical cross stratified beds consist of high angle stoss side layers with shallow angle to sub-parallel lee side layers (Fig. 5.1d). Massive deposits are present and lack any internal structure, however grading is present in some of the massive deposits.

The elongate and lunate beds are comparable to beds of the same name found in Douillet et al. (2013); and the cross stratified and asymmetrical cross stratified are comparable to the type A and D beds found in Cole (1991) respectively.

5.2 Bedforms

5.2.1 Elongate beds

The elongate bedforms are subparallel with slightly steeper lee sides (E8: 2.53°; E14: 10.4°; E24: 8.53°) than the stoss side (E8: 0.270°; E14: 0.834°; E24: 0.719°). The beds contain initial normal vertical and horizontal grading, the vertical grading later becomes reverse grading. These beds are predominantly fines rich, initially only consisting of 45-90 µm particles (Fig. 5.2), although in the more disperse currents there are elongate beds rich in coarser material (Fig. 5.3, 5.4).

The most common bedform in these experimental deposits is elongate beds. The presence of elongate beds suggests that during this period of deposition the flow had a high transport capacity and high competence, with aggradation occurring primarily on the stoss side (Douillet et al., 2013) forming long shallow backset beds.

These beds form in nearly all the deposits as prior to the development of topographic obstacles the flume is sub-parallel so the main basal deposit that can form will reflect the surface topography of the flume. Once these elongate beds have deposited the flume topography varies which can produce topographic obstacles which makes the production of bedforms such as lunate beds and asymmetrical cross stratified beds possible.

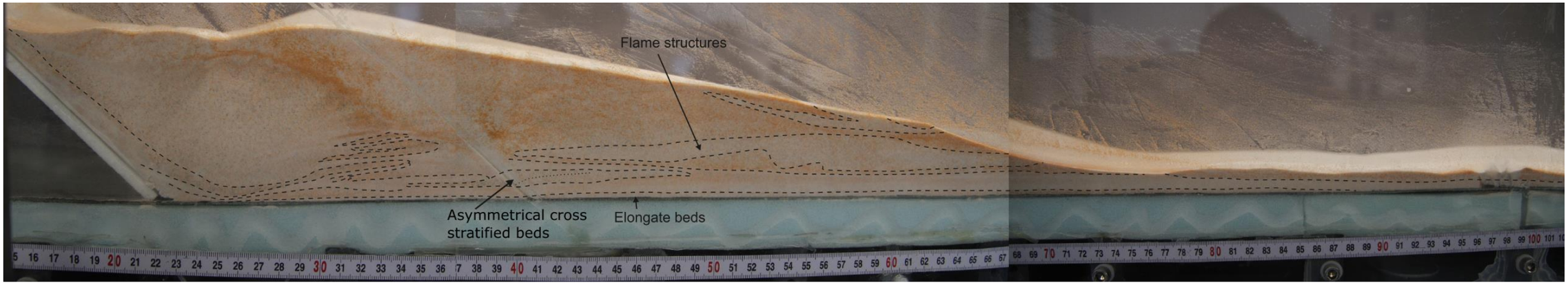

Figure 5.2: Annotated photograph of the deposit from the fine bi-disperse current showing basal fine elongate beds

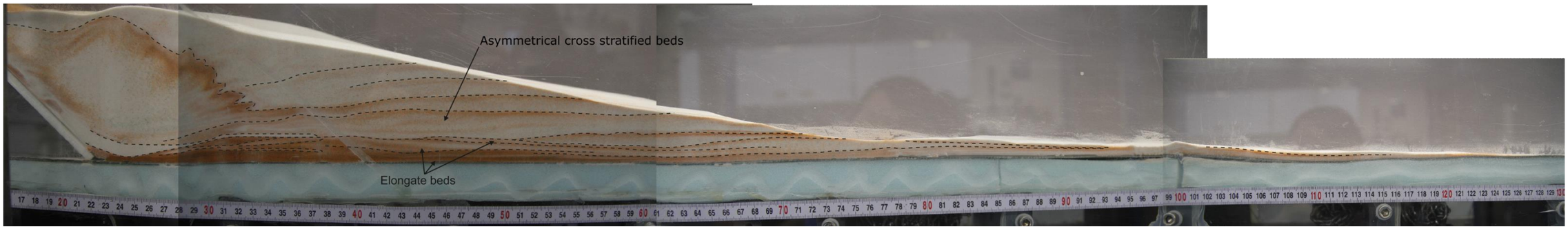

Figure 5.3: Annotated photograph of the deposit from the fine tri-disperse current showing basal coarse elongate beds

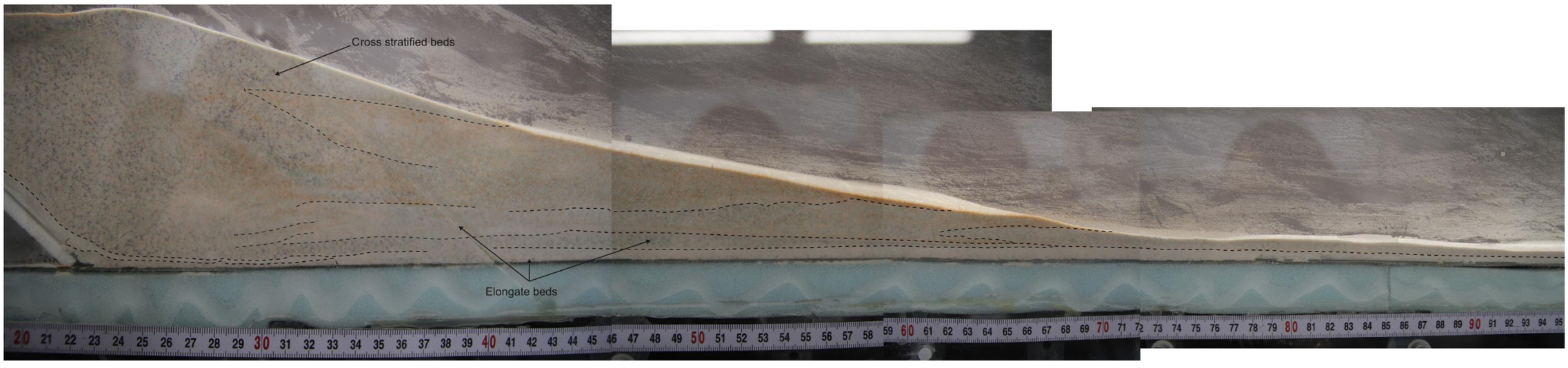

Figure 5.4: Annotated photograph of the deposit from the quad-disperse current showing basal coarse elongate beds

5.2.2 Lunate beds

The lunate beds consist of a steep (E10: 7.79°; E11; 24.1°; E20: 13.1°) lee side and shallow (E10: 1.01°; E11: 0.707°; E20: 1.16°) stoss side. The beds are 39.8 to at least 55.7 cm long and 1.04 to 1.32 cm thick and predominantly consist of the finest particles within the current.

The lunate beds indicate the number of pulses within the current, however their composition varies depending on location within the deposit. In the coarse bi-disperse currents where the lunate bedforms are the basal deposit (Fig. 5.5a) the bed is fines rich (45-90 μm) and laminations are unclear but there is slight normal vertical grading with no evidence of horizontal grading. However, there is horizontal grading in the tri-disperse currents. While when the lunate beds form higher in the deposit (Fig. 5.5b) they are richer in coarse particles and contain normal horizontal and reverse vertical grading.

The lunate beds indicate that at the time of deposition the flow was turbulent, dilute and had a low transport capacity. The number of lunate beds within the deposit indicates the number of pulses of material within the current (Douillet et al., 2013). In the deposits from the coarse bi-disperse currents (Fig. 5.5a) there are three lunate beds which suggests that formed in three pulses of material occurred; while in the second set of deposits of the coarse bi-disperse currents (Fig. 5.5b) there are two lunate beds which suggests that formed in two pulses of material occurred. By comparing to the number of pulses in the currents which formed these deposits (Chapter 4; Table 4.1) we can see for Fig 5.5a and 5.10 this interpretation is accurate as three pulses occurred in these currents and three elongate beds were deposited. However, for Fig 5.5b this interpretation is not as accurate as three pulses occurred within this current (Chapter 4; Table 4.1), it is likely that this variation is due to difficulty identifying individual beds within the deposit.

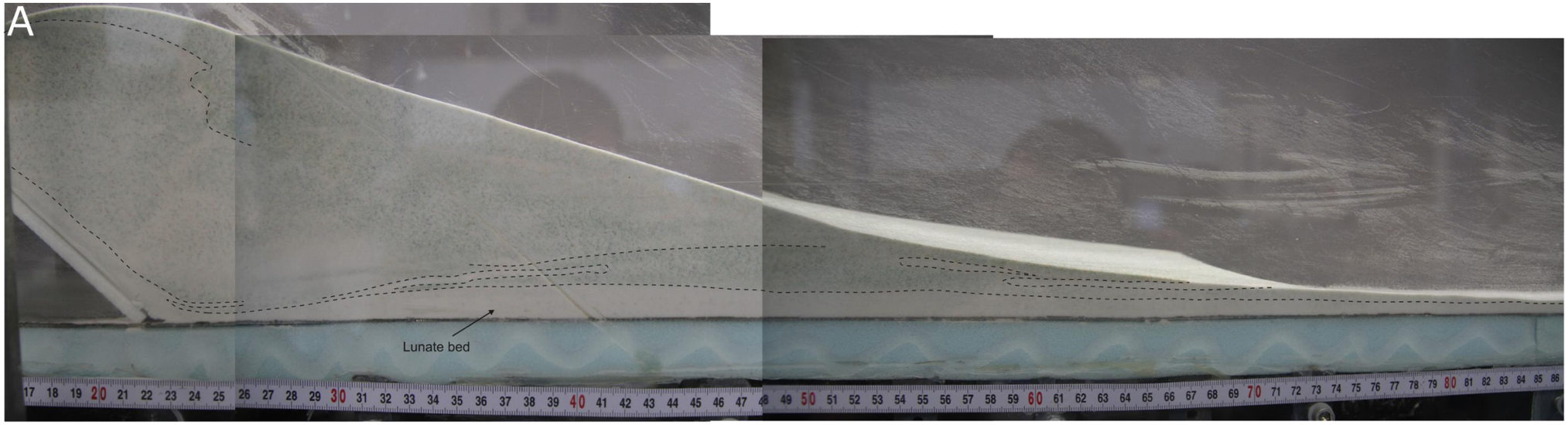

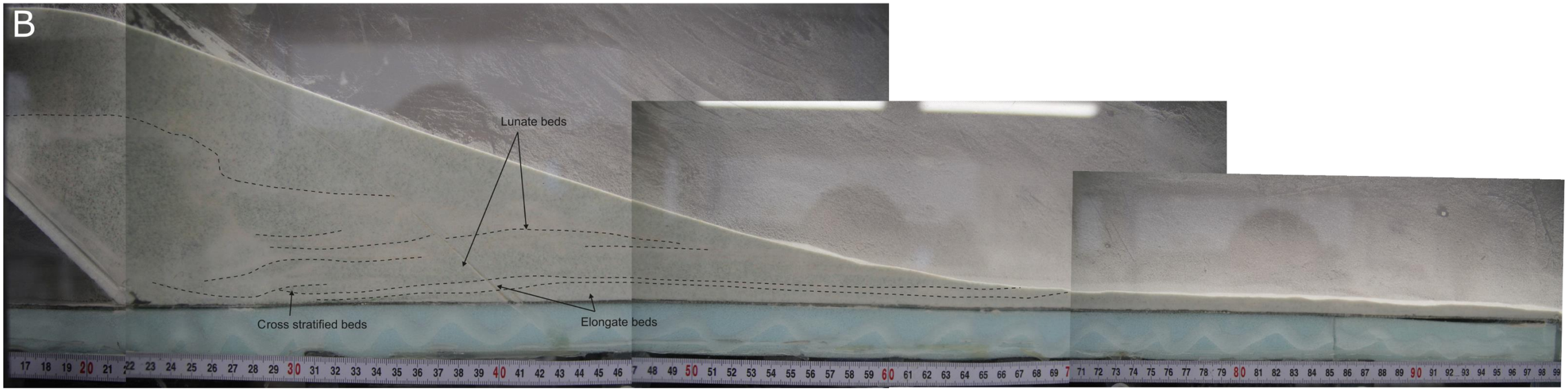

Figure 5.5: Annotated photographs of the coarse bi-disperse currents. (A) Experiment 10, showing basal lunate beds; (B) Experiment 11, showing lunate beds higher up in the deposit

5.2.3 Cross stratified beds

The cross stratified beds have a steep angled stoss side (E15: 7.17°; E17: 9.95° to 15.7°; E19: 13.0°) overlying a sub-parallel (E15: 2.68° E17: 3.64°; E19: 2.68°) deposit. The beds show reverse vertical and normal horizontal grading (Fig. 5.6). These bedforms are regressive and overlie previously deposited sub-planar elongate beds, where present these beds make up the majority of the deposit (Fig. 5.7).

The structure of these beds suggests slight reworking of material from the earlier laminations within the beds and underlying deposits (Fig. 5.8), where bedload tractional sorting causing selective entrainment of smaller particles leading to remobilisation of the 45-90 µm particles. This entrainment is due to the surface roughness effect or turbulence causing fine particles to reincorporate into the current until the turbulence is low enough to allow for deposition (Branney & Kokelaar, 2002).

The cross stratified beds show progressive aggradation occurred at this time at a lower energy than during the deposition of the asymmetrical cross stratified bedforms described below (Schmincke et al., 1973; Branney & Kokelaar, 2002). The cross stratified beds deposited when the current was travelling at 0.86 and 1.75 ms^{-1} while the asymmetrical cross stratified beds deposited when the current was traveling at 1.35 and 1.37 ms^{-1}. This suggests that the previous interpretation of Schmincke et al. (1973) aren't entirely correct as some cross stratified beds are forming at a higher energy than the asymmetrical cross stratified beds.

The deposition occurred in a traction-dominated flow boundary zone, which indicates high rates of shear within the flow and low current concentration resulting in few inter-particle collisions; with bedforms forming from interactions between the current and underlying deposits, which causes grading from planar beds to cross stratification (Branney & Kokelaar, 2002). However, as these experimental currents are dense granular currents it is likely that the deposition occurred in a granular flow dominated flow boundary zone.

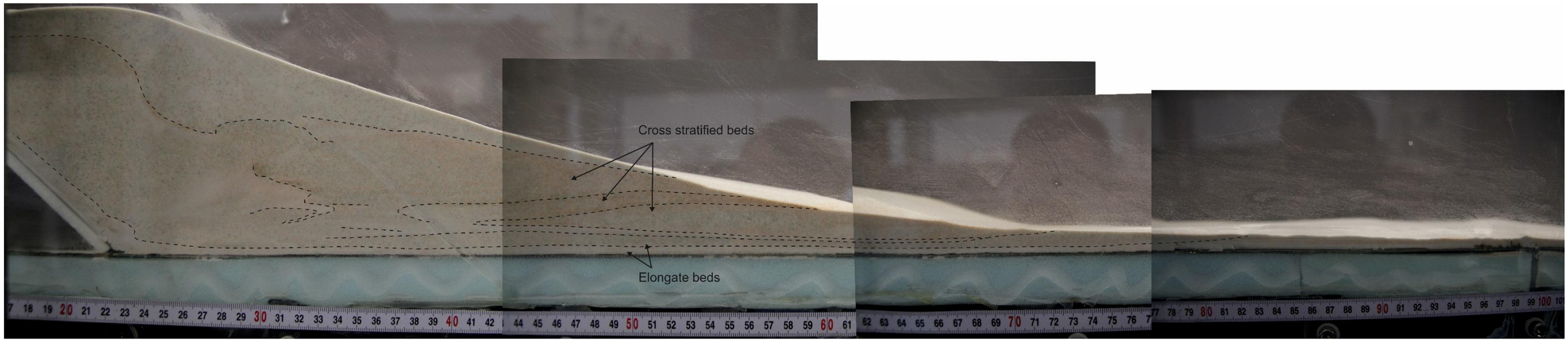

Figure 5.6: Annotated photograph showing the deposit from the fine tri-disperse current showing cross stratified beds

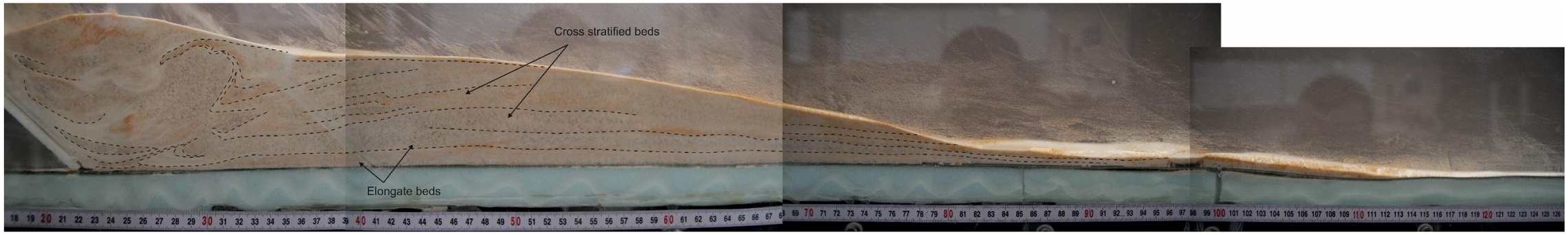

Figure 5.7: Annotated photograph of the coarse tri-disperse current showing cross stratified beds making up most of the deposit

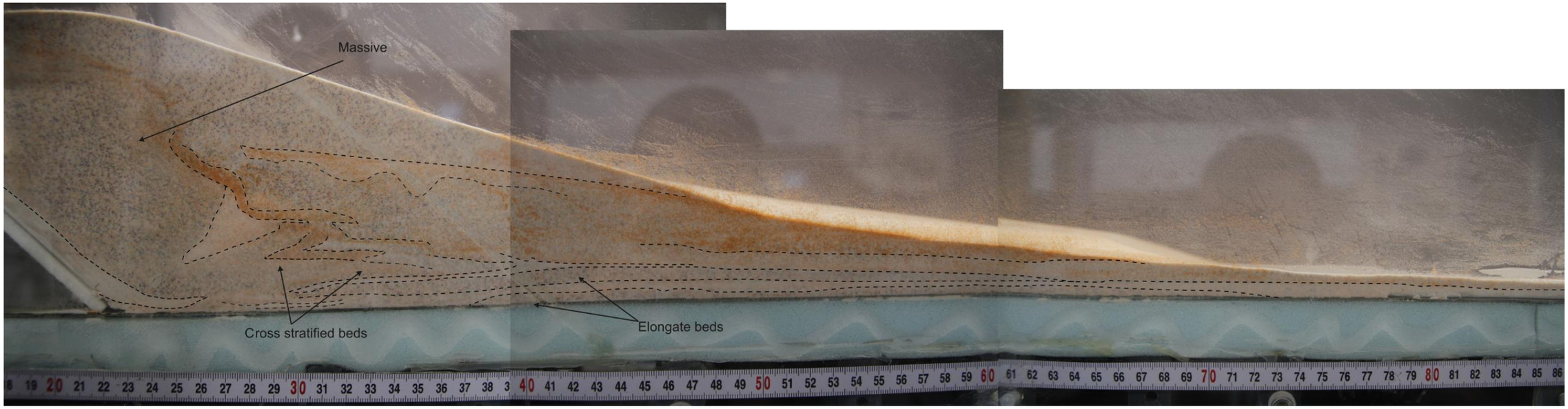

Figure 5.8: Annotated photograph of the deposit from the coarse tri-disperse current showing reverse graded cross stratified beds

5.2.4 Asymmetrical cross stratified beds

The asymmetrical cross stratified beds show a range of angles with lee side deposits ranging from 24.5° to 13.8° and stoss side deposits at an 0.363° to 1.32° angle. These bedforms are 13.7 (E8) to 26.2 (E14) cm long and 0.793 (E8) to 1.19 (E14) cm thick.

The asymmetrical cross stratified beds show very strong normal horizontal grading (Fig. 5.3) and reverse grading within each lamination (Fig. 5.2, 5.3). However, in the coarser currents the laminations are less clear (Fig. 5.9) while grading is still present within the laminations.

The asymmetrical cross stratified beds are interpreted as forming in a high energy environment, where after the flow passes along the chute a hydraulic jump occurs (Schmincke et al., 1973). These beds primarily deposit on the stoss side of previously deposited bedforms, with slight deposition on the lee side of the dune typically horizontal due to the previous bedform. As this current is a dry granular flow rather than a fluvial system the change in flow behaviour occurs as the result of a granular jump (Branney & Kokelaar, 2002).

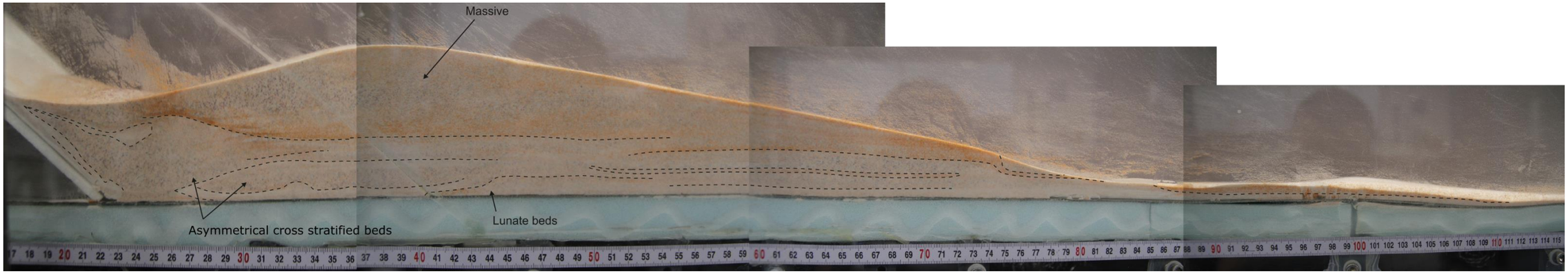

Figure 5.9: Annotated photograph of the deposit from the coarse tri-disperse current with poorly laminated asymmetrical cross stratified beds

5.2.5 Massive deposits

The massive deposits vary across the currents with grading present in some deposits. In massive deposits which consisted predominantly of the finest material (45-90 μm) (Fig. 5.2, 5.9) or the coarsest material (Fig. 5.8, 5.10) there was no grading present in the deposit. While in deposits consisting of a range of grain sizes with no clear primary grain size, there was variations, with some deposits showing no grading (Fig. 5.5, 5.6, 5.9, 5.8) and others showing reverse vertical and normal horizontal grading (Fig. 5.12).

The massive deposits suggest that deposition occurred in a quasi-steady current with a fluid escape dominated flow boundary zone rather than a tractional shear dominated flow boundary zone. The presence of the finest material (45-90 μm) indicates that while the flow boundary zone is characterised by fluid escape, the amount of elutriation was insufficient to remove all the fine particles, which could have remained due to particle agglomeration (Branney & Kokelaar, 2002). As in the experimental currents there was no moisture or temperature input it is likely that the cohesion was due to interparticle forces or ambient moisture.

While most of the massive deposits were deposited from the flow boundary zone, some deposited due to the fall out of fine particles from the suspended overriding cloud. Here the deposition occurred due to a reduction in energy resulting in the overriding cloud being unable to support the particles or some of the particles agglomerated and the flow did not have the energy required to transport particles of that size; as the overriding cloud continued to propagate it is likely that deposition from fall out occurred as a combination of the two with a gradual reduction in energy.

Figure 5.10: Annotated photograph of the deposit from the quad-disperse current showing an ungraded massive deposit of coarse material

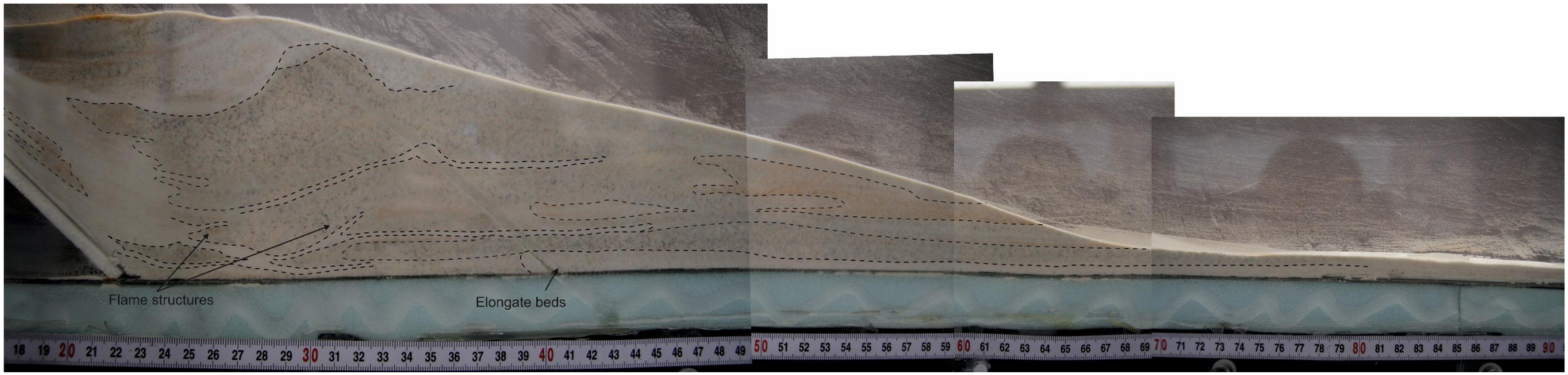

Figure 5.11: Annotated photograph of the deposit from the quad-disperse current showing a graded massive deposit

5.2.6 Flame structures

Flame structures are interpreted as forming when larger particles are deposited above the fine surface deposit. The deposit develops and degasses, allowing the deposit to collapse with the overlying coarse particles sinking filling voids. This sinking is stopped by the increasing yield strength with depth during degassing which produces lobes of coarser material within the fine beds (Fig 5.12) (Branney & Kokelaar, 2002). In some deposits the finest particles have been remobilized within the overlying flow (Fig. 5.7, 5.10). These flame structures likely formed due to loading as shown in Fig 5.12, as the coarser overlying layer pushed into the fine layer below creating tongues of fine material.

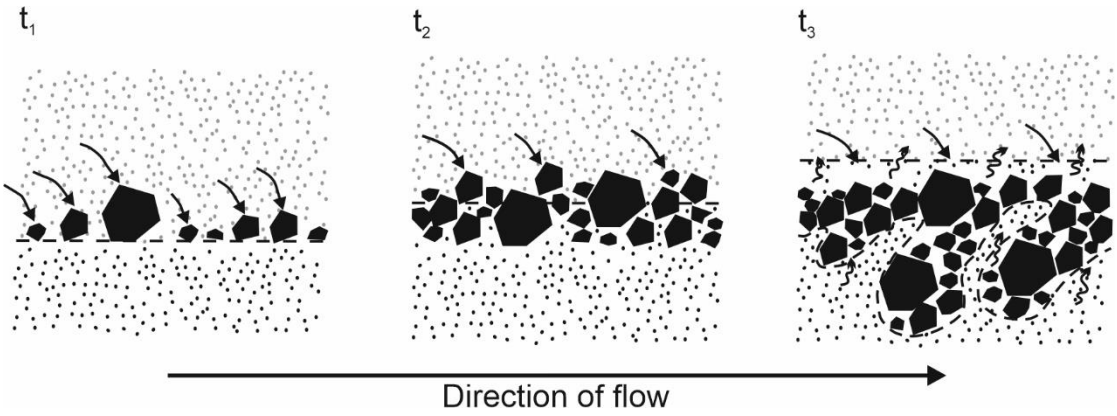

Figure 5.12: Sketch showing how coarser particles deposited over previously deposited fines can sink. Straight lines show particle movement and squiggled arrows show degassing (Adapted from (Branney & Kokelaar, 2002))

Flame structures are created by shearing flow across an existing deposit, similar to the development of Kelvin-Helmholz instabilities (Rowley et al., 2011). In other deposits, coarser particles have been remobilized within the faster fines rich overlying flow (Fig. 5.2, 5.10). As the fine layer is unlikely to be able to produce load structures into the coarse layer below these structures are possibly related to Kelvin-Helmholz instabilities. The Kelvin-Helmholz instabilities suggest that shear instabilities are causing the reincorporation of the coarse deposit temporarily into the flow allowing these structures to generate.

5.2.7 Grading

The normal vertical grading shows that deposition occurred as part of a waning unsteady current, this waning means that the current does not have the capacity to carry larger particles resulting in their deposition. This grading may also suggest an increase in the rate of shear in the flow boundary zone which leads to greater granular segregation. By increasing granular segregation selective filtering of particles occurs which leads to percolation of fine particles (Branney & Kokelaar, 2002). However, in the deposits there is normal grading in the initial deposits from the current when the current will have been waxing, this suggests that the presence of normal grading cannot necessarily be used to interpret the current conditions. This normal grading may occur in a waxing current where the energy is growing but the current is not energetic enough to carry the coarsest particles resulting in their deposition. The lateral normal grading shows that the fine particles (45-90 µm and 125-250 µm) had a greater run-out distance than the coarser particles, this is possibly due to reducing

energy in the current resulting in a lower carrying capacity meaning that the larger particles cannot travel as far.

Inverse grading suggests that deposition occurred as part of a waxing unsteady current, which means that the current has the capacity to transport larger particles for a greater distance. Another possibility is that as the current is unsteady the shear rate changes as the flow propagates, by reducing the shear rate the larger particles are able to segregate downwards towards the flow boundary zone and deposit later than previous fines (Fig 5.13). It is also possible that because the larger clasts travel slower than the larger clasts they arrive at the same location as the previously deposited fines later and therefore deposit in an inverse graded deposit (Branney & Kokelaar, 2002).

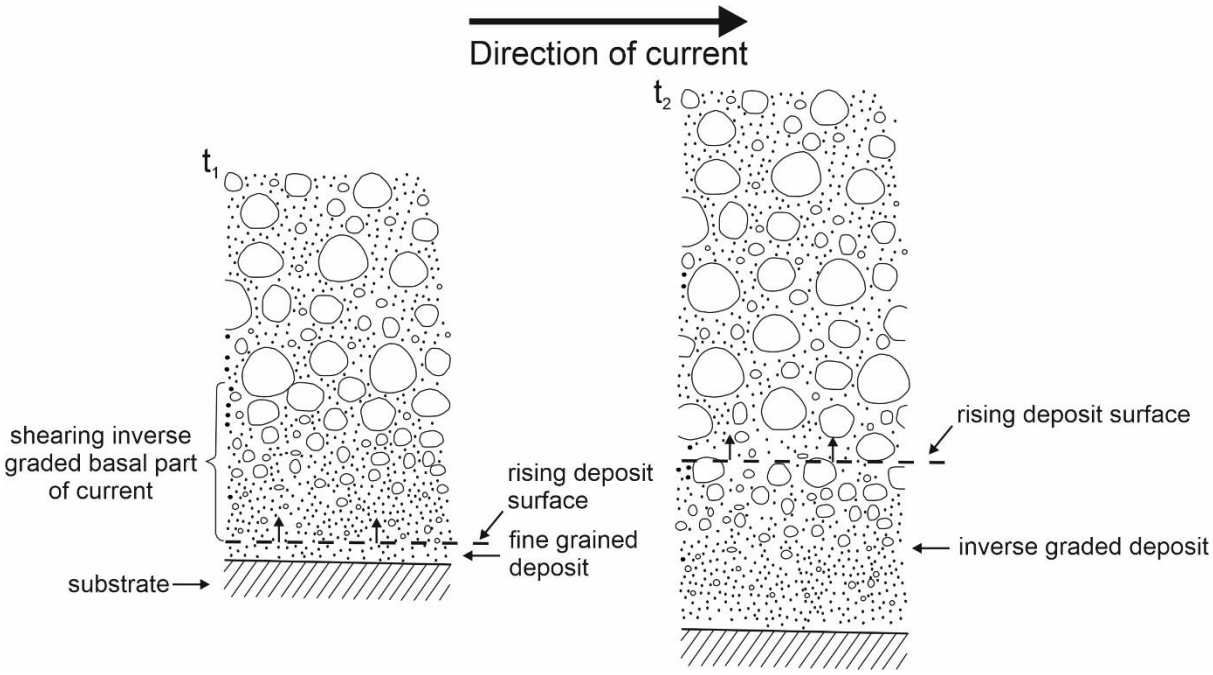

Figure 5.13: Sketch showing the deposition of an inverse graded deposit in a granular fluid-based PDC. At time t_1 the high shear prevents the large particles from descending within the current, while fine particles percolate downwards and deposit. At time t_2, the shear rate has changed due to unsteadiness within the current leading to the larger particles descending within the current to the flow boundary zone where deposition occurs (Branney & Kokelaar, 2002)

5.3 Discussion

Table 5.1 indicates which of the bedforms were present in each of the deposits from the currents. By comparing the bedforms present in different currents it is possible to see how the flow boundary zone changed with varying proportions of fines.

Table 5.1: Table showing bedform features which are present in each deposit

	Elongate	Lunate	Cross stratified	asymmetrical cross stratified	Massive	Reverse grading	Normal grading	Flame structures
Fine bi-disperse	✓			✓	✓	✓		✓
Coarse bi-disperse		✓			✓			
	✓	✓	✓		✓	V	H	
	✓				✓	V	H	✓
Fine tri-disperse	✓			✓	✓	asymmetrical cross stratified	elongate	✓
	✓		✓		✓		✓	✓
	✓		✓		✓	✓		
	✓		✓		✓	cross stratified		
Coarse tri-disperse	✓		✓		✓	V	H	✓
	✓		✓			✓		✓
		✓		✓	✓	V	H	✓
	✓		✓		✓	V	H	✓
Quad-disperse	✓				✓		✓	✓
	✓				✓	V	H	✓
	✓		✓			2^{ND} + V	1^{ST} + L	✓
	✓				✓	V (distal H)	H	

In all the deposits the horizontal grading is normal, which suggests that the currents had a high transport capacity for the fines (45-90 μm) allowing them to have the largest run-out distance of any particle. And most vertical grading is reverse grading, which suggests that the currents were unsteady and waxing, with a high transport capacity (Branney & Kokelaar, 2002). It is also possible that the reverse grading suggests a waning flow where the carrying capacity is reduced. This means that the coarser particles are deposited earlier in the current resulting in a later fines-rich deposit.

The deposits from fine bi-disperse currents contain basal deposits of elongate beds which suggests that initial deposition occurred when the flow had a high transport capacity and high competence (Douillet et al., 2013) this suggests at this point the current was waxing. Later deposition formed asymmetrical cross stratified beds suggests that deposition was still occurring in a high energy environment with the underlying beds producing a barrier allowing for the formation of these bedforms. The presence of flame structures in this deposit suggests that there was high shear in the flow boundary zone, which allowed for the reincorporation of fines into the flow.

The deposits from coarse bi-disperse currents contain basal deposits of elongate beds which suggests that initial deposition occurred when the flow had a high transport capacity and high competence (Douillet et al., 2013) this suggests at this point the current was waxing. The presence of lunate beds suggests that the transport capacity of the flow reduced and therefore much thicker beds could be deposited then the thin underlying elongate beds. The presence of overlying massive deposits suggests that as the current propagated, the current became steady, and the flow boundary zone conditions changed from shear dominated, either tractional or granular flow dominated, to fluid escape dominated.

The deposits from both the fine and coarse tri-disperse currents contain basal deposits of elongate beds. The elongate beds suggest that initial deposition occurred when the flow had a high transport capacity and high competence (Douillet et al., 2013), which suggests at this point the current was waxing. However, the presence of normal grading in the elongate beds suggests either a waxing or waning unsteady current (Branney & Kokelaar, 2002), so it is possible that the current conditions varied as the bedforms grew. The overlying cross stratified beds suggest that the energy in the flow reduced and the flow boundary zone at this time was traction dominated with a high rate of shear and low concentration within the current (Branney & Kokelaar, 2002). However, as these currents are dense rather than dilute the flow boundary zone would be dominated by granular flow. As these cross stratified beds are reverse graded the current was still unsteady and waxing at this time with a high transport capacity, suggesting only a slight reduction in energy (Branney & Kokelaar, 2002). The presence of overlying massive deposits suggests that as the current propagated, the current became steady, and the flow boundary zone conditions changed from granular flow dominated to fluid escape dominated.

The deposits from quad-disperse currents contain basal deposits of elongate beds which suggests that initial deposition occurred when the flow had a high transport capacity and high competence (Douillet et al., 2013) this suggests at this point the current was waxing. The presence of overlying massive deposits suggests that as the current propagated, the current

became steady, and the flow boundary zone conditions changed from shear dominated, either tractional or granular flow dominated, to fluid escape dominated.

6 Discussion

This project aimed to investigate the relationship between the range of grain sizes in PDCs and the mobility of these currents, especially with regards to the run-out distance and velocity. Additionally, it aimed to investigate how the range of grain sizes became structured within the deposits of PDCs.

This study expands on the theory of Sparks (1976) that the high mobility of PDCs is due to the fluidisation of fines within the current. Sparks (1976) suggested that the proportion of fines within the current impacts the mobility of PDCs causing greater velocities and run-outs. This has previously been examined on mono-disperse and bi-disperse currents (Savage & Lun, 1988; Chedeville & Roche, 2014; Rowley et al., 2014; Smith et al., 2018, 2020), but work on poly-disperse currents has been limited.

The deposition of ignimbrites was classically believed to occur *en masse* from dense or dilute currents (Sparks, 1976), with dense currents producing massive deposits and dilute PDCs (previously known as "surges") producing deposits containing bedforms. Later work by Branney and Kokelaar (1992, 2002) suggested that ignimbrite deposition can be progressive, where material gradually deposits, or stepwise, where packages within the current deposit. Work by Smith et al. (2020) has shown that dense granular currents can produce bedforms, such as backset beds, previously thought to indicate dilute currents (Cas & Wright, 1987; Cole, 1991; Douillet et al., 2013). This study, like that of Smith et al. (2020), shows that dense granular currents can produce bedforms previously thought to be indicative of dilute currents.

In Chapters 4 and 5 of this thesis, flow behaviours were identified using current descriptions to describe common behaviours and variations with grain size, and currents were quantitatively compared in terms of run-out distance, velocity, and acceleration. The deposits were then classified by bedforms present before interpretations of flow boundary zone conditions were made.

In this chapter, themes emerging from the results chapters will be discussed and the application of these findings to our interpretation of ignimbrites and natural PDC behaviours will be evaluated. This chapter will focus on the impact of grain size distribution on mobility, comparing the experimental deposits of Chapter 5 with natural ignimbrites, comparing the current behaviours in Chapter 4 with other analogue experiments, the limitations of the experimental set up used, and potential future work based on this research.

6.1 How does grain size distribution impact current mobility?

6.1.1 Run-out and grain size distribution

Pyroclastic density currents are known to be highly mobile, which can lead to high run-out distances and velocities (Lube et al., 2007; Rowley et al., 2014; Dufek, 2016). This mobility is often attributed to material properties. For example, the fine fraction is likely a key element in current mobility; Sparks (1976) proposed that PDCs are to some extent lubricated by the fine fraction (<125 μm) within the current, where fluidisation of the fines reduces the yield strength of the current. The presence of the fine fraction within the current also means that pore pressure is increased, which reduces the rate of pore pressure diffusion. This means that

the current is able to remain fluidised for longer and therefore be more mobile increasing the potential run-out (Dufek & Manga, 2008; Roche et al., 2010).

The relationship between run-out distance and fines was tested in this study. When run-out distance is plotted against proportion of fines (45-90 μm) in the current, a weak relationship is apparent (Fig 4.15). As the proportion of fines increases from 80% to 90%, run-out distance increases from 1.34 to 1.78 m (32.8% increase). However, the high variation in run-out distances for different currents that contained 90% fines suggests that fines content alone is not controlling run-out distance.

When run-out distance is plotted against the sorting parameter (Method of moments; Chapter 3), a clearer trend appears (Fig 4.13). Typically, the better sorted the original current, the further the run-out distance. This is possibly due to weaker frictional forces and fewer interparticle interactions; better sorted currents have fewer inter-particle collisions because there is less potential for sorting to occur. Sorting effects such as percolation and diffusion involve inter-particle collisions and contacts which increases the inter-particle friction. Percolation causes smaller particles fill voids between larger particles, increasing the contact between particles; and diffusion involves inter-particle collisions which cause the downward movement of fine particles (Vallance & Savage, 2000). In the better sorted currents, more gravitational potential energy from release from the hopper is converted to horizontal kinetic energy rather than lost through these collisions, which means that the flow is more energetic allowing for longer run-out (Bernard et al., 2014; Roche et al., 2021).

The most poorly sorted current has a greater run-out distance than some better sorted currents. This is possibly because the gas fluidisation provides a high pore pressure which reduces the internal friction (Roche et al., 2004). In the more poorly sorted currents, there is a greater difference in the maximum and minimum grain sizes (maximum of 710 μm and minimum of 45 μm). By applying the equation of Sohn and Chough (1993) (Section 6.1.5) these ranges are above the threshold for percolation to occur ($d_s/d_L < 0.25$), and therefore sorting would be expected to happen more readily. Through percolation this sorting then creates a fines rich base, observed in experiments 15 and 17 (Chapter 4) whereby the basal friction is reduced allowing for a greater run-out distance (Dade & Huppert, 1996). However, in experiment 14 (Chapter 4) the basal layer is predominantly coarse particles and the upper layer is fines rich, this suggests that in this instance the gas fluidisation prevents percolation occurring as expected.

These trends suggest that in general the reduction of friction due to less inter-particle interactions is the dominant control over run-out distance. However, the increase in run-out for the most poorly sorted indicates that percolation and other sorting effects are key to this reduction in friction; it is likely that percolation becomes a major control over run-out distance for the most poorly sorted currents.

6.1.2 Velocity and grain size distribution

This study investigated how grain size distribution is related to velocity as a variable of mobility. In the results from this study there is a linear relationship between the velocity and sorting parameter (Fig. 4.17), where the more poorly sorted currents have a lower velocity. The flow front velocity of the currents shows similar trends to the run-out distance, in that

there is a weak relationship between the proportion of fines and the bulk velocity. This likely has the same cause as the run-out, with fewer interparticle collisions meaning that more gravitational potential energy from the fall is converted to horizontal kinetic energy rather than lost through these collisions. Also, reducing the inter-particle collisions reduces the friction within the current allowing for a higher velocity in the current. This is because the reduction of frictional forces within a current is associated with a high gas pore pressure (Druitt et al., 2007; Roche et al., 2008) and this has been identified by Smith et al. (2018) as controlling the flow velocity.

The flow front velocity along the flume indicates that all currents produced in this study were non-uniform with lateral variations in velocity. Fig 4.18 illustrates that in all the currents the velocity varies as the flow propagates. The more poorly sorted currents have greater lateral variations in velocity than the less poorly sorted currents, displaying greater non-uniformity. The fine tri-disperse current is less poorly sorted than the coarse bi-disperse current and shows greater non-uniformity, suggesting that the grain size range is a more important factor in controlling the degree of uniformity within the current than the initial sorting of the current.

The high flow velocities at the base of the current are likely a result of the enrichment of fine particles which causes a reduction in effective surface roughness and frictional energy losses (Fig. 6.1). This has been observed in non-fluidized granular currents where fine particles (150-250 μm and 300-425 μm) were released over a substrate of coarse particles (0.75-1 mm) (Kokelaar et al., 2014), and particles (5 mm and 14 mm) were placed on a moving belt to simulate continual current propagation (Gajjar et al., 2016).

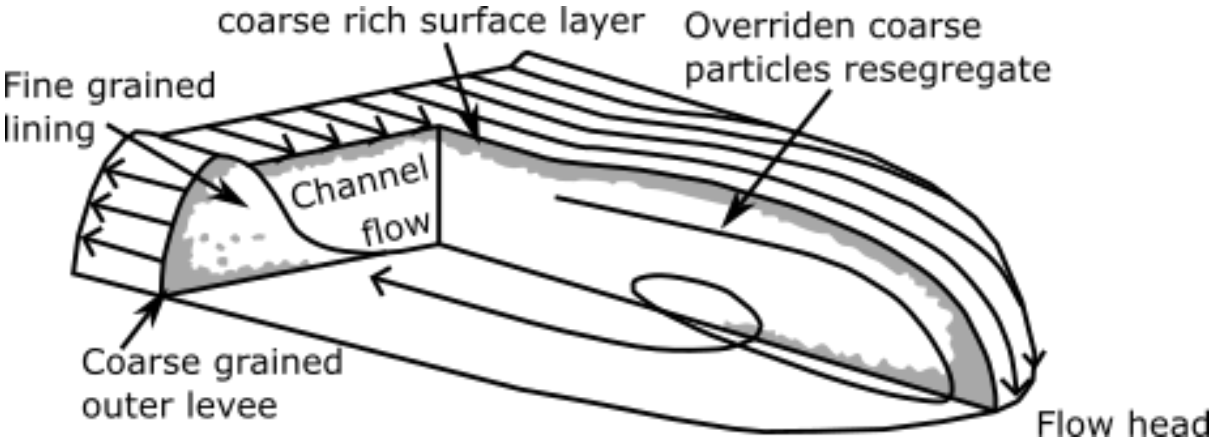

Figure 6.1: Diagram showing the generation of levees and a fines rich lining reducing the surface roughness and frictional energy loss (Kokelaar et al., 2014)

In the experiments of Kokelaar et al. (2014) and Gajjar et al. (2016) analogue currents formed internal channels and levees where fine particles lined the base of the flow reducing the surface roughness. This reduced the frictional energy losses and substrate permeability which allows for enhanced pore-fluid pressure retention, resulting in a more energetic and mobile current (Kokelaar et al., 2014).

The formation of basal fines is shown in this study by the stratified fine tri-disperse currents which have a greater velocity than the non-stratified coarse tri-disperse current (Fig. 4.13). In

the majority of experimental currents in this study, the currents are only stratified prior to the formation of current pulses. This may allow for early deposition of fines producing the fine rich internal channels and levees allowing for the highly mobile coarser currents. These levees could not be observed from the deposit surface or sidewall of these currents. To investigate the basal fines and the formation of levees further in constrained and aerated currents the series of experimental currents from this study could be repeated and sectioned to make detailed cross sections of the channel. This would allow for detailed observations about the presence of these features and interpretations on their impact on mobility. However, the experiments of Kokelaar et al. (2014) and Gajjar et al. (2016) are unfluidised, so the potential impact of current fluidisation on the formation of levees is unclear.

Previous work by Chedeville and Roche (2014) has suggested that increasing the surface roughness of the substrate can cause current auto-fluidisation as gas escapes from inter-particle voids. Auto-fluidisation can lead to an increase in the velocity and run-out distance of the current (Chedeville & Roche, 2014). In the experimental currents the later pulses have a greater velocity than the initial current, especially in the more polydisperse currents. The greater velocity in the more poly-disperse currents is likely caused by auto-fluidisation from gases releasing from the interparticle voids created by the coarser particles.

It is likely that the dominant mechanism for the high current velocities varies depending on the proportion of fines in the current. In currents with a high proportion of fines it is likely that the levees proposed by Kokelaar et al. (2014) cause the high velocities observed. While in currents and pulses with a lower proportion of fines it is likely that the auto-fluidisation proposed by Chedeville and Roche (2014) causes the high velocities observed.

6.1.3 The role of unsteadiness

Unsteadiness has been defined as variation in the current parameters (such as velocity, acceleration or competence) at a fixed location through time (Branney & Kokelaar, 2002). Either waxing when a parameter increases, waning when a parameter decreases, or quasi-steady when a parameter fluctuates only slightly (Branney & Kokelaar, 2002). Unsteadiness within a PDC impacts current mobility through time (for example, run-out) and therefore the nature of the deposit (Andrews, 2019).

The main type of unsteadiness observed in the experimental currents is variation in velocity, as shown in Chapter 4. There is also unsteadiness in the spatial and temporal grain-size distribution of the currents, for example when a coarse-rich pulse passes over a fines-rich current. In currents with varying grain sizes, each grain size may travel at a different velocity, meaning that as the flow propagates there will be temporal variations in current velocity and composition. Pulses are clear evidence for unsteadiness, characteristically displaying different velocities, accelerations, and composition to the underlying flow. In the experiments of Andrews (2019), pulses start with a lower velocity than the initial flow head but as they propagate the velocity reduces at a lower rate than the initial flow head velocity. This is similar to the results of this study, but the impact of grain size cannot be compared as Andrews (2019) used a mono-disperse current.

It is possible to use variations in flow front acceleration and velocity to interpret the presence of unsteadiness. The currents that contain a greater range of particle sizes, such as the fine

and coarse tri-disperse currents, have a greater range in acceleration than the mono and bi-disperse currents (Fig. 4.19). This suggests that the range of maximum and minimum grain sizes has a greater impact on the acceleration within the current than the initial sorting of the current. The subsequent pulses have greater velocities than the initial flow head (Fig. 4.18), this supports the work of Andrews (2019) that suggests that unsteadiness impacts the mobility by increasing the velocity.

6.1.4 Generation of pulses in dense granular currents

Pulses were observed to impact current mobility in this study, but their formation is not well understood. Previous analogue experiments have suggested that pulses are generated from the interaction between the current and topography generated by the aggrading deposit (Rowley et al., 2014). Other work based on field deposits has suggested that pulses are generated through fluctuations in the source (Báez et al., 2020; Risica et al., 2022). Fluctuations in the source which produce pulses can include pulsatory collapse of the eruption column (Giordano et al., 2008) and pulsatory variations in mass flux (Báez et al., 2020; Risica et al., 2022). The pulses in this study are likely to be related to the interactions between currents and topography proposed by Rowley et al. (2014), as this study did not involve any variations in material supply.

In this study, pulses generated spontaneously within the currents and occurred at multiple points along the flume, not just at the base of the ramp. This suggests that the generation of pulses is not simply an effect of release from the hopper, and/or impinging on the ramp, but is related to behaviours within the current. This generation of pulses does not follow the theory of Báez et al. (2020) or Risica et al. (2022) instead it is similar to the work of Rowley et al. (2014) as current behaviours are related to the pulses.

Pulses occur in all currents except the fine tri-disperse currents, but the number of pulses varies. The number of pulses formed during each experiment is independent of the grain size distribution, current sorting, runout distance and current duration (Fig. 6.2).

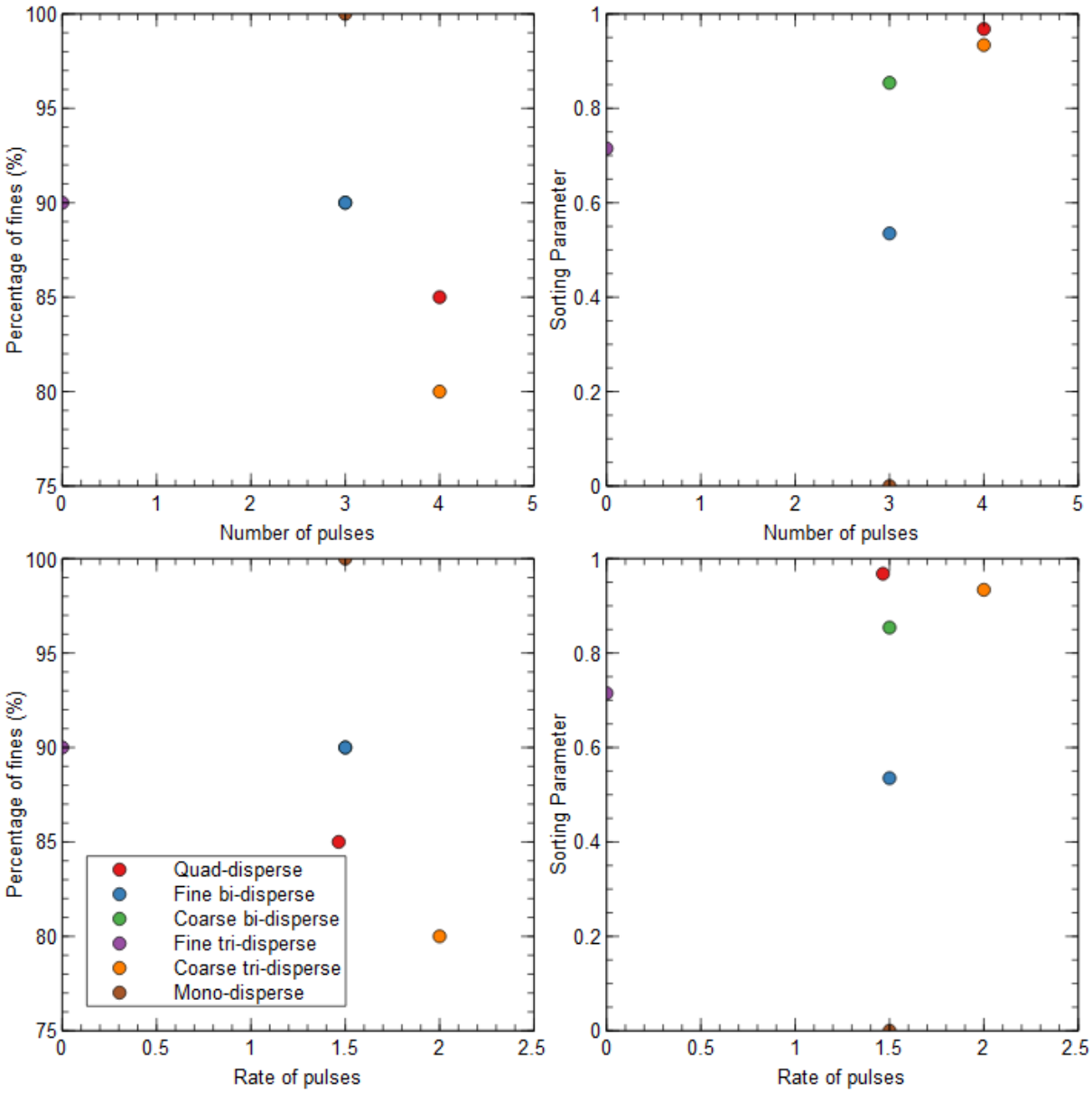

Figure 6.2: Graphs showing the relationship between the number of pulses and (a) grain size distribution, (b) current sorting, (c) run-out distance, and (d) current duration

The pulses are not present in the stratified fine tri-disperse currents and are observed to prevent stratification in the bi-disperse and quad-disperse currents, which contain some stratification prior to the pulses. It is likely that the pulses prevent stratification as they are more energetic than the previous flow head and overpass the flow head causing rapid changes in velocity (Fig. 4.18). By overtaking the flow head the pulse can recirculate previous material and mixes with the underlying current thereby the grain size equilibrium forming stratification cannot occur.

The cause of current pulses is unclear and needs further investigation. It is possible that pulses occur when there is more material in the current than the carrying capacity, which produces a backwards-propagating wave of excess mobile particles. This is unclear but may be observed occurring within the coarse bi-disperse current (Experiment 10 at 0.68 seconds). However, picking out the movement of individual particles makes observing this a challenge. In future

experiments, particle image velocimetry could be used to track the movement of individual particles at the onset of a pulse, allowing interpretation of the interactions causing pulse generation.

6.1.5 Quantifying percolation

Percolation is the process where particles move downwards into empty space due to gravity. Small particles percolate downwards more frequently than large particles, producing inverse grading. Percolation is important to quantify as it is believed to be a key method for sorting within dense granular currents (Vallance & Savage, 2000).

Numerical models created by Sohn and Chough (1993) for flow behaviours in natural PDCs suggest that percolation should occur instantly when the ratio of the smallest grain size to the largest grain size in the current is less than 0.25. This would lead to rapid organisation into a stratified current.

Table 6.1: Values calculated using the equation from (Sohn & Chough, 1993) where d_s is the smallest grain size and d_L is the largest grain size in the current

Current	$\frac{d_s}{d_L}$
Fine bi-disperse	0.06
Coarse bi-disperse	0.13
Fine tri-disperse	0.09
Coarse tri-disperse	0.09
Quad-disperse	0.09

For each experiment in this study the d_s/d_L value is less than the threshold for instant percolation of grains (Table 6.1), which suggests that all the experimental currents should have become stratified. However, the results in Chapter 4 show that this is not the case. Highly likely to be due to the gas fluidisation causing uplifting of fines within the current allowing for circulation of particles. The Sohn and Chough (1993) model does not consider fluidisation, and this study suggests that this has an important control on grain percolation. Unfluidised models may not accurately represent the grain segregation observed in natural gas-fluidised PDCs.

6.2 Comparing experimental deposits with ignimbrites

Ignimbrites are one of the main sources of data for studying the behaviour of natural PDCs, along with methods of directly collecting data shown in Table 2.2. By comparing the deposits of experimental currents with ignimbrites it is possible to apply the interpretations of the experimental current behaviours to the behaviours of natural PDCs.

Many features of ignimbrites can be used to infer PDC dynamics. For example, the aspect ratio of distal ignimbrites has been used to infer whether the depositing PDC was dilute or granular (e.g. the Taupo ignimbrite, Dade and Huppert, 1996). This suggested that low aspect ratio (e.g. high run-out distance) ignimbrites are deposited from dilute PDCs (Dade & Huppert, 1996). More recent work has suggested that large volume PDCs that are highly mobile can

have a dense basal section. The current which deposited the Peach Springs Tuff likely consisted of an upper more dilute zone allowing for deposition on topographic highs, with proximal velocities > 100 ms^{-1} prior to deceleration in distal areas. This suggests that high velocity currents or dilute currents are not necessary to deposit ignimbrites with a large run-out distance or low aspect ratio (Roche et al., 2016).

6.2.1 Ignimbrite interpretation paradigms – *en masse* deposition vs progressive aggradation at the flow boundary zone

Theories behind the emplacement of ignimbrites have changed rapidly within the last 60 years. Deposition was initially thought to be occurring through progressive aggradation whereby coarse and fine particles can be deposited without a decrease in current velocity (Fisher, 1966). In the 1970s, seminal publications (e.g. by Sparks, 1976 and Wright and Walker, 1981) proposed and developed a paradigm for ignimbrite emplacement whereby high-concentration pyroclastic flows were interpreted to deposit material en masse, by plug flow (Sparks, 1976; Wright & Walker, 1981). However more recent work has found this paradigm to likely reflect only the end-member of a spectrum of PDC deposition, with the majority of ignimbrites forming through progressive deposition at the flow boundary zone (Branney & Kokelaar, 1992, 2002) (Chapter 2).

Ignimbrites can be used to interpret the conditions of the flow boundary zone at the time of deposition, especially with regards to shear rate and velocity. The experimental currents in this study are all dense, granular flows where a granular flow dominated FBZ would be expected (Fig. 6.3). Being able to relate the experimental conditions at the flow boundary zone and the deposits allows for improved interpretations of flow boundary zone conditions from ignimbrites. Based on the current density and deposits (Chapter 5), the conditions at the flow boundary zone show little variation between the currents and are predominantly a granular flow-dominated FBZ. The main variation is within the deposition rate and rate of shear, the variation in deposition rate can be related to variation in deposition methods and from periods where the current was more mobile therefore no deposition occurred. The variation in rate of shear correlates with a lower current velocity which suggests that either individual particles within the current had different velocities resulting in different rates of shear, or the current was waxing or waning which caused varying velocities and therefore rates of shear. This suggests that to understand these variations in flow boundary zone conditions more detailed work needs to be carried out using particle image velocimetry (PIV) to allow for detailed quantification of individual grain velocities. Using this it can be quantified if the change in FBZ conditions is related to a whole current change or change in individual grain sizes.

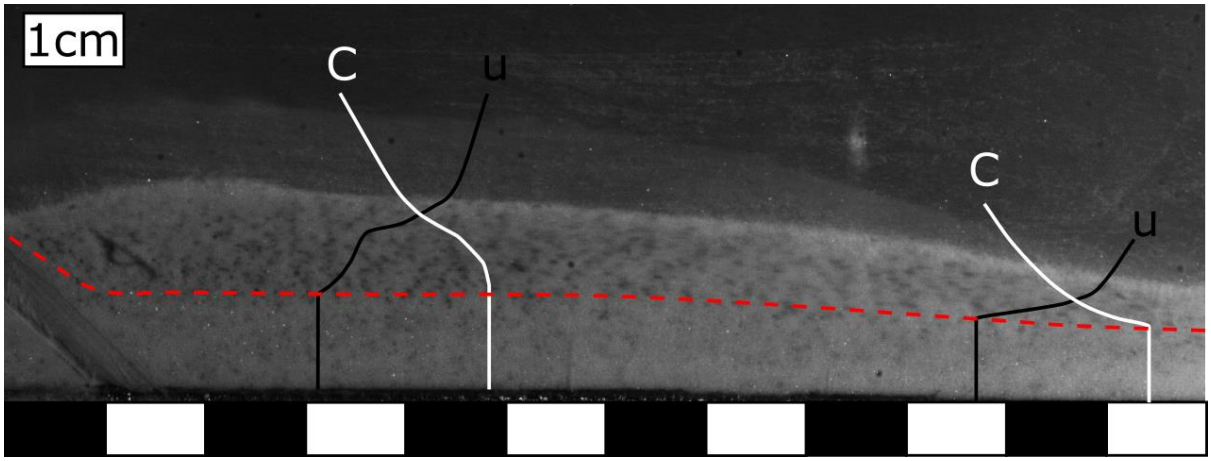

Figure 6.3: Suggested model of the flow boundary zone conditions for the quad-disperse currents (Image of Experiment 23 at 0.648 seconds). C = concentration, u = velocity. Red dashed line indicates the boundary between the deposit and the current.

There is little variation between the different deposits as in every deposits there are similar grading patterns, reverse vertical and normal lateral grading; and bedforms, elongate beds and cross stratification. The similar grading patterns in the deposits suggest that currents display some common behaviours regardless of the proportion of fines. Reverse vertical grading suggests that percolation, occurs in every current regardless of the proportion of fines. And the normal lateral grading shows that the finer particles have a greater run-out than coarser particles due to having a higher energy. The absence of variation in bedforms by current suggests that the proportion of fines within the current does not control the bedform generation.

The massive deposits, cross stratified beds and asymmetrical cross stratified beds in these experiments have gradually aggraded from the flow boundary zone (Fig. 6.4b). This gradual aggradation adds further evidence towards deposition from the flow boundary zone, as proposed by Branney and Kokelaar (1992) and now a widely accepted paradigm in the community, rather than through *en-masse* freezing, as proposed by Sparks (1976). The deposit packages, such as individual lunate beds, indicate a degree of step-wise aggradation occurs. Previously this was thought to form when there is successive *en-masse* deposition of plugs of material where each plug develops a high enough yield strength to deposit either from friction or particle adhesion (Fig. 6.4a) (Branney & Kokelaar, 1992). In the experimental videos the step-wise aggradation can be seen to occur gradually with each plug gradually aggrading prior to a pause in deposition due to changing conditions in the FBZ (Fig. 6.4c).

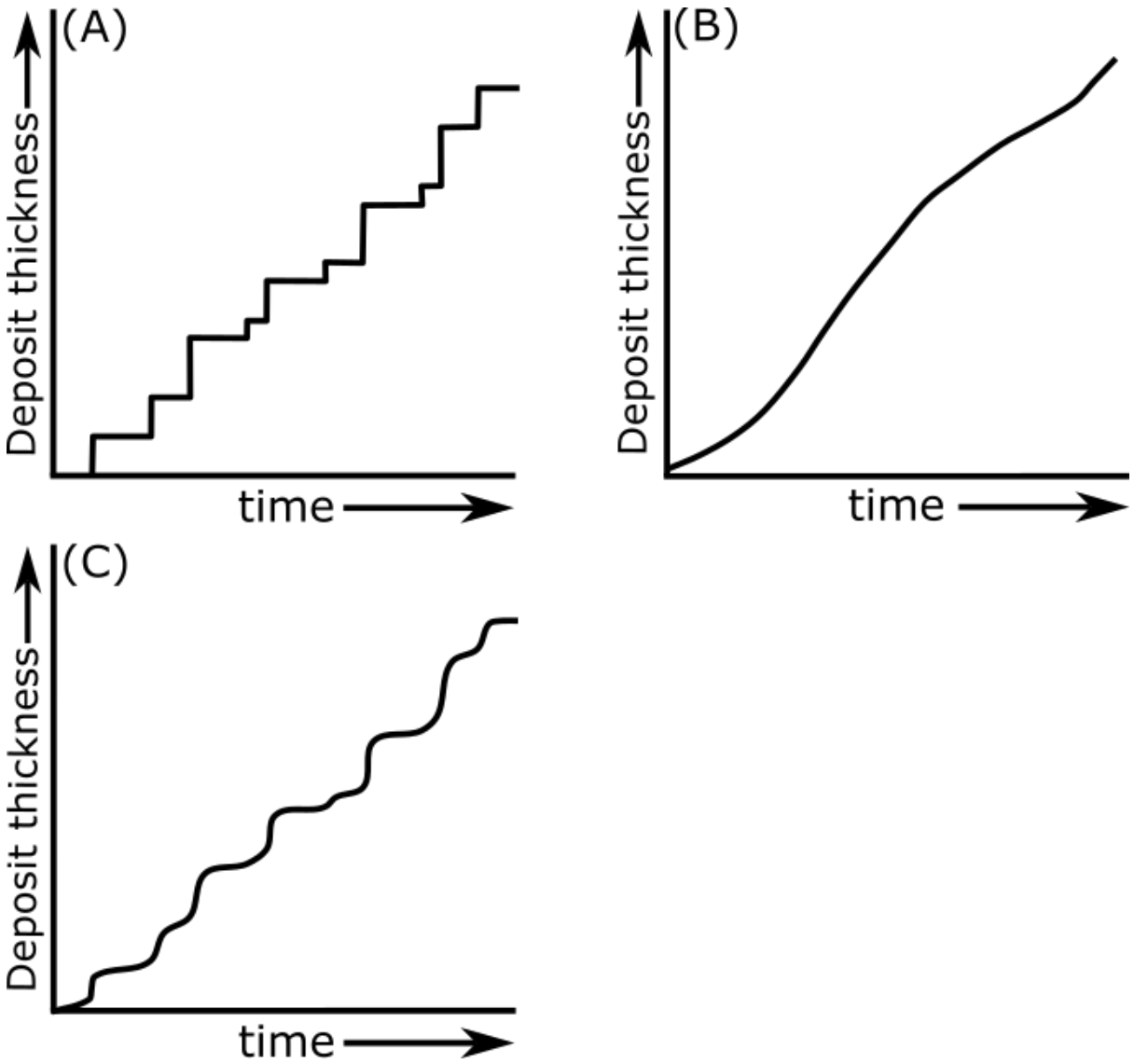

Figure 6.4: Sketch of deposition rates for (A) stepwise aggradation, where there is en masse freezing of plugs of material; *(B) gradual aggradation, where direct suspension sedimentation occurs; (C) the combination proposed in this study, where individual plugs of material gradually deposit. Adapted from (Branney & Kokelaar, 1992)*

6.2.2 Comparing experimental deposits to ignimbrites

There are a number of bedforms reported from the field, such as transverse bedforms, observed at Tungurahua, Ecuador (Douillet et al., 2013); and scour and fill, observed at Pantelleria, (Dowey & Williams, 2022), that were not replicated in this study. This may be because the experimental currents in this study did not replicate the flow conditions necessary to form these bedforms. Or, because these bedforms fundamentally cannot be formed from constrained dense, granular currents. By comparing the deposits observed in the flume to ignimbrites it is possible to compare interpretations and validate that the bedforms produced in the flume reflect natural ignimbrites.

6.2.2.1 Elongate

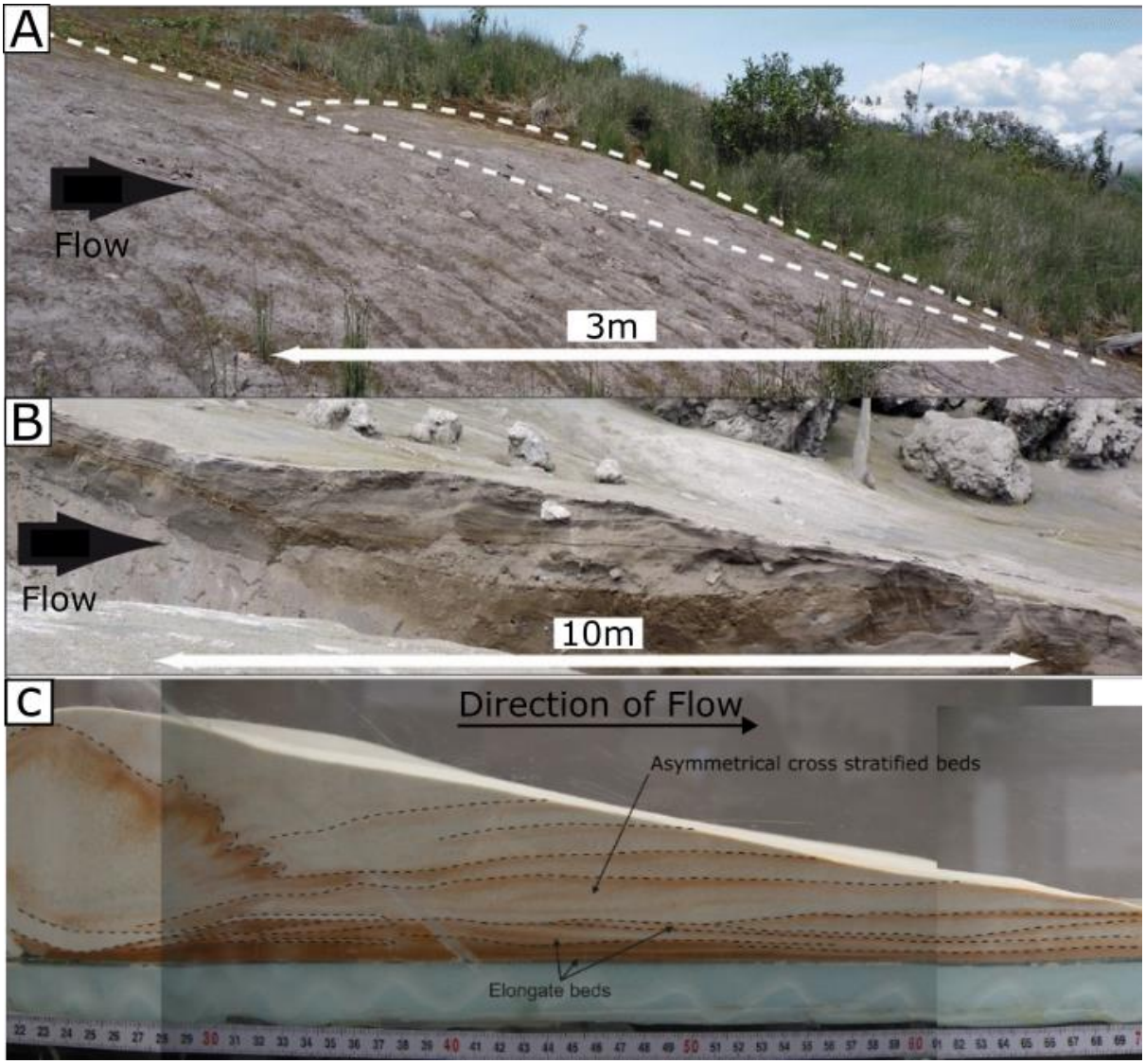

Figure 6.5: (a) outer shape of an elongate bed, (b) internal structure of a different elongate bed (Douillet et al., 2013) (c) deposit from the fine tri-disperse current showing elongate beds (Fig. 5.3)

Elongate bedforms observed in deposits at Tungurahua volcano, Ecuador (Fig. 6.5a and b). The elongate bedforms here have been interpreted to be deposited in a high capacity and competence dense current due to the presence of large blocks. These deposits were observed in the proximal zone on steep slopes with nucleation occurring independent from the underlying topography (Douillet et al., 2013).

Experimental elongate bedforms are able to form on a low angle slope (~4 °) which suggests that contrary to the natural deposits slope angle does not impact their deposition. Experimental elongate bedforms formed independent of the underlying topography, similar to the field deposits, as they mainly formed basal deposits.

6.2.2.2 Lunate

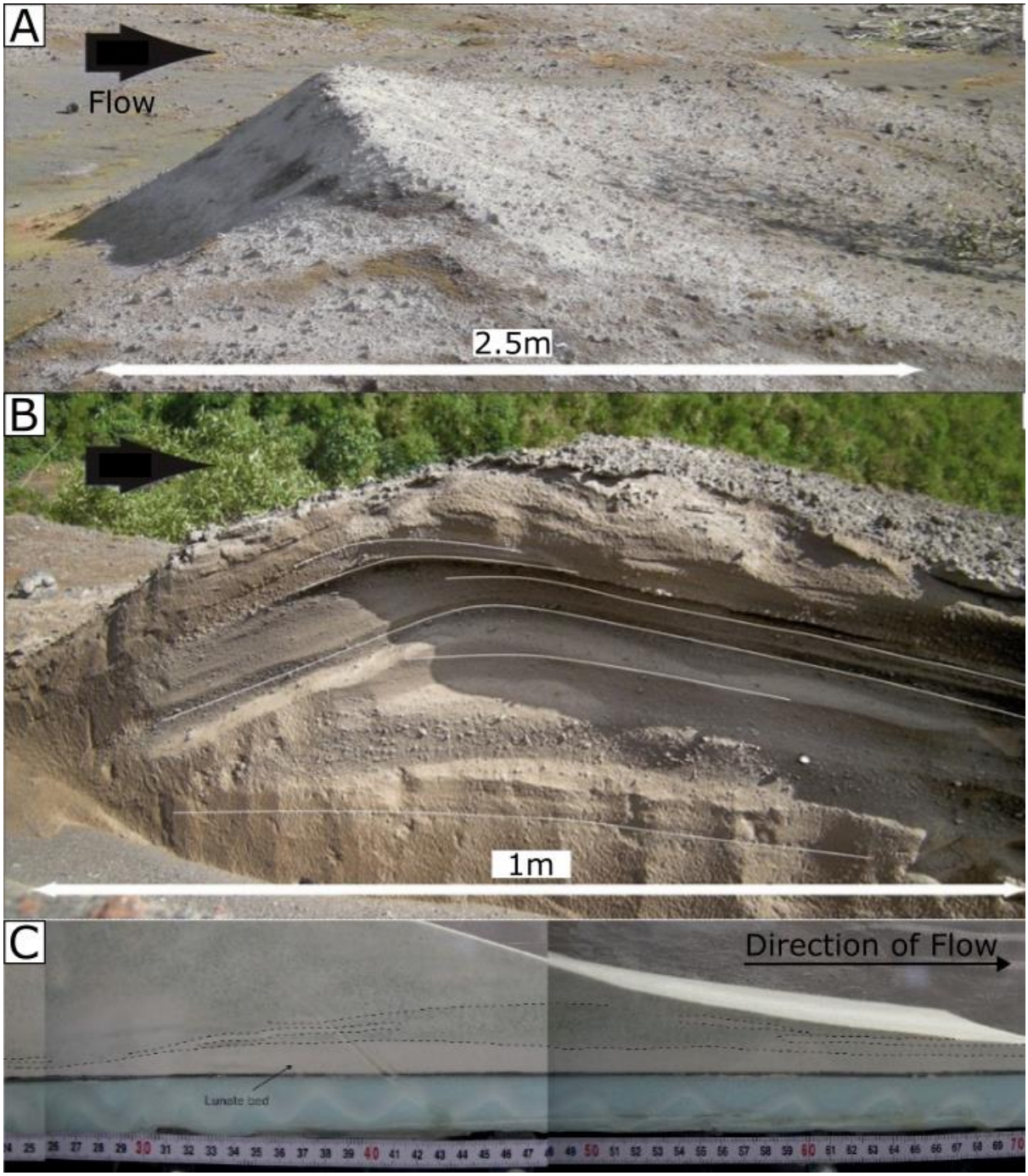

Figure 6.6: (a) outer shape of a lunate bed (b) internal structure of a different lunate dune bedform, Tungurahua volcano, Ecuador (Douillet et al., 2013) (c) deposit from the coarse bi-disperse current showing lunate beds (Fig. 5.5)

Lunate bedforms observed in deposits at Tungurahua volcano, Ecuador (Fig. 6.6a and b), have been interpreted to nucleate from flat streambeds, independent of underlying morphology. Lunate bedforms are interpreted to deposit from a tractional flow boundary zone in a dilute, turbulent current with a low carrying capacity (Douillet et al., 2013). As this study used dense granular currents, the presence of lunate beds within the deposits demonstrates that lunate beds can be deposited from a dense current, likely in a granular flow dominated flow boundary zone.

The experimental lunate bedforms generally form independent from the underlying morphology. Although it is possible that the underlying deposits impact the shape of the lunate beds as the bed morphologies in Fig 5.5b are related to the morphology of the underlying elongate bed unlike in Fig. 5.5a. To investigate this further, experimental repeats should be carried out over a flume topography to observe any differences in bed morphology with underlying topography.

6.2.2.3 Cross stratified

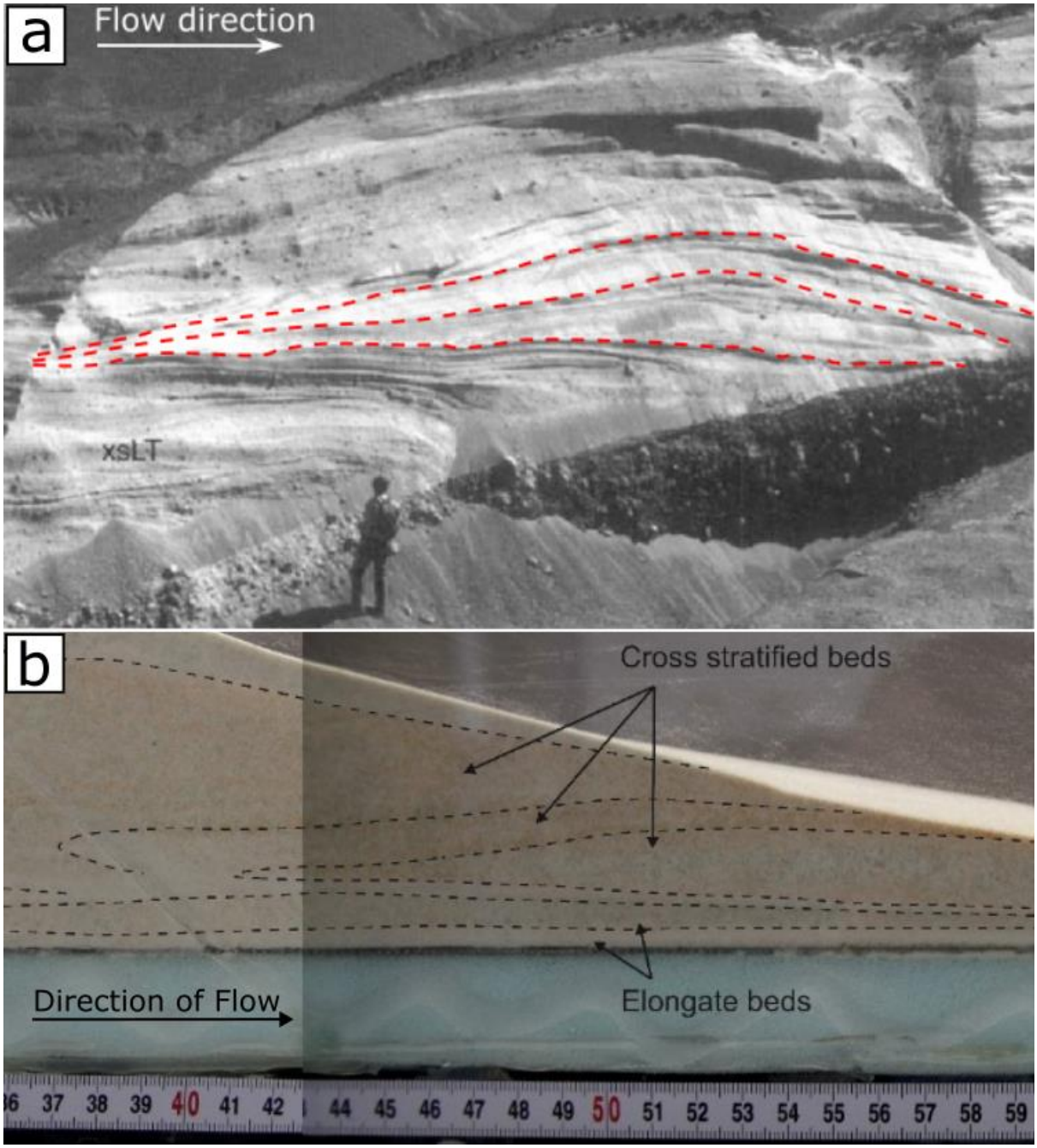

Figure 6.7: (a) Proximal cross stratified lapilli tuff, 18th May 1980 Mt St Helens ignimbrite. Flow direction was left to right (Branney & Kokelaar, 2002), (b) deposit from the fine tri-disperse current showing cross stratified beds (Fig. 5.6)

Cross stratified beds observed at Mt St Helens (Fig. 6.7a) have been interpreted to have deposited as part of a traction dominated flow boundary zone. In this current the fine clasts were supported by fluid turbulence and denser/larger clasts transported by saltation, sliding, or rolling. As this unit correlates with a massive unit further away, the flow boundary zone is interpreted as gradational between traction dominated and direct fallout dominated (Branney & Kokelaar, 2002).

The experimental findings of this study have supported the transport mechanisms proposed by Branney and Kokelaar (2002). These currents however were dense, granular currents suggesting that the flow boundary zone was granular flow dominated rather than traction dominated which requires a more dilute current.

6.2.2.4 Chute and pool

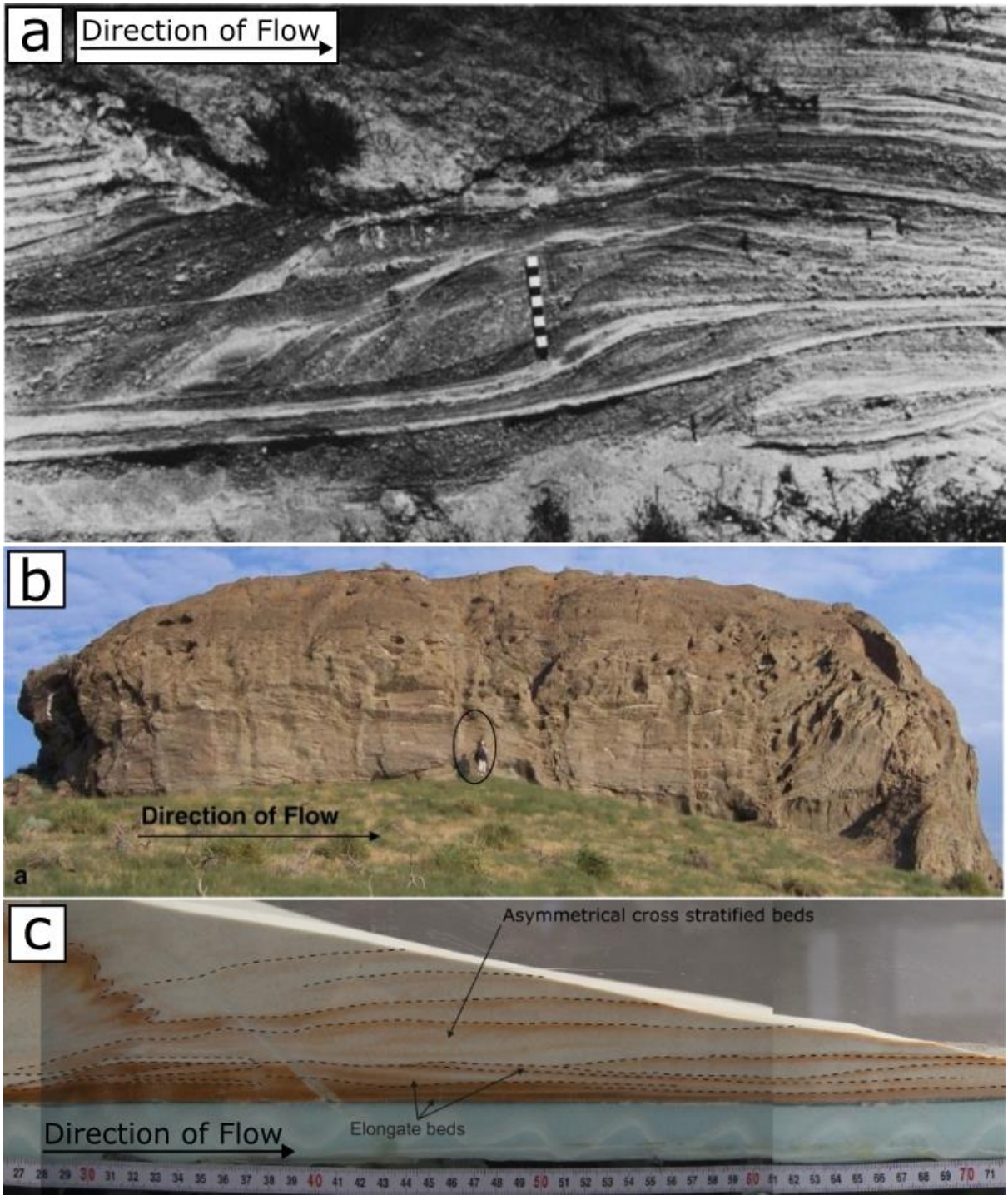

Figure 6.8: (a) Chute and pool structure at Laacher See. Scale is 1 m. Flow direction is left to right (Schmincke et al., 1973), (b) Large chute and pool structure within surge deposits. The outcrop is 40 m in length and 13 m tall (Brand & Clarke, 2009), (c) deposit from the fine tri-disperse current showing asymmetrical cross stratified beds (Fig. 5.3)

Chute and pool structures are high angle bedforms with steeply dipping stoss side deposits and shallower angled, parallel beds depositing on the lee side of the dune (Schmincke et al., 1973). At Laacher See, Germany (Fig. 6.8a) they were interpreted as being deposited from very high energy surges (Schmincke et al., 1973). Similar bedforms in Oregon, USA (Fig. 6.8b)

have been interpreted as recording changes in flow conditions at a hydraulic jump where the flow changed from supercritical to sub-critical. It has also been suggested that these bedforms represent a surge current surmounting a previously existing obstacle (Brand & Clarke, 2009).

Chute and pool bedforms are similar in appearance to the asymmetrical cross stratified beds observed in the experimental currents (Chapter 5), which are interpreted as depositing in a high energy environment. However distinct ‘surges’ are not visible when these bedforms are deposited, and rather than turbulent dilute flow (surge) the experimental currents are dense, granular flows. This demonstrates that either chute and pool bedforms can form in both dense and dilute currents making them unsuitable as a diagnostic feature of current type or that different processes can produce bedforms with a similar appearance. As all of the currents have supercritical Froude numbers (Fig. 6.13), the experimental currents lack any evidence of a granular jump. Based on this and the experimental bedforms overlying the crest of previous bedforms (Fig. 5.9) it is likely that the asymmetrical cross stratified beds formed from surmounting obstacles in the flume as suggested by Brand and Clark (2009).

6.2.2.5 Massive deposits

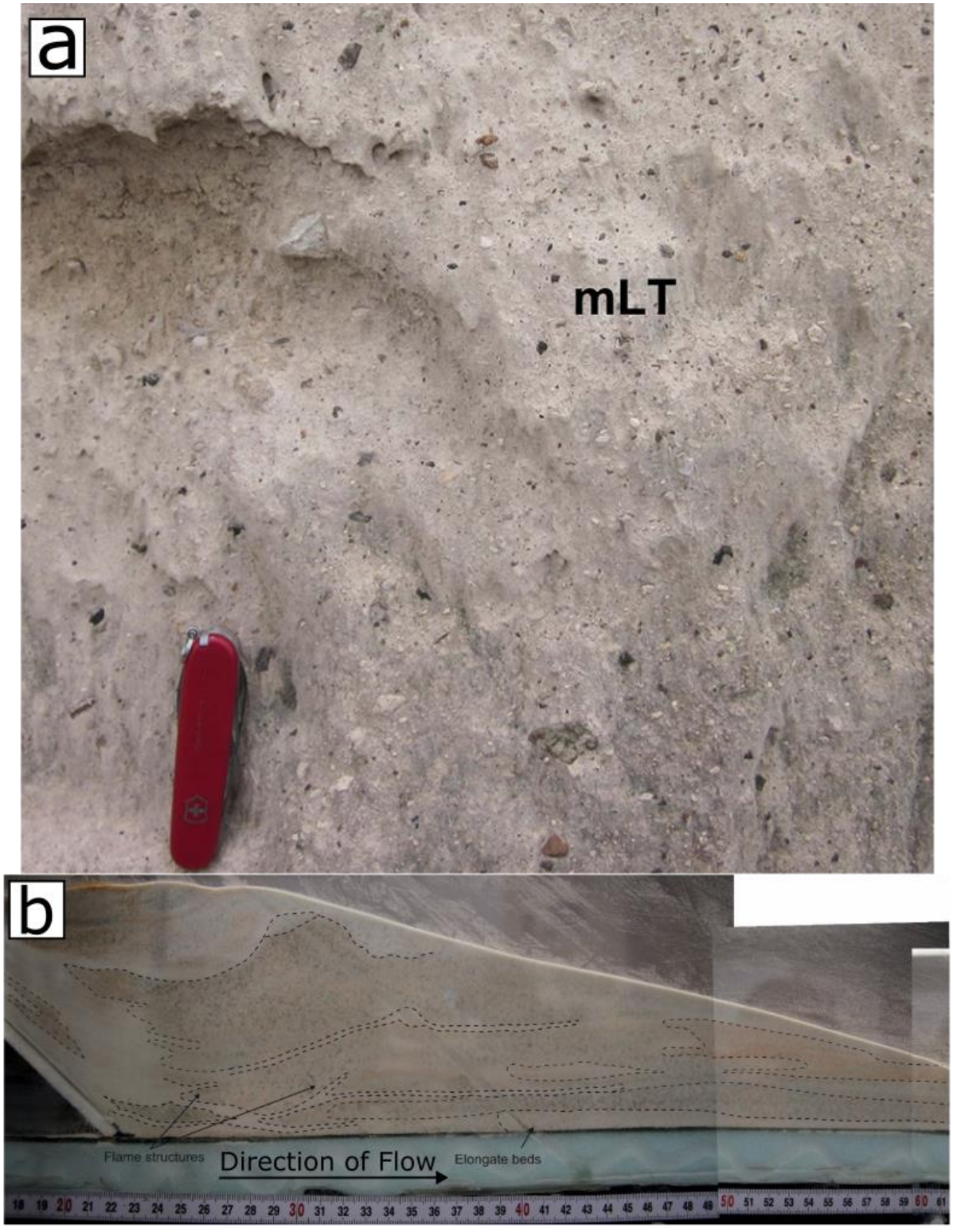

Figure 6.9: (a) Massive non-welded lapilli tuff deposit from Lower Huichapan Ignimbrite, Mexico (Pacheco-Hoyos et al., 2020) (b) deposit from quad-disperse current showing a massive deposit (Fig. 5.11)

Massive deposits, such as in the Huichapan Ignimbrite, Mexico (Fig. 6.9) are interpreted as forming in a current where tractional segregation from turbulent shear is suppressed leading

to a fluid escape dominated flow boundary zone. These deposits are often fines depleted due to the elutriation of fines but the interlocking of particles means that not all of the fine ash is elutriated (Branney & Kokelaar, 2002).

Massive deposits have previously interpreted as depositing *en masse* (Sparks, 1976) while more recent research has suggested that gradual deposition occurs (Branney & Kokelaar, 1997, 2002). The gradual aggregation is supported by the presence of grading and onlap relationships between massive deposits and topography (Branney & Kokelaar, 2002).

The massive deposits in the experimental currents of this thesis are interpreted as depositing from a fluid escape dominated flow boundary zone. These deposits can be observed to gradually aggrade which further supports the work of Branney and Kokelaar (1997, 2002).

6.2.2.6 Flame structures

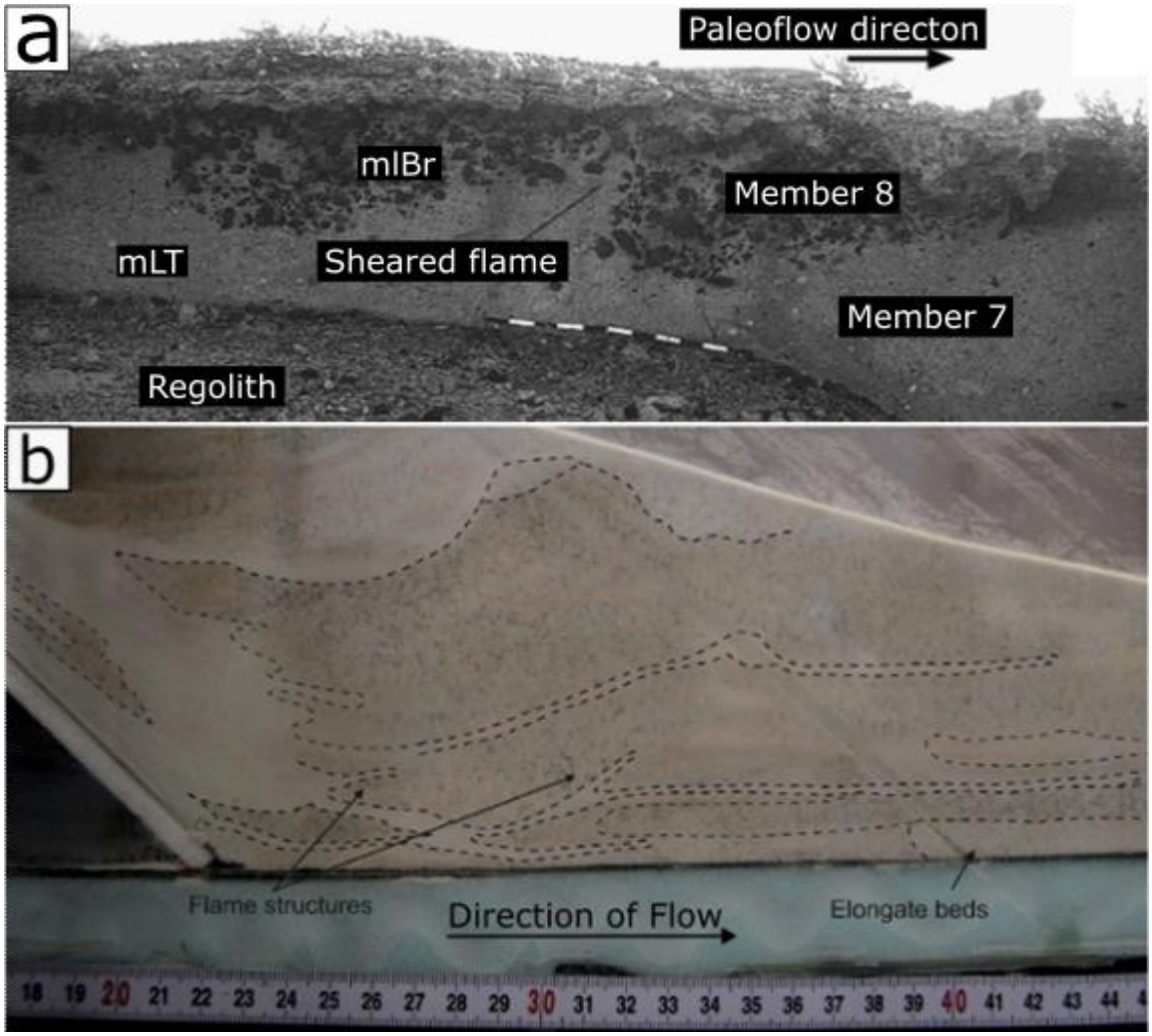

Figure 6.10: (a) Upper members of the Poris Formation, Tenerife. Sheared load structures in lithic breccia at La Mareta, indicating loading of breccia during deposition (Brown & Branney, 2004), (b) deposit from the quad-disperse current showing flame structures (Fig. 5.11)

Asymmetrical load structures (Fig. 6.10a) have been interpreted as forming when a massive lithic breccia (mlBr) flowed over gas rich unconsolidated massive lapilli tuff (mLT). The

direction of the flames indicates downslope shear which suggests that the flames were generated prior to the cessation of downslope movement. The lithic breccia formed discrete pods through loading of discrete depositional packages, through particle segregation and elutriation during deposition, or post-depositional segregation where convective instabilities at the lower contact generated load balls (Brown & Branney, 2004).

Load structures are similar to the flame structures observed in the experimental deposits, suggesting that they formed in a similar environment. The formation of flame structures in the experimental deposits is likely from loading or particle segregation and elutriation, which are two of the proposed methods of Brown and Branney (2004). The flame shapes (Fig. 5.2) indicate that shear was present at the time of generating these structures, this suggests that the current was still flowing, and these structures are not evidence of post-depositional segregation.

6.2.2.7 Two Dimensional

Figure 6.11: Photograph of 2D dune bedforms observed at Tungurahua volcano, Ecuador (Douillet et al., 2013)

Two-dimensional dunes have been observed at Tungurahua volcano, Ecuador (Fig. 6.11). 2D bedforms are interpreted as forming when flow propagation is dominated by lateral transport over downstream transport in unconstrained currents. These bedforms are not observed in the experimental deposits due to the narrow flume used not allowing for lateral transport, showing that the flume represents a constrained current.

6.2.2.8 Outcrop showing multiple bedforms

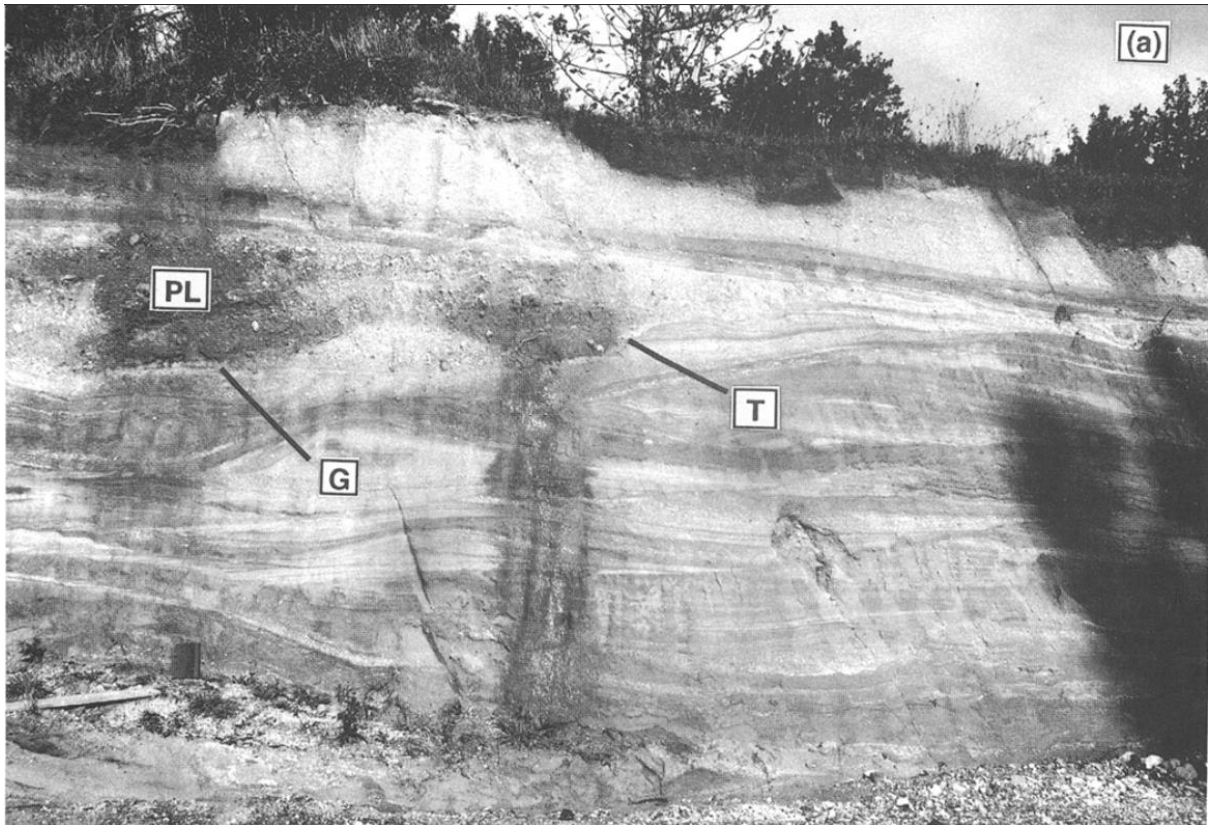

Figure 6.12: photograph of exposure near Marzano town. PL = pumice layer, T = truncated bedding at contact between PL and underlying deposit, G = gradational contact. (Valentine & Giannetti, 1995)

Fig. 6.12 shows cross stratification, chute and pool structures and other bedforms which are interpreted as depositing in a dilute current (Valentine & Giannetti, 1995). However, the presence of these bedforms in the experimental deposits suggests that these currents are not necessarily dilute. This bedform formation can be related to the underlying topography through granular jamming where the current is blocked by topography (Douillet et al., 2019), which have been shown to occur in dense granular currents (Smith et al., 2020). This suggests that chute and pool generation is not necessarily related to changes in current conditions as proposed by Schmincke, Fisher and Waters (1973).

6.2.3 What do the deposits of fines mean?

Thin beds of fines occurred within all of the deposits generated by the experimental runs of this study. These fines were observed to be deposited from fallout of the overriding cloud between pulses and within some of the pulses. This deposition from the experimental overriding cloud, which has not been reported in previous volcanology experiments, is analogous to deposition of fines from the co-ignimbrite cloud in natural PDCs.

In previous studies, the presence of ash fall-out units (as well as pumice fall units or reworked horizons) has been interpreted as marking the cessation of current activity, even briefly, at a specific location. Such layers have been used as markers to define discrete ignimbrite “flow units” (Brown & Branney, 2004). The change of ignimbrites with height do not necessarily

indicate a change in flow unit as this can record a change in material from the source or a hiatus in deposition (Branney & Kokelaar, 2002).

In the currents of this study the fallout is deposited during the temporary cessation of deposition related to stepwise aggradation and from fallout into the thin aggrading currents, which changes the current composition and behaviours. The current is therefore unsteady due to changing the composition of the currents, which means that the FBZ conditions can change varying the depositional behaviour. The experimental fall out deposits from the overriding cloud have major impacts on field interpretations of ignimbrites as previously the presence of fall out deposits was interpreted as forming during a hiatus of PDC activity.

Flow unit boundaries can be variable as a sustained current propagates, and its flow direction varies, meaning that one location may experience sustained passage of the current while another location may experience interrupted flow (Branney & Kokelaar, 2002). This spatial variation in the arrangement of flow units has been shown in well preserved successions, such as in Tenerife (Brown & Branney, 2004; Smith & Kokelaar, 2013). This variation records a contradictory picture of PDC behaviour during an eruptive event, and that the stratigraphic record can be influenced by a number of factors such as current unsteadiness and syn-depositional interactions.

6.3 Comparison to other analogue experiments

6.3.1 Small scale analogue experiments

Previous work on small scale analogue experiments have been carried out by Savage and Lun (1988), Vallance and Savage (2000), Bareschino et al. (2008), Roche et al. (2008, 2010), Rowley (2010), Rowley et al. (2014), Andrews (2019) and Smith et al. (2018, 2020). In the experiments by Savage and Lun (1988) and Vallance and Savage (2000) the currents were observed inversely grade due to percolation of fine particles within the current. In this study reverse grading occurs in the deposit but stratified currents as per Savage and Lun (1988) are not present in every current. The absence of stratified currents is most likely due to the basal gas supply which causes elutriation of fines and resegregation. The work by Andrews (2019) shows similar current behaviours with pulses caused by current unsteadiness propagating faster than the initial current head. The work of Andrews (2019) is less suitable for direct comparison with this study as the experiments involved mono-disperse dilute currents meaning that different behaviours would be expected. In this discussion the primary focus will be on comparisons with Smith et al. (2018, 2020) as these experiments used a similar experimental set up to this study.

Smith et al. (2018; 2020) investigated mono-disperse dense PDCs using the same flume used in this study. For the equivalent U_{mf}, the experiments of Smith et al. (2018) had a run out of 2 m and 2.5 m for slopes angled at 2° and 4° respectively. These values are 22% and 47% larger than the run-out distance of the monodisperse currents of this study. Slope angle has been identified as causing an increase of up to 50% in run-out between a 2° and 4° slope (Smith et al., 2018). Therefore, it is likely that the variation in flume angle had a major control over the run-out distance. The degree of variation caused by a change in slope angle suggests that comparing the run-out distances of this study and Smith et al. (2018) is not possible.

By comparing the flow front velocity of this study with the equivalent U_{mf} conditions in Smith et al. (2018) the mono-disperse currents show similar velocities. This suggests that the flume angle has less control over the flow front velocity, allowing for comparisons between these studies. The more poly-disperse currents show greater velocities than the monodisperse currents of this study and Smith et al. (2018) (Fig. 4.18). The variation between this study and Smith et al. (2018) suggests that the range of grain sizes in the current has a greater impact over flow front velocity than the slope angle. The variation in velocity between mono-disperse and poly-disperse currents could be related to the surface roughness impacting the basal friction. Surface roughness has been identified as a factor controlling mobility by Kokelaar et al. (2014) in non-aerated currents flowing over existing topography. In this study it has not been possible to quantify the impact of surface roughness on the basal velocity during each current. The impact of surface roughness could be investigated by using PIV analysis to examine how velocity at the base of the current varies as the substrate varies through deposition.

Smith et al. (2020) was able to define a phase diagram which quantified the parent currents of a variety of deposits based on velocity, current thickness, Froude number and friction number. When results from this study are plotted on to these phase diagrams, we find that they all plot in the planar bedform space (Fig. 6.13).

Froude number is calculated using eqn. 9:

$$Fr = \frac{U}{\sqrt{gH}} \qquad \text{(eq. 9)}$$

Where U is the current velocity and H is the current thickness, and were calculated at the flow from of the depositing part of the current. The value for Froude number is important as Fr > 1 shows a supercritical flow, Fr = 1 shows critical flow and Fr < 1 shows a subcritical flow. Supercritical flows occur as part of a higher energy environment than subcritical flows so can be used to interpret current energy.

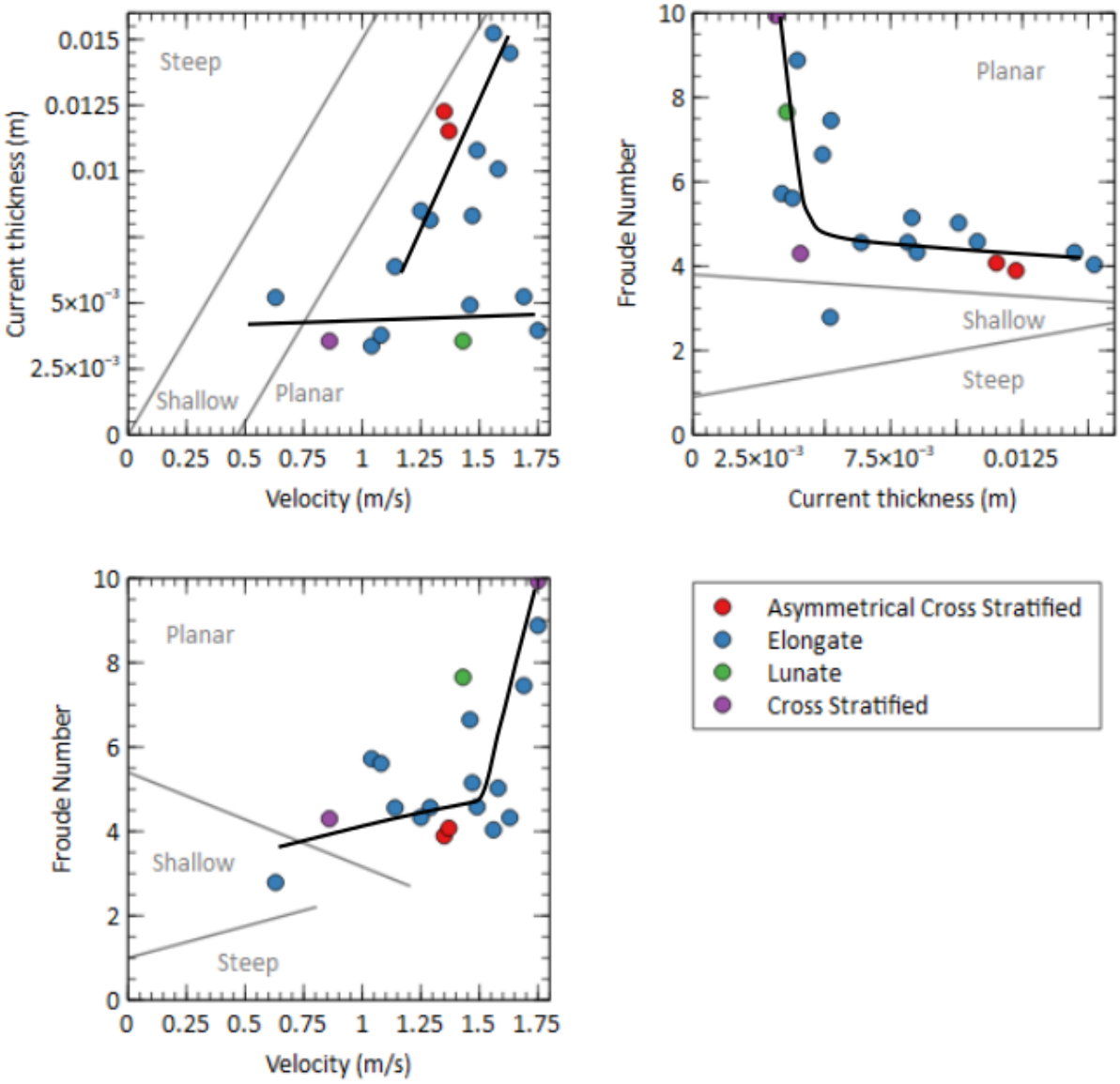

Figure 6.13: Phase diagram showing current conditions during the deposition of each bedform. Phase boundaries in grey from Smith et al. (2020), possible trends shown in black

The variations in grain size within these experimental currents may account for the deposition of non-planar bedforms at higher velocities as larger particles increase the roughness of the surface. By creating this rough surface, it is easier for smaller particles to deposit in the interparticle spaces. This then allows for deposition to occur in the high energy currents rather than just in low energy currents as expected. This suggests that while the boundaries of Smith et al. (2020) are valid for a waning or monodisperse current but as the range of grain sizes in the current changes the boundaries will vary too.

The steep bedforms of Smith et al. (2020) are similar to the 'asymmetrical cross stratified beds' bedforms of the experiments presented here, in that they contained a steep stoss side. These high angle bedforms of Smith et al. (2020) deposited towards the end of a waning flow, unlike in this study where deposition occurred during waxing and waning of the current. The differences in velocity suggests that the velocity is related to the timing of deposition rather

than being indicative of the velocities at which these bedforms deposit. As higher velocities are expected in the currents of this study based on eqn. 9, higher Froude numbers would be expected as the currents are similar in thickness. There are possible trends in the data, shown in Fig. 6.13, that suggest that the control of Froude number by the current thickness or current velocity changes. However, this requires further investigation and data to strengthen the trends and allow for identification of at what current conditions the control changes.

Variations in the experimental conditions can impact the mobility and therefore the results of the phase diagram, as flow volume and discharge rate impact mobility (Sulpizio et al., 2014). For example, the discharge rate is equivalent to the mass flux which can vary depending on the release mechanism. The trapdoor release mechanism used in Smith et al. (2020) provides a different mass flux to the horizontal lock gate used and means that some energy is lost as particles collide with the trapdoor. The experimental set up of Smith et al. (2020) also didn't use a ramp as in this study, which suggests that more lateral propagation could have occurred resulting in a higher current velocity. Both the experiments by Smith et al. (2020) and the ones in this thesis used a 10 kg charge, but the mass of material in each pulse which deposited is unlikely to be constant.

6.4 Limitations

6.4.1 Flume limitations

The flume was designed with Perspex side walls to allow for video analysis of currents and image analysis of deposits. However, there are limitations to this design. In analogue experiments carried out by Ancey (2001) the frictional forces from the sidewall caused a reduction in velocity between the centre line and sidewall of 30% to 50% (Ancey, 2001). These experiments were carried out using dry, granular currents consisting of 2 mm diameter glass particles. In the experiments of this study, as the particle size is smaller the effect of friction on each particle will be smaller, so the sidewall effect will be present but will have less of an impact on current behaviours.

For small particle sizes (250 μm), the sidewall effects are prominent within 50 mm of the flume edge (Rowley et al., 2011) this means that the deposits observed at the sidewall are not fully indicative of features present within the deposit. Based on the deposits of Rowley et al. (2011) it is possible that features such as Kelvin-Helmholtz instabilities and reworking of material which appear minor at the side wall are more developed towards the centre of the flume. However, it is also possible that these structures formed in this study at the sidewall due to the identified sidewall effects.

6.4.2 Data limitations

Due to using a black and white high-speed camera it is not possible to completely identify particles using their colour in the high-speed video. By using the colour photographs of the deposits, it is possible to identify general trends in grain sizes which allows for descriptions of variations in behaviour based on grain size. As the grain size of the particles is too small for PIV the inability to be completely accurate in identifying the grain size of individual grains did not impact the qualitative results.

Due to time constraints on this project, some experimental data has a large standard deviation (Section 4.2) whereby this data is not statistically significant. This is because less repeats were carried out to allow for investigation into a greater range of polydisperse currents. By covering a large range of parameters it is possible to define the trends more clearly than by using a smaller range of parameters but with more repeats (giving a smaller standard deviation). The standard deviation is larger in the mono and bi-disperse currents as more repeats were carried out for the tri- and quad-disperse currents to allow for more reliable interpretations of these currents which lack previous investigation. To improve the significance of some of this data further repeats could be carried out as needed, especially on the 100% 45-90 μm and fine bi-disperse currents as these have the largest standard deviations.

One aspect of the data which could have been strengthened is analysis using PIV techniques, however the grain sizes used meant that even with the high-quality images available the software did not effectively work. By over analysing the video over exaggerated interpretations of the data were produced. In future work on this topic, it would be beneficial to use a higher resolution and higher FPS colour high-speed camera whereby PIV analysis would be possible and internal behaviours, such as recirculation, could be observed.

6.4.3 Scaling issues

Scaling is a common issue in relating analogue experiments to natural currents. In order to minimise the impacts of scaling either appropriate parameters must be used, or large scale work is carried out (Chapter 2). In the case of small scale analogue experiments it is vital to ensure that the parameters such as density, grain size and aspect ratio are appropriate. By ensuring that the experimental parameters of this study are a useful comparison to natural PDCs it is possible to carefully apply the interpretations of the experiments to natural PDCs.

Table 6.2 provides a summary of how a range of parameters and dimensionless values of the experimental currents relate to natural PDCs. By comparing these values, it is possible to show that the experimental currents are well scaled for dense PDCs allowing for interpretations of the experimental currents to be carefully applied to the natural currents.

Table 6.2: Parameters of natural dense PDCs (Data from Roche, 2012) compared with experimental currents in this work and Smith (2020)

Parameter	Natural PDCs (Roche, 2012)	Previous experiments (Smith, 2020)	These experiments
Particle Diameter (m)	$2 \times 10^{-5} - 5 \times 10^{-4}$	$4.5 \times 10^{-5} - 2.5 \times 10^{-4}$	$4.5 \times 10^{-5} - 7.1 \times 10^{-4}$
Particle Density (kgm^{-3})	500-2500	2500	2500
Fluid Density (kgm^{-3})	~1	1.225 – 2	1.185
Flow Thickness (m)	$10^{0} - 5 \times 10^{1}$	$10^{-3} - 1.2 \times 10^{-1}$	$4 \times 10^{-3} - 1 \times 10^{-2}$
Flow Length (m)	10^{3} – 10^{4}	0.5 – 3	1.34 – 1.76

Aspect Ratio	0.001 – 0.005	0.002 – 0.04	0.002 – 0.006
Froude Number	1.6 – 3	0.7 – 7	3.9 – 9.9

As previously identified (Chapter 3) the particle size was chosen to provide similarities with the material within natural PDCs. Table 6.2 shows that the ash component of PDCs has similar parameter values to the ballotini of these experiments. However, natural PDCs contain much larger blocks than the ash matrix range above which means that this data cannot be entirely representative of natural PDCs but shows an example of how a range of grain sizes affects current mobility.

The density of both the particles and fluid suggest that the currents can be used to simulate natural PDCs as both the particle and fluid densities controls the degree of fluidisation (Roche, 2012). The particle density in these experiments is not totally representative of the densities of particles in natural PDCs. This was done to allow isolated investigation into the effect of grain size without adding in the complication of the effect of density as described in Chapter 3.

The main variation is in the Froude number where these experiments have a higher value than natural PDCs. As the values for these experiments and natural currents are greater than 1 both experimental and natural currents display supercritical behaviour. The similarity in flow conditions mean that this variation is negligible. Previous work by Smith (2020) has shown that the currents can be subcritical, however this is due to current blocking leading to a thicker current which reduces the Froude number.

6.4.4 Comparison to other granular flows

By comparing the behaviours observed in the small-scale analogue currents with large scale analogue currents and natural granular currents it is possible to accurately increase the scale of these results. By scaling up the results of this study it is possible to apply the interpretations to natural PDCs.

6.4.4.1 Large scale analogue experiments

The current behaviour results described in Chapter 4 can be compared to the results of other analogue experiments carried out by Lube et al. (2015) and Breard et al. (2016) on the PELE flume. The experimental set up consists of an aerated and heated hopper and was described in Chapter 2. The PELE flume experiments use Taupo ignimbrite material in a flume of 13x37 m dimensions (12-20 orders of magnitude larger than the flume used in this study). The use of natural material and the scale of the flume begins to approach natural behaviours seen in natural pyroclastic density currents. Some of the behaviours observed in the PELE flume experiments are consistent with those observed in this study; this includes the formation of a concentrated basal flow and an overriding cloud. The concentrated basal flow shows fingers forming (Fig. 6.14 H), similar to the mm scale flow fronts observed in this study. The larger pumice fragments travelled by saltation (Fig. 6.14 I), similar to the transport by saltation of the 500-710 µm particles. The overriding cloud shows detachment (Fig. 6.14 H) and an expelled front travelling ahead of the dense flow (Fig. 6.14 C), this can be observed in the experimental currents of this study. However, Kelvin-Helmholtz instabilities are generated within the overriding cloud unlike the experimental currents of this thesis (Breard & Lube,

2017). The elutriation of fines generating an overriding cloud, shown in Fig. 6.14 A and H, can also be observed occurring in the experimental currents of this study. The deposits from these experiments also show that the finest ash has a greater thin run out distance than the main flow body; with internally graded lobes forming in the deposit, where the deposit coarsens outwards towards the flow head and lobe edges.

The currents typically propagate at initial velocities of 16 ms^{-1}, reducing to 10 ms^{-1} at 3.1 m along the flume and then reducing to 5 ms^{-1} at 10.6 m along the flume (Breard et al., 2016). These velocities in Breard et al. (2016) are 6-20 orders of magnitude larger than the velocities of this study. As these velocities are similar to the scaling for the two experimental set ups, it is highly likely that the results of this study are valid for larger scale currents).

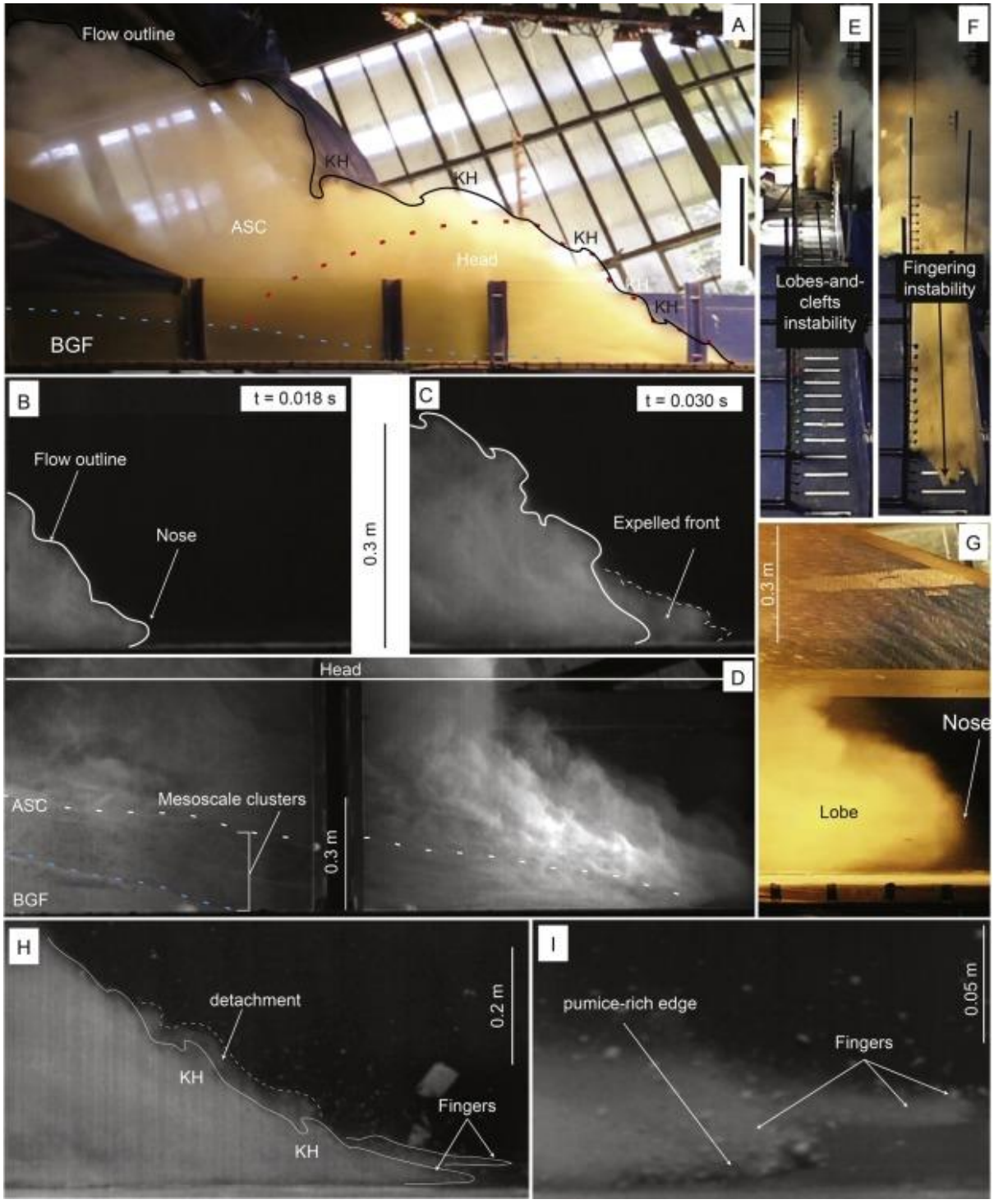

Figure 6.14: Photographs of various aspects portion and processes occurring within the head of experimental currents. A: Side view photograph showing the nearly semi-elliptical head shape with a wedge front. Note Kelvin–Helmholtz instabilities that grew in size up current. Dashed and solid lines indicate the different outlines of the ash-cloud surge (ACS), basal granular–fluid flow (BGF) and head. B: Close-up photograph of the snout of the head, which developed a small elevated nose. C: Photograph of the same front after 0.012 s (after B) that depicts a transient expelled flow front. D: Picture of the internal structure of the flow head shows three zones: the lowermost one is the BGF, separated by a sharp interphase from the intermediate concentrated zone where mesoscales structures develop. Particles gather in

clusters of dendritic pattern. E: Frontal view of the flow in the proximal area showing lobes-and-clefts instabilities. F: Flow front develop finger instabilities in the medial and distal area. G: Cross-section through a lobe developed nose. H: Close-up photographs showing a cross section through the flow front with finger instabilities. Note the thin <1 cm thick fingers. I: Finger instabilities can transport large particles (pumices) at the front. (Breard & Lube, 2017)

The experiments of Breard and Lube (2017) show similar behaviours to the analogue experiments carried out for this thesis, suggesting that the results of the small-scale analogue experiments can be scaled up to a large-scale analogue experiments. The similarities also suggests that the materials used are displaying similar behaviours to the natural PDC material used in the PELE experiments which improves the reliability of the use of silica-glass ballotini beads in analogue experiments. Based on these similarities, as the PELE experiments can be scaled to natural PDCs it is possible to apply the findings of this study to natural PDCs.

The presence of the saltating large particles and fingers in the dense basal current of both large- and small-scale experiments suggests that these are key behaviours of the flow front. With eddies and instabilities in the overriding cloud key to the elutriation of fines and the interactions between the overriding cloud and basal current.

6.4.4.2 Ice and Snow Avalanches

Snow avalanches consist of cold, dry and cohesionless material which has variable material properties that can possibly change within the flow. Materials such as snow and ice within the flow consist of a range of grain sizes with frictional forces between the particles (Naaim et al., 2003). Due to these behaviours snow avalanches are a comparable dry granular flow to the analogue PDC experiments in this study, however they are not a complete analogue for PDCs as they lack the exsolution of gas, variations in methods of entrainment of air and different density particles.

Snow avalanches in Marmolada, Italy (03/07/22) consist of a dense basal layer with an overriding cloud of fines. The main flow head was dominated by fines with large particles travelling by saltation at the front of the current (Fig. 6.15a). As the flow propagated lobes were generated as pulses of material travelled through the current, with coarser particles travel along the surface of the current and fines escaping the flow into the overriding cloud (Fig. 6.15b) (Evolution Crisis, 2022).

Figure 6.15: (a) Photograph of the Marmolada avalanche showing snow traveling as a cloud and larger particles traveling by saltation. No scale available. (b) Photograph of the Marmolada avalanche showing the formation of lobes at the flow front. (c) Photograph of the avalanche in the Tian Shan mountains showing the overriding cloud of snow and saltating larger particles. (d) Photograph of the avalanche in the Tian Shan mountains showing the formation of lobes after surpassing a topographic barrier, lateral spreading once the avalanche is unconstrained and fines preceding the coarser particles (Evolution Crisis, 2022; Shimmin, 2022).

The snow avalanche in the Tian Shan Mountains, Kyrgyzstan (08/07/22) consisted of a single supply of material from an ice wall collapse with pulses of material forming as the current propagated. The main flow head was dominated by fines with large particles travelling by saltation at the front of the current and within the current (Fig. 6.15c). As the flow surpassed topographic barriers lobes were generated and fines escaped the flow into the overriding cloud. The current contained a range of grain sizes with fines forming a thin flow front ahead of the main body of the current (Fig. 6.15d) (Shimmin, 2022).

Snow avalanches display similar behaviours to the analogue granular flows, such as the generation of pulses and saltation of large particles. These similarities mean it is possible to use the observations to accurately interpret other large scale natural dry granular flows. Also, as the analogue flume displays similar side wall effects to valley constrained avalanches, we it is possible to infer that the flume displays some sidewall effects which were unexpected. These sidewall effects mean that these analogue experiments are best used to interpret valley constrained PDCs.

However, it is not possible to see if the avalanches reincorporated material into the flow as observed in this study. This prevents us for comparing the degree of reincorporation within the currents.

6.5 Other potential future work

Future topics of research have been identified throughout the chapter. On top of these potential topics of research previously identified there is a possibility for further work into the impact of fluidisation on the current mobility and deposition. Wilson (1980) created a classification system for the degree of fluidisation based on the deposits. In the deposits of this study, there are similar grading patterns suggesting similar degrees of fluidisation. This is expected as there was no variation in gas supply in this series of experiments. By repeating these experiments with varying gas supply, it is possible to investigate how accurate this classification system is and if the degree of fluidisation controls sorting patterns more than the grain size distribution.

6.6 Conclusions

This study aimed to investigate the mobility of PDCs and the role of grain size distribution has in controlling that mobility. This aim has two main focuses, first the mobility of PDCs, and secondly the relationship between the grain size distribution and the deposits. Mobility has been considered with regards to the current velocity and run-out distance. This study has shown that:

- Both the percentage of fines and initial current sorting control the run-out distance.
- The variation in the run-outs for currents with a 90% fines content shows that initial current sorting is more important than percentage of fines in controlling run-out. This means that the more well sorted currents have a greater run-out distance than the poorly sorted currents.
- The less well sorted currents have a greater velocity than the more well sorted currents. This means that initial current sorting is more important than percentage of fines in controlling bulk velocity.
- Percentage of fines is more important than initial current sorting in controlling the degree of non-uniformity (i.e., lateral variation in velocity) of the current velocity. Currents with a lower proportion of fines (i.e. quad-disperse) have more non-uniform velocities than mono-disperse currents.
- As mobility is a related to both run-out and velocity, both grain size distribution and the initial current sorting can be said to impact mobility.

Examining the deposits from currents with varying ranges of grain sizes has shown that:

- The phase diagrams of Smith et al. (2020) do not apply to poly-disperse currents. This suggests that lab and field deposit bedforms cannot currently be used to create accurate interpretations of current conditions using this system.
- Unsteadiness can cause variations of shear rate within the current. This controls the position of each grain size within the current.
- Controlling the position of each grain within the current, controls when each grain size reaches the FBZ to deposit. This influences the timing of deposition of the various grain sizes.

- Variations in time of deposition can create grading patterns within the deposits. Therefore, grading patterns in deposits do not necessarily indicate a waxing/waning current.
- Analogue experiments have provided evidence that deposition does not occur *en-masse* but is a combination of gradual and stepwise aggradation. The deposition in stepwise packages is also gradual not *en-masse.*
- Deposition of fines within the experimental currents from the overriding cloud shows a temporary cessation or sufficient waning for fall-out deposition. This indicates that for natural PDCs the co-ignimbrite cloud can be recorded in the deposit and does not necessarily indicate hiatus in eruptive activity.

References

Ancey, C. (2001) Dry granular flows down an inclined channel: Experimental investigations on the frictional-collisional regime. *Physical Review E*, 65(1), 011304. Available online: https://doi.org/10.1103/PhysRevE.65.011304.

Andrews, B. & Manga, M. (2011) Effects of topography on pyroclastic density current runout and formation of coignimbrites. *Geology*, 39(12), 1099–1102. Available online: https://doi.org/10.1130/g32226.1.

Andrews, B.J. (2019) Recognizing unsteadiness in the transport systems of dilute pyroclastic density currents. *Bulletin of Volcanology*, 81(2), 5. Available online: https://doi.org/10.1007/s00445-018-1266-5.

Arattano, M. & Marchi, L. (2008) Systems and Sensors for Debris-flow Monitoring and Warning. *Sensors*, 8(4). Available online: https://doi.org/10.3390/s8042436.

Auker, M.R., Sparks, R.S.J., Siebert, L., Crosweller, H.S. & Ewert, J. (2013) A statistical analysis of the global historical volcanic fatalities record. *Journal of Applied Volcanology 2013 2:1*, 2(1), 1–24. Available online: https://doi.org/10.1186/2191-5040-2-2.

Báez, W., de Silva, S., Chiodi, A., Bustos, E., Giordano, G., Arnosio, M., Suzaño, N., Viramonte, J.G., Norini, G. & Groppelli, G. (2020) Pulsating flow dynamics of sustained, forced pyroclastic density currents: insights from a facies analysis of the Campo de la Piedra Pómez ignimbrite, southern Puna, Argentina. *Bulletin of Volcanology*, 82(7), 53. Available online: https://doi.org/10.1007/s00445-020-01385-5.

Bareschino, P., Lirer, L., Marzocchella, A., Petrosino, P. & Salatino, P. (2008) Self-fluidization of subaerial rapid granular flows. *Powder Technology*, 182(3), 323–333. Available online: https://doi.org/10.1016/J.POWTEC.2007.12.010.

Bernard, J., Kelfoun, K., Le Pennec, J.-L. & Vallejo Vargas, S. (2014) Pyroclastic flow erosion and bulking processes: comparing field-based vs. modeling results at Tungurahua volcano, Ecuador. *Bulletin of Volcanology*, 76(9), 858. Available online: https://doi.org/10.1007/s00445-014-0858-y.

Blott, S.J. & Pye, K. (2001) GRADISTAT: a grain size distribution and statistics package for the analysis of unconsolidated sediments. *Earth Surface Processes and Landforms*, 26(11), 1237–1248. Available online: https://doi.org/10.1002/ESP.261.

Brand, B.D. & Clarke, A.B. (2009) The architecture, eruptive history, and evolution of the Table Rock Complex, Oregon: From a Surtseyan to an energetic maar eruption. *Models and Products of Mafic Explosive Activity*, 180(2), 203–224. Available online: https://doi.org/10.1016/j.jvolgeores.2008.10.011.

Brand, B.D., Mackaman-Lofland, C., Pollock, N.M., Bendaña, S., Dawson, B. & Wichgers, P. (2014) Dynamics of pyroclastic density currents: Conditions that promote substrate erosion and self-channelization — Mount St Helens, Washington (USA). *Journal of Volcanology and Geothermal Research*, 276, 189–214. Available online: https://doi.org/10.1016/J.JVOLGEORES.2014.01.007.

Branney, M.J. & Kokelaar, P. (1992) A reappraisal of ignimbrite emplacement: progressive aggradation and changes from particulate to non-particulate flow during emplacement of high-grade ignimbrite. *Bulletin of Volcanology 1992 54:6*, 54(6), 504–520. Available online: https://doi.org/10.1007/BF00301396.

Branney, M.J. & Kokelaar, P. (2002) *Pyroclastic Density Currents and the Sedimentation of Ignimbrites*. London: Geological Society of London.

Branney, M.P. & Kokelaar, P. (1997) Giant bed from a sustained catastrophic density current flowing over topography: Acatlán ignimbrite, Mexico. *Geology*, 25(2), 115–118. Available online: https://doi.org/10.1130/0091-7613(1997)025<0115:GBFASC>2.3.CO;2.

Breard, E.C.P., Dufek, J. & Roche, O. (2019) Continuum Modeling of Pressure-Balanced and Fluidized Granular Flows in 2-D: Comparison With Glass Bead Experiments and Implications for Concentrated Pyroclastic Density Currents. *Journal of Geophysical Research: Solid Earth*, 124(6), 5557–5583. Available online: https://doi.org/10.1029/2018JB016874.

Breard, E.C.P. & Lube, G. (2017) Inside pyroclastic density currents – uncovering the enigmatic flow structure and transport behaviour in large-scale experiments. *Earth and Planetary Science Letters*, 458, 22–36. Available online: https://doi.org/10.1016/J.EPSL.2016.10.016.

Breard, E.C.P., Lube, G., Jones, J.R., Dufek, J., Cronin, S.J., Valentine, G.A. & Moebis, A. (2016) Coupling of turbulent and non-turbulent flow regimes within pyroclastic density currents. *Nature Geoscience 2016 9:10*, 9(10), 767–771. Available online: https://doi.org/10.1038/ngeo2794.

Brown, R.J. & Branney, M.J. (2004) Event-stratigraphy of a caldera-forming ignimbrite eruption on Tenerife: the 273 ka Poris Formation. *Bulletin of Volcanology*, 66(5), 392–416. Available online: https://doi.org/10.1007/s00445-003-0321-y.

Brown, R.J. & Branney, M.J. (2013) Internal flow variations and diachronous sedimentation within extensive, sustained, density-stratified pyroclastic density currents flowing down gentle slopes, as revealed by the internal architectures of ignimbrites on Tenerife. *Bulletin of Volcanology 2013 75:7*, 75(7), 1–24. Available online: https://doi.org/10.1007/S00445-013-0727-0.

Bursik, M.I. & Woods, A.W. (1996) The dynamics and thermodynamics of large ash flows. *Bulletin of Volcanology 1996 58:2*, 58(2), 175–193. Available online: https://doi.org/10.1007/S004450050134.

Cagnoli, B. & Manga, M. (2005) Vertical segregation in granular mass flows: A shear cell study. *Geophysical Research Letters*, 32(10), 1–4. Available online: https://doi.org/10.1029/2005GL023165.

Cagnoli, B. & Romano, G.P. (2010) Effect of grain size on mobility of dry granular flows of angular rock fragments: An experimental determination. *Journal of Volcanology and Geothermal Research*, 193(1–2), 18–24. Available online: https://doi.org/10.1016/J.JVOLGEORES.2010.03.003.

Cagnoli, B. & Romano, G.P. (2012) Effects of flow volume and grain size on mobility of dry granular flows of angular rock fragments: A functional relationship of scaling parameters. *Journal of Geophysical Research: Solid Earth*, 117(B2), 2207. Available online: https://doi.org/10.1029/2011JB008926.

Calder, E.S., Cole, P.D., Dade, W.B., Druitt, T.H., Hoblitt, R.P., Huppert, H.E., Ritchie, L., Sparks, R.S.J. & Young, S.R. (1999) Mobility of pyroclastic flows and surges at the Soufriere Hills Volcano, Montserrat. *Geophysical Research Letters*, 26(5), 537–540. Available online: https://doi.org/10.1029/1999GL900051.

Calder, E.S., Sparks, R.S.J. & Gardeweg, M.C. (2000) Erosion, transport and segregation of pumice and lithic clasts in pyroclastic flows inferred from ignimbrite at Lascar Volcano, Chile. *Journal of Volcanology and Geothermal Research*, 104(1), 201–235. Available online: https://doi.org/10.1016/S0377-0273(00)00207-9.

Carn, S.A., Watts, R.B., Thompson, G. & Norton, G.E. (2004) Anatomy of a lava dome collapse: the 20 March 2000 event at Soufrière Hills Volcano, Montserrat. *Journal of Volcanology and Geothermal Research*, 131(3–4), 241–264. Available online: https://doi.org/10.1016/S0377-0273(03)00364-0.

Cas, R.A.F., Wright, H.M.N., Folkes, C.B., Lesti, C., Porreca, M., Giordano, G. & Viramonte, J.G. (2011) The flow dynamics of an extremely large volume pyroclastic flow, the 2.08-Ma Cerro Galán Ignimbrite, NW Argentina, and comparison with other flow types. *Bulletin of Volcanology*, 73(10), 1583–1609. Available online: https://doi.org/10.1007/S00445-011-0564-Y/FIGURES/9.

Cas, R.A.F. & Wright, J.V. (1987) *Volcanic successions, modern and ancient: a geological approach to processes, products, and successions*. London: Allen & Unwin.

Charbonnier, S.J. & Gertisser, R. (2011) Deposit architecture and dynamics of the 2006 block-and-ash flows of Merapi Volcano, Java, Indonesia. *Sedimentology*, 58(6), 1573–1612. Available online: https://doi.org/10.1111/J.1365-3091.2011.01226.X.

Chedeville, C. & Roche, O. (2014) Autofluidization of pyroclastic flows propagating on rough substrates as shown by laboratory experiments. *Journal of Geophysical Research: Solid Earth*, 119(3), 1764–1776. Available online: https://doi.org/10.1002/2013JB010554.

Clarke, B.A., Tierz, P., Calder, E.S. & Yirgu, G. (2020) Probabilistic Volcanic Hazard Assessment for Pyroclastic Density Currents From Pumice Cone Eruptions at Aluto Volcano, Ethiopia. *Frontiers in Earth Science*, 0, 348. Available online: https://doi.org/10.3389/FEART.2020.00348.

Cole, P.D. (1991) Migration direction of sand-wave structures in pyroclastic-surge deposits: Implications for depositional processes. *Geology*, 19(11), 1108. Available online: https://doi.org/10.1130/0091-7613(1991)019<1108:MDOSWS>2.3.CO;2.

Collins, G.S. & Melosh, H.J. (2003) Acoustic fluidization and the extraordinary mobility of sturzstroms. *Journal of Geophysical Research: Solid Earth*, 108(B10). Available online: https://doi.org/10.1029/2003JB002465.

Criswell, C.W. (1987) Chronology and pyroclastic stratigraphy of the May 18, 1980, Eruption of Mount St. Helens, Washington. *Journal of Geophysical Research: Solid Earth*, 92(B10), 10237–10266. Available online: https://doi.org/10.1029/JB092IB10P10237.

Dade, W.B. & Huppert, H.E. (1996) Emplacement of the Taupo ignimbrite by a dilute turbulent flow. *Nature 1996 381:6582*, 381(6582), 509–512. Available online: https://doi.org/10.1038/381509a0.

Dade, W.B. & Huppert, H.E. (1998) Long-runout rockfalls. *Geology*, 26(9), 803–806. Available online: https://doi.org/10.1130/0091-7613(1998)026<0803:LRR>2.3.CO;2.

Deal, E., Venditti, J.G., Benavides, S.J., Bradley, R., Zhang, Q., Kamrin, K. & Perron, J.T. (2021) Grain shape effects in bed load sediment transport. *EarthArXiv* [Preprint]. Available online: https://doi.org/10.31223/X55033.

Delannay, R., Valance, A., Mangeney, A., Roche, O. & Richard, P. (2017) Granular and particle-laden flows: from laboratory experiments to field observations. *Journal of Physics D: Applied Physics*, 50(5), 053001. Available online: https://doi.org/10.1088/1361-6463/50/5/053001.

Dellino, P., Dioguardi, F., Doronzo, D.M. & Mele, D. (2020) A discriminatory diagram of massive versus stratified deposits based on the sedimentation and bedload transportation rates. Experimental investigation and application to pyroclastic density currents. *Sedimentology*, 67(4), 2013–2039. Available online: https://doi.org/10.1111/SED.12693.

Douillet, G.A., Bernard, B., Bouysson, M., Chaffaut, Q., Dingwell, D.B., Gegg, L., Hoelscher, I., Kueppers, U., Mato, C., Ritz, V.A., Schlunegger, F. & Witting, P. (2019) Pyroclastic dune bedforms: macroscale structures and lateral variations. Examples from the 2006 pyroclastic currents at Tungurahua (Ecuador). *Sedimentology*, 66(5), 1531–1559. Available online: https://doi.org/10.1111/sed.12542.

Douillet, G.A., Pacheco, D.A., Kueppers, U., Letort, J., Tsang-Hin-Sun, È., Bustillos, J., Hall, M., Ramón, P. & Dingwell, D.B. (2013) Dune bedforms produced by dilute pyroclastic density currents from the August 2006 eruption of Tungurahua volcano, Ecuador. *Bulletin of Volcanology*, 75(11), 1–20. Available online: https://doi.org/10.1007/S00445-013-0762-X/FIGURES/12.

Dowey, N. & Williams, R. (2022) Simultaneous fall and flow during pyroclastic eruptions: A novel proximal hybrid facies. *Geology* [Preprint]. Available online: https://doi.org/10.1130/G50169.1.

Druitt, T.H. (1998) Pyroclastic Density Currents. In Gilbert, J.S. & Sparks. R.S.J. (eds) *The Physics of Explosive Volcanic Eruptions*. London: Geological Society, 145–182.

Druitt, T.H., Avard, G., Bruni, G., Lettieri, P. & Maez, F. (2007) Gas retention in fine-grained pyroclastic flow materials at high temperatures. *Bulletin of Volcanology 2007 69:8*, 69(8), 881–901. Available online: https://doi.org/10.1007/S00445-007-0116-7.

Druitt, T.H., Bruni, G., Lettieri, P. & Yates, J.G. (2004) The fluidization behaviour of ignimbrite at high temperature and with mechanical agitation. *Geophysical Research Letters*, 31(2). Available online: https://doi.org/10.1029/2003GL018593.

Dufek, J. (2016) The Fluid Mechanics of Pyroclastic Density Currents. *Annual Review of Fluid Mechanics*, 48, 459–485. Available online: https://doi.org/10.1146/ANNUREV-FLUID-122414-034252.

Dufek, J. & Bergantz, G.W. (2007) Suspended load and bed-load transport of particle-laden gravity currents: the role of particle–bed interaction. *Theoretical and Computational Fluid Dynamics 2007 21:2*, 21(2), 119–145. Available online: https://doi.org/10.1007/S00162-007-0041-6.

Dufek, J. & Manga, M. (2008) In situ production of ash in pyroclastic flows. *Journal of Geophysical Research: Solid Earth*, 113(B9). Available online: https://doi.org/10.1029/2007JB005555.

Esposti Ongaro, T., Komorowski, J.-C., Legendre, Y. & Neri, A. (2020) Modelling pyroclastic density currents from a subplinian eruption at La Soufrière de Guadeloupe (West Indies, France). *Bulletin of Volcanology 2020 82:12*, 82(12), 1–26. Available online: https://doi.org/10.1007/S00445-020-01411-6.

Evolution Crisis (2022) *Avalanche in Italian Marmolada mountain due glacier collapse*. Available online: https://youtu.be/JeDNh7GvWy4.

Fenner, C.N. (1923) *The origin and mode of emplacement of the great tuff deposit of the Valley of Ten Thousand Smokes*. Geophysical Laboratory, Carnegie Institution of Washington.

Fisher, R.V. (1966) Mechanism of deposition from pyroclastic flows. *American Journal of Science*, 264(5), 350–363. Available online: https://doi.org/10.2475/ajs.264.5.350.

Fisher, R.V., Orsi, G., Ort, M. & Heiken, G. (1993) Mobility of a large-volume pyroclastic flow — emplacement of the Campanian ignimbrite, Italy. *Journal of Volcanology and Geothermal Research*, 56(3), 205–220. Available online: https://doi.org/10.1016/0377-0273(93)90017-L.

Fisher, R.V. & Schmincke, H. (1984) *Pyroclastic rocks*. 1st edition. Berlin, Heidelberg: Springer Berlin, Heidelberg.

Flemming, B.W. (2000) The role of grain size, water depth and flow velocity as scaling factors controlling the size of subaqueous dunes. In Trentesaux, A. & Garlan, T. (eds) *Proceedings, Marine Sandwave Dynamics, International Workshop, March 23-24 2000, University of Lille 1, France*. Lille, 55–60.

Francis, P.W. & Baker, M.C.W. (1977) Mobility of pyroclastic flows. *Nature*, 270(5633), 164–165. Available online: https://doi.org/10.1038/270164a0.

Gaffney, E.S. & Melosh, H.J. (1982) Noise and target strength degradation accompanying shallow-buried explosions. *Journal of Geophysical Research: Solid Earth*, 87(B3), 1871–1879. Available online: https://doi.org/10.1029/JB087IB03P01871.

Gajjar, P., Vaart, K. van der, Thornton, A.R., Johnson, C.G., Ancey, C. & Gray, J.M.N.T. (2016) Asymmetric breaking size-segregation waves in dense granular free-surface flows. *Journal of Fluid Mechanics*, 794, 460–505. Available online: https://doi.org/10.1017/JFM.2016.170.

Geldart, D. (1973) Types of gas fluidization. *Powder Technology*, 7(5), 285–292. Available online: https://doi.org/10.1016/0032-5910(73)80037-3.

Gilbertson, M.A. (2019) Estimation of the minimum fluidisation velocities in well-mixed bi-disperse fluidised beds. *Powder Technology*, 346, 433–440. Available online: https://doi.org/10.1016/J.POWTEC.2019.02.019.

Gilbertson, M.A. & Eames, I. (2003) The influence of particle size on the flow of fluidised powders. *Powder Technology*, 131(2–3), 197–205. Available online: https://doi.org/10.1016/S0032-5910(02)00343-1.

Giordano, G. & Cas, R.A.F. (2021) Classification of ignimbrites and their eruptions. *Earth-Science Reviews*, 220, 103697. Available online: https://doi.org/10.1016/j.earscirev.2021.103697.

Giordano, G., Porreca, M., Musacchio, P. & Mattei, M. (2008) The Holocene Secche di Lazzaro phreatomagmatic succession (Stromboli, Italy): evidence of pyroclastic density current origin deduced by facies analysis and AMS flow directions. *Bulletin of Volcanology*, 70(10), 1221–1236. Available online: https://doi.org/10.1007/s00445-008-0198-x.

Hayashi, J.N. & Self, S. (1992) A comparison of pyroclastic flow and debris avalanche mobility. *Journal of Geophysical Research: Solid Earth*, 97(B6), 9063–9071. Available online: https://doi.org/10.1029/92JB00173.

Hibert, C., Mangeney, A., Grandjean, G. & Shapiro, N.M. (2011) Slope instabilities in Dolomieu crater, Réunion Island: From seismic signals to rockfall characteristics. *Journal of Geophysical Research*, 116(F4). Available online: https://doi.org/10.1029/2011JF002038.

Iverson, R.M., Costa, J.E. & LaHusen, R.G. (1992) *Debris-flow flume at H. J. Andrews Experimental Forest, Oregon*. U.S. Geological Survey, Dept. of the Interior.

Kieffer, S.W. (1981) Fluid Dynamics of the May 18 Blast at Mount St. Helens. In Lipman, P.W. & Mullineaux, D.R. (eds) *The 1980 Eruptions of Mount St. Helens, Washington. U.S. Geological Survey Professional Paper*. Washington D.C.: University of Washington Press, 379–400.

Kokelaar, B.P., Graham, R.L., Gray, J.M.N.T. & Vallance, J.W. (2014) Fine-grained linings of leveed channels facilitate runout of granular flows. *Earth and Planetary Science Letters*, 385, 172–180. Available online: https://doi.org/10.1016/J.EPSL.2013.10.043.

Legros, F. & Kelfoun, K. (2000) On the ability of pyroclastic flows to scale topographic obstacles. *Journal of Volcanology and Geothermal Research*, 98(1), 235–241. Available online: https://doi.org/10.1016/S0377-0273(99)00184-5.

Levy, C., Mangeney, A., Bonilla, F., Hibert, C., Calder, E.S. & Smith, P.J. (2015) Friction weakening in granular flows deduced from seismic records at the Soufrière Hills Volcano, Montserrat. *Journal of Geophysical Research: Solid Earth*, 120(11). Available online: https://doi.org/10.1002/2015JB012151.

Loughlin, S.C., Baxter, P.J., Aspinall, W.P., Darroux, B., Harford, C.L. & Miller, A.D. (2002) Eyewitness accounts of the 25 June 1997 pyroclastic flows and surges at Soufrière Hills Volcano, Montserrat, and implications for disaster mitigation. *Geological Society, London, Memoirs*, 21(1), 211–230. Available online: https://doi.org/10.1144/GSL.MEM.2002.021.01.10.

Lube, G., Breard, E.C.P., Cronin, S.J. & Jones, J. (2015) Synthesizing large-scale pyroclastic flows: Experimental design, scaling, and first results from PELE. *Journal of Geophysical Research: Solid Earth*, 120(3), 1487–1502. Available online: https://doi.org/10.1002/2014JB011666.

Lube, G., Cronin, S.J., Platz, T., Freundt, A., Procter, J.N., Henderson, C. & Sheridan, M.F. (2007) Flow and deposition of pyroclastic granular flows: A type example from the 1975 Ngauruhoe eruption, New Zealand. *Journal of Volcanology and Geothermal Research*, 161(3), 165–186. Available online: https://doi.org/10.1016/J.JVOLGEORES.2006.12.003.

Lucas, A. & Mangeney, A. (2007) Mobility and topographic effects for large Valles Marineris landslides on Mars. *Geophysical Research Letters*, 34(10). Available online: https://doi.org/10.1029/2007GL029835.

Malin, M.C. & Sheridan, M.F. (1982) Computer-Assisted Mapping of Pyroclastic Surges. *Science*, 217(4560), 637–640. Available online: https://doi.org/10.1126/SCIENCE.217.4560.637.

Manga, M., Patel, A. & Dufek, J. (2011) Rounding of pumice clasts during transport: Field measurements and laboratory studies. *Bulletin of Volcanology*, 73(3), 321–333. Available online: https://doi.org/10.1007/S00445-010-0411-6/FIGURES/12.

McCoy, S.W., Tucker, G.E., Kean, J.W. & Coe, J.A. (2013) Field measurement of basal forces generated by erosive debris flows. *Journal of Geophysical Research: Earth Surface*, 118(2), 589–602. Available online: https://doi.org/10.1002/JGRF.20041.

Miller, T.P. & Smith, R.L. (1977) Spectacular mobility of ash flows around Aniakchak and Fisher calderas, Alaska. *Geology*, 5(3), 173–176. Available online: https://doi.org/10.1130/0091-7613(1977)5<173:SMOAFA>2.0.CO;2.

Murai, I. (1961) A Study of the Textural Characteristics of Pyroclastic Flow Deposits in Japan. *Bulletin of the Earthquake Research Institute*, 39(2), 133–253.

Naaim, M., Faug, T. & Naaim-Bouvet, F. (2003) Dry Granular Flow Modelling Including Erosion and Deposition. *Surveys in Geophysics 2003 24:5*, 24(5), 569–585. Available online: https://doi.org/10.1023/B:GEOP.0000006083.47240.4C.

Newhall, C.G. & Punongbayan, R. (eds) (1996) *Fire and mud: eruptions and lahars of Mount Pinatubo, Philippines*. Quezon City: Philippine Institute of Volcanology and Seismology.

Pacheco-Hoyos, J.G., Aguirre-Díaz, G.J. & Dávila-Harris, P. (2020) Elutriation pipes in ignimbrites: An analysis of concepts based on the Huichapan Ignimbrite, Mexico. *Journal of Volcanology and Geothermal Research*, 403, 107026. Available online: https://doi.org/10.1016/J.JVOLGEORES.2020.107026.

Palladino, D.M. & Giordano, G. (2019) On the mobility of pyroclastic currents in light of deposit thickness and clast size trends. *Journal of Volcanology and Geothermal Research*, 384, 64–74. Available online: https://doi.org/10.1016/J.JVOLGEORES.2019.07.014.

Ripepe, M., De Angelis, S., Lacanna, G., Poggi, P., Williams, C., Marchetti, E., Donne, D.D. & Ulivieri, G. (2009) Tracking Pyroclastic Flows at Soufrière Hills Volcano. *Eos, Transactions American Geophysical Union*, 90(27). Available online: https://doi.org/10.1029/2009EO270001.

Risica, G., Rosi, M., Pistolesi, M., Speranza, F. & Branney, M.J. (2022) Deposit-Derived Block-and-Ash Flows: The Hazard Posed by Perched Temporary Tephra Accumulations on Volcanoes; 2018 Fuego Disaster, Guatemala. *Journal of Geophysical Research: Solid Earth*, 127(6), e2021JB023699. Available online: https://doi.org/10.1029/2021JB023699.

Roche, O. (2012) Depositional processes and gas pore pressure in pyroclastic flows: an experimental perspective. *Bulletin of Volcanology*, 74(8), 1807–1820. Available online: https://doi.org/10.1007/s00445-012-0639-4.

Roche, O., Azzaoui, N. & Guillin, A. (2021) Discharge rate of explosive volcanic eruption controls runout distance of pyroclastic density currents. *Earth and Planetary Science Letters*, 568. Available online: https://doi.org/10.1016/j.epsl.2021.117017.

Roche, O., Buesch, D.C. & Valentine, G.A. (2016) Slow-moving and far-travelled dense pyroclastic flows during the Peach Spring super-eruption. *Nature Communications*, 7(1), 10890. Available online: https://doi.org/10.1038/ncomms10890.

Roche, O., Gilbertson, M.A., Phillips, J.C. & Sparks, S.S.J. (2004) Experimental study of gas-fluidized granular flows with implications for pyroclastic flow emplacement. *Journal of Geophysical Research: Solid Earth*, 109(10). Available online: https://doi.org/10.1029/2003JB002916.

Roche, O., Montserrat, S., Niño, Y. & Tamburrino, A. (2008) Experimental observations of water-like behavior of initially fluidized, dam break granular flows and their relevance for

the propagation of ash-rich pyroclastic flows. *Journal of Geophysical Research: Solid Earth*, 113(B12), 12203. Available online: https://doi.org/10.1029/2008JB005664.

Roche, O., Montserrat, S., Niño, Y. & Tamburrino, A. (2010) Pore fluid pressure and internal kinematics of gravitational laboratory air-particle flows: Insights into the emplacement dynamics of pyroclastic flows. *Journal of Geophysical Research: Solid Earth*, 115(B9). Available online: https://doi.org/10.1029/2009JB007133.

Rowley, P. (2010) *Analogue modelling of pyroclastic density current deposition*. Royal Holloway, University of London. Available online: https://pure.royalholloway.ac.uk/portal/en/publications/analogue-modelling-of-pyroclastic-density-current-deposition(a6f4b96b-805d-42f2-8e81-5c352cef78f6).html [Accessed 29/09/2021].

Rowley, P.J., Kokelaar, P., Menzies, M. & Waltham, D. (2011) Shear-Derived Mixing in Dense Granular Flows. *Journal of Sedimentary Research*, 81, 874–884. Available online: https://doi.org/10.2110/jsr.2011.72.

Rowley, P.J., Roche, O., Druitt, T.H. & Cas, R. (2014) Experimental study of dense pyroclastic density currents using sustained, gas-fluidized granular flows. *Bulletin of Volcanology*, 76(9), 1–13. Available online: https://doi.org/10.1007/S00445-014-0855-1.

Savage, S.B. & Lun, C.K.K. (1988) Particle size segregation in inclined chute flow of dry cohesionless granular solids. *Journal of Fluid Mechanics*, 189, 311–335. Available online: https://doi.org/10.1017/S002211208800103X.

Schellart, W.P. (2000) Shear test results for cohesion and friction coefficients for different granular materials: scaling implications for their usage in analogue modelling. *Tectonophysics*, 324(1–2), 1–16. Available online: https://doi.org/10.1016/S0040-1951(00)00111-6.

Schmincke, H., Fisher, R.V. & Waters, A.C. (1973) Antidune and chute and pool structures in the base surge deposits of the Laacher See area, Germany. *Sedimentology*, 20(4), 553–574. Available online: https://doi.org/10.1111/J.1365-3091.1973.TB01632.X.

Schneider, C.A., Rasband, W.S. & Eliceiri, K.W. (2012) NIH Image to ImageJ: 25 years of image analysis. *Nature Methods*, 9(7), 671–675. Available online: https://doi.org/10.1038/nmeth.2089.

Schwarzkopf, L.M., Spieler, O., Scheu, B. & Dingwell, D.B. (2006) Fall-experiments on Merapi basaltic andesite and constraints on the generation of pyroclastic surges. *EEarth Discussions*, 1(2), 81–96.

Shimmin, H. (2022) *9 Brits and 1 American on a guided tour of the Tian Shan mountains in Kyrgyzstan... Instagram*. Available online: https://www.instagram.com/p/CfyT6xcA27D/?igshid=YmMyMTA2M2Y%3D&fbclid=IwAR07UwSFRSV-8z7iBl4s8PX_mD-Qz--SKLy-00s37YJt2Zu6f6PfX-qw-iw.

Smith, G. (2020) *Propagation of Aerated Pyroclastic Density Current Analogues: Flow Behaviour and the Formation of Bedforms and Deposits*. University of Hull.

Smith, G., Rowley, P., Williams, R., Giordano, G., Trolese, M., Silleni, A., Parsons, D.R. & Capon, S. (2020) A bedform phase diagram for dense granular currents. *Nature Communications*, 11(1), 1–11. Available online: https://doi.org/10.1038/s41467-020-16657-z.

Smith, G., Williams, R., Rowley, P. & Parsons, D. (2018) Investigation of variable aeration of monodisperse mixtures: implications for pyroclastic density currents. *Bulletin of Volcanology 2018 80:8*, 80(8), 1–12. Available online: https://doi.org/10.1007/S00445-018-1241-1.

Smith, N.J. & Kokelaar, B.P. (2013) Proximal record of the 273 ka Poris caldera-forming eruption, Las Cañadas, Tenerife. *Bulletin of Volcanology*, 75(11), 768. Available online: https://doi.org/10.1007/s00445-013-0768-4.

Smith, R.L. (1960) Ash Flows. *GSA Bulletin*, 71(6), 795–841. Available online: https://doi.org/10.1130/0016-7606(1960)71[795:AF]2.0.CO;2.

Sohn, Y.K. & Chough, S.K. (1993) The Udo tuff cone, Cheju Island, South Korea: transformation of pyroclastic fall into debris fall and grain flow on a steep volcanic cone slope. *Sedimentology*, 40(4), 769–786. Available online: https://doi.org/10.1111/j.1365-3091.1993.tb01359.x.

Sparks, R.S.J. (1976) Grain size variations in ignimbrites and implications for the transport of pyroclastic flows. *Sedimentology*, 23(2), 147–188. Available online: https://doi.org/10.1111/J.1365-3091.1976.TB00045.X.

Sparks, R.S.J., Self, S. & Walker, G.P.L. (1973) Products of Ignimbrite Eruptions. *Geology*, 1(3), 115–118. Available online: https://doi.org/10.1130/0091-7613(1973)1<115:POIE>2.0.CO;2.

Staron, L. & Lajeunesse, E. (2009) Understanding how volume affects the mobility of dry debris flows. *Geophysical Research Letters*, 36(12). Available online: https://doi.org/10.1029/2009GL038229.

Staudt, F., Mullarney, J.C., Pilditch, C.A. & Huhn, K. (2017) The role of grain-size ratio in the mobility of mixed granular beds. *Geomorphology*, 278, 314–328. Available online: https://doi.org/10.1016/J.GEOMORPH.2016.11.015.

Sulpizio, R., Dellino, P., Doronzo, D.M. & Sarocchi, D. (2014) Pyroclastic density currents: state of the art and perspectives. *Journal of Volcanology and Geothermal Research*, 283, 36–65. Available online: https://doi.org/10.1016/J.JVOLGEORES.2014.06.014.

Tanner, W.F. (1967) Ripple mark indices and their uses. *Sedimentology*, 9(2), 89–104. Available online: https://doi.org/10.1111/j.1365-3091.1967.tb01332.x.

Thornton, A.R., Gray, J.M.N.T. & Hogg, A.J. (2006) A three-phase mixture theory for particle size segregation in shallow granular free-surface flows. *Journal of Fluid Mechanics*, 550, 1–25. Available online: https://doi.org/10.1017/S0022112005007676.

Trolese, M., Cerminara, M., Esposti Ongaro, T. & Giordano, G. (2019) The footprint of column collapse regimes on pyroclastic flow temperatures and plume heights. *Nature Communications 2019 10:1*, 10(1), 1–10. Available online: https://doi.org/10.1038/s41467-019-10337-3.

Valentine, G.A. & Giannetti, B. (1995) Single pyroclastic beds deposited by simultaneous fallout and surge processes: Roccamonfina volcano, Italy. *Journal of Volcanology and Geothermal Research*, 64(1), 129–137. Available online: https://doi.org/10.1016/0377-0273(94)00049-M.

Vallance, J.W. & Savage, S.B. (2000) Particle Segregation in Granular Flows Down Chutes. In Rosato, A.D. & Blackmore, D.L. (eds). Cape May, NJ, U.S.A.: Springer, Dordrecht, 31–51. Available online: https://doi.org/10.1007/978-94-015-9498-1_3.

Walker, G.P.L. (1981) Generation and dispersal of fine ash and dust by volcanic eruptions. *Journal of Volcanology and Geothermal Research*, 11(1), 81–92. Available online: https://doi.org/10.1016/0377-0273(81)90077-9.

Walker, G.P.L. (1985) Origin of coarse lithic breccias near ignimbrite source vents. *Journal of Volcanology and Geothermal Research*, 25(1–2), 157–171. Available online: https://doi.org/10.1016/0377-0273(85)90010-1.

Wang, A., Marashdeh, Q., Teixeira, F.L. & Fan, L.-S. (2015) Applications of capacitance tomography in gas–solid fluidized bed systems. In *Industrial Tomography*. Elsevier, 529–549. Available online: https://doi.org/10.1016/B978-1-78242-118-4.00020-4.

Wilson, C.J.N. (1980) The role of fluidization in the emplacement of pyroclastic claws: An experimental approach. *Journal of Volcanology and Geothermal Research*, 8(2–4), 231–249. Available online: https://doi.org/10.1016/0377-0273(80)90106-7.

Wilson, C.J.N. (1985) The Taupo eruption, New Zealand. II. The Taupo Ignimbrite. *Philosophical Transactions of the Royal Society of London. Series A, Mathematical and Physical Sciences*, 314(1529), 229–310. Available online: https://doi.org/10.1098/RSTA.1985.0020.

Wohletz, K.H., Sheridan, M.F. & Brown, W.K. (1989) Particle size distributions and the sequential fragmentation/transport theory applied to volcanic ash. *Journal of Geophysical Research: Solid Earth*, 94(B11), 15703–15721. Available online: https://doi.org/10.1029/JB094IB11P15703.

Wright, J.V. & Walker, G.P.L. (1981) Eruption, transport and deposition of ignimbrite: A case study from Mexico. *Journal of Volcanology and Geothermal Research*, 9(2), 111–131. Available online: https://doi.org/10.1016/0377-0273(81)90001-9.

Yamasato, H., Kitagawa, S. & Komiya, M. (1998) Effect of rainfall on dacitic lava dome collapse at Unzen volcano, Japan. *Papers in Meteorology and Geophysics*, 48(3), 73–78. Available online: https://doi.org/10.2467/MRIPAPERS.48.73.

Yang, W.C. (2007) Modification and re-interpretation of Geldart's classification of powders. *Powder Technology*, 171(2), 69–74. Available online: https://doi.org/10.1016/J.POWTEC.2006.08.024.

Appendix I: Material information

Table I.1: Grain size data for each experiment carried out. Red indicates experiments which were discounted, see notes for reason

Mix Name	Experiment Number	Experiment Name	45-90 µm	125-355 µm	355-500 µm	500-710 µm	Notes
Quad-disperse	1	-	85	5	5	0	Prior to insertion of the impingement ramp
	2	-	85	5	5	0	
Fine bi-disperse	3	-	90	10	0	0	
	4	-	90	10	0	0	
	5	-	90	10	0	0	
	6	Chamber 1	90	10	0	0	
	7	-	90	10	0	0	Loss of gas supply to chambers 2 and 3
	8	Wide Angle	90	10	0	0	
Monodisperse	9	Wide Angle	100	0	0	0	
Coarse bi-disperse	10	Wide Angle	90	0	10	0	
	11	First Chamber	90	0	10	0	
	12	2nd first chamber	90	0	10	0	
Monodisperse	13	2nd Wide Angle	100	0	0	0	
Fine tri-disperse	14	Chamber one	90	5	5	0	
	15	2nd Chamber one	90	5	5	0	
	16	3rd Chamber one	90	5	5	0	
	17	Wide Angle	90	5	5	0	
Coarse tri-disperse	18	Wide Angle	80	10	10	0	
	19	Chamber one	80	10	10	0	
	20	2nd Chamber one	80	10	10	0	
	21	Close up of mid-chamber one	80	10	10	0	
Quad-disperse	22	First chamber	85	5	5	5	

	23	Close up of mid-chamber 1	85	5	5	5	
	24	Close up of chamber 1 end	85	5	5	5	
	25	Wide angle	85	5	5	5	

Appendix II: Current Descriptions

Monodisperse currents

Experiment 9

In this flow the initial flow head is very stable with an overriding plume generated as the material impinged on the baseplate. At 0.674 seconds the flow head is at 65cm along the flume, at 56 cm along the flume the basal layer is 0.6 cm thick and the overriding cloud is 11 cm thick. At 0.654 seconds the flow near the baseplate became unsteady and was followed by a 2nd pulse at approximately 46 cm along the flume.

Initial deposition starts at 1.15 seconds, with the formation of shallow backset beds around 70cm along the flume, initially through progressive aggradation then through regressive aggradation which causes rapid deposition. As the wedge aggrades at 1.226 seconds the deposit between 60 and 80 cm remobilises and travels 17 cm further.

Experiment 13

This current consists of a basal current and overriding cloud (formed at 0.14 seconds when the material impinged the ramp). When the flow head was at 55 cm along the flume (0.654 seconds) the overriding cloud detached from the head of the flow and the current became unsteady with waves and turbulence, where a pulse generates. This unsteadiness was followed by a second pulse in the current (0.7 seconds). Progressive aggradation of the deposit at the base of the ramp (at 0.696 seconds) is followed by greater unsteadiness in the current, shown by the turbulent waves and elutriation of fines into the overriding cloud. The newly-formed deposit at the base of the ramp at t = 0.844 seconds is thicker than the deposit at 4.00 seconds, once the current has stopped propagating.

Fine bi-disperse currents

Experiment 6

At 0.2 seconds a thicker stable flow follows the initial thin flow head with unsteadiness observed at 0.34 seconds at 57cm along the flume while the head of flow was at 70cm along the flume. After the main flow head a 2nd pulse follows at 0.39 seconds with a possible 3rd pulse at 0.516 seconds, which mixes with the 2nd pulse by 0.678 seconds.

There is a turbulent overriding cloud of fine particles which is approximately 46.4% thicker than the basal flow.

Initial deposition consists of regressive aggradation which becomes progressive aggradation forming from 0.76 seconds. With later deposition is mainly from fall out from overriding cloud forming shallow backset beds.

Experiment 8

In this current the overriding cloud generated very rapidly as the material impinged on the baseplate. The initial flow head was a few millimetres thick overtaken by a thicker pulse at 0.332 seconds, 60cm along the flume. Following this overtaking the current became turbulent with the flow head becoming unsteady, this turbulence ends at 0.44 seconds, 75cm along the flume, at the same time 50cm along the flume a second pulse generates following this unsteadiness. During the initial flow the overriding cloud reaches approximately 15cm high, whereas the basal layer is only 1cm thick.

At 0.502 seconds as the flow progresses, the head of the 2nd pulse reaches 57cm along the flume, while at 40cm along the flume the 2nd pulse becomes unsteady. At 0.538 seconds a 3rd pulse generates at 32 cm along the flume; at this point (0.66 seconds) the overriding cloud reaches height of 18.6cm.

Progressive aggradation is the most common method of deposition, however, at 1.08 seconds regressive aggradation begins to occur just after hopper at approximately 40cm along the flume.

Coarse bi-disperse currents

Experiment 10

In this current at 0.346 seconds when the current impinges on the base plate an overriding cloud is present. Between t = 0.346 seconds and t = 0.440 seconds the flow is steady after which the flow becomes unsteady with a pulse generating at t = 0.534 seconds. This pulse 'jumps' over the initial flow head at t = 0.584. Following this a second pulse of material generates at t = 0.604 seconds, at 0.680 seconds the head of the flow and second pulse become laminar and a third pulse is generated behind the second pulse. At 0.742 seconds the third pulse mixes in with the preceding flow and at t = 0.774 there is a package of coarser material which when it overruns the finer current forms a minor surge and elutriates into the overriding cloud. At 0.774 seconds there is progressive aggradation of the deposit at the end of the ramp (22 cm along the flume) which continues until 1.39 seconds when deposition is dominated by regressive aggradation from 40 cm along the flume. At 2.412 seconds there is some slight progressive aggradation of the last of the material which forms the uppermost deposit from this current.

Experiment 11

In this current the initial flow head is steady, followed by an unsteady 2nd pulse after 0.432 seconds. This unsteady pulse catches up with the initial flow head and becomes steady as it mixes, after 0.54 seconds. This results in a laminar flow with an overriding cloud of fine material. After 0.826 seconds, the flow then develops unsteadiness which is coeval with the generation of a 3rd pulse of material.

Experiment 12

In this current the initial flow head is steady but at 0.344 seconds 20cm from the flow head the flow becomes unsteady, this is followed at 0.39 seconds by the generation of a 2nd pulse which primarily consists of coarser material. Following this pulse, the flow becomes increasingly unsteady which is followed by the generation of a 3rd pulse, at 0.516 seconds, which contains waves where crests of finer material appear. Above the main body of the flow is an overriding cloud which carries more fines than before and shows greater turbulence.

After 0.75 seconds deposition starts at 70 cm along the flume with progressive aggradation of fine particles from fall out from suspension of the overriding cloud but as the deposit grows the overriding cloud cannot flow over the deposit and reverse aggradation occurs. This initial deposit from suspension is then followed by deposition form the basal layer of the flow.

Fine tri-disperse currents

Experiment 14

In this current the overriding cloud precedes the basal flow head. The initial flow head is steady with a thicker unsteady flow unit catching up with the flow head. In this unsteady thicker pulse, the fine particles travel faster than the coarse particles causing both vertical and lateral grading where initially the current is stratified.

Deposition occurred initially with the coarse particles depositing first with a less coarse mix flowing over the top. This flow behaviour leads to progressive aggradation, appearing as backset beds or regressive features.

Experiment 15

In this current the turbulent overriding cloud precedes flow head, which is stable and consists of fine material a few millimetres thick.

At 0.34 seconds, the current is unsteady 3cm from the flow head, this is followed by a coarse pulse at 0.354 seconds forming 10 cm behind the flow head. The flow initially shows some stratification and then as the pulse catches up with the flow head and the flow becomes unsteady mixing occurs and before the flow head is fully mixed and the underlying segregated fines are deposited. This unsteadiness continues and a pulse of fine material occurs at 0.502 seconds, 25cm from the flow head.

Deposition increases after 0.612 seconds at 70cm along the flume before growing towards 80cm and then after 0.69 seconds towards 60cm from 70cm, initially this deposition is of the fine basal layer while the coarse material flows over the deposit and eventually the coarse material progressively aggrades. After 0.784 seconds progressive aggradation occurs growing from 60cm along the flume towards 70 cm along the flume, here fine material flows over this progressively aggrading bedform, where deposition is mainly coarser material with some fines deposited.

Experiment 16

In this current at 0.356 seconds the overriding cloud preceded the flow head by 17 cm. The initial flow head, at 0.356 seconds, is 1 millimetre thick and fines rich. At 0.368 seconds, 1.85 cm behind the flow head the current becomes unsteady and is dominated by coarse material flowing in a similar way to experiment 14 with fines overrunning the coarser material. After 0.36 seconds of unsteadiness the current becomes steady again.

Deposition is primarily of coarser material with fine material continuing to flow, with the initial deposit forming backset beds which deposits around 70 cm before propagating forwards and backwards.

Experiment 17

In this current is laminar from 0.228 seconds until 0.330 seconds where unsteadiness develops at 30cm along the flume, however, at 0.432 seconds as the amount of material supplied increased the point where unsteadiness is generated moved towards 22cm where the ramp meets the baseplate.

An overriding cloud generates as the material falls and impinges on the baseplate at 0.21 seconds, this overriding cloud flows 4.07cm ahead of basal layer at 0.528 seconds.

Following the unsteadiness in the current particles formed “waves” that “jumped” over the main flow, at 0.468 seconds, and travelled 24.5cm before the fines are elutriated into the overriding cloud and coarser material falls back into basal layer, at 0.608 seconds.

At 0.652 seconds, a pulse of coarse material with a fine surface is generated, this pulse shows lateral grading with fines dominating the front of the pulse.

At 0.678 seconds as the current is highly unsteady, the fine particles were travelling faster than coarse particles which slowly moved as part of the wedge, this is causing regressive aggradation in the top layer of deposits from 40cm to 22cm. At 0.93 seconds the flow becomes laminar and stratified, with a coarse upper layer.

At 2.56 seconds, the last of the material falling from the hopper isn't mixing in the flow at all but fines are detaching forming an overriding cloud which is travelling over the stationary deposit to approximately 60cm.

Coarse tri-disperse currents

Experiment 18

In this current the overriding cloud was visible at 0.3 seconds as the material reaches the flume baseplate from the ramp. This turbulent overriding cloud grows in volume as the flow propagates and after flowing at 1.46 seconds, 50 cm along the flume, the detached cloud is reaching 17.9 cm above the base of the flume (13.8 cm above the top of the deposit and overriding current). After the basal part of the flow has stopped travelling the overriding cloud is still transporting the finest material.

At 0.472 seconds the flow became unsteady, 30cm along the flume. The material falling from the hopper then limited the motion of a large wedge of coarse material at the base of the ramp, after this the flow became more unsteady and is followed by 2 later pulses of material. The 2nd pulse of material, generated at 0.646 seconds, largely consists of coarse material, and the 3rd pulse of material, generated at 0.684 seconds, also largely consists of coarse material although there were fine particles causing lateral grading towards the head of the pulse, this was most visible after 1.008 seconds at 56 cm along the flume.

Experiment 19

In the current the initial flow head, at 0.172 seconds, is quasi-steady and shows as the flow propagates lateral and vertical normal grading occur. The initially coarse-grained flow head becomes gradually more unsteady, at 0.388 seconds, prior to deposition of the coarse particles and the fine particles continued to propagate as part of the flow.

At 0.516 seconds, the unsteadiness is followed by the generation of a 2nd pulse of coarse material with a turbulent overriding cloud of fine particles. This pulse overpasses the previous deposits and begins to progressively aggrade at 0.66 seconds, with coarser particles depositing first, this leads to vertical and lateral normal grading of the flow as coarser particles deposit first.

The fines rich flow then begins to aggrade forming a deposit that is 0.676cm thick; then the flow becomes richer in coarse particles again. This flow then progressively aggrades until the basal layer stops flowing after 1.65 seconds, where the 14.55cm thick turbulent overriding cloud continues to transport the finest materials along the flume.

Experiment 20

In the current the initial flow head was steady and consisted of fine material, with an overriding cloud 1cm behind the flow head, at 0.172 seconds. At 0.224 seconds, 8cm behind the steady flow head is an unsteady pulse of coarser material, the wavelength increases and the pulse appeared quasi-stable as the pulse overtook the initial flow head at 0.42 seconds, 83cm along the flume where the pulse 'jumps' over the flow head.

At 0.378 seconds, there is a quasi-steady and coarse particle rich 3rd pulse, which laterally grades with the head becoming rich in fine particles and absorbs into the previous pulse. Then at 0.528 seconds a 4th pulse appears with a dense overriding cloud 0.59cm thick hugging the basal layer and the less dense turbulent overriding cloud is 17.28cm thick. This pulse is dominated by a flow head rich in fine particles which is 0.68cm thick while the coarser parts of the flow are 0.39cm thick. The coarser material from the 4th pulse begins to progressively aggrade with the overriding cloud continuing faster than the

basal layer. Between 0.82 and 1.176 seconds the flow became stable flowing over the aggrading deposit, before the fines rich flow became unstable again at 1.176 seconds.

Experiment 21

In the flow at 0.104 seconds, the coarse grains (>355 µm) travelled by saltation and a cloud of fine particles (45-90 µm) that preceded the main flow head (consisting primarily of 500-710 µm particles in a matrix of fine material either 45-90 µm or 125-355 µm), which is highly unsteady and coarse rich at 0.206 seconds. The saltating particles are travelling approximately 8.21cm ahead of flow head, and the overriding cloud is travelling approximately 6.59cm ahead of the flow head; this suggest that these sparse outlier particles initially the coarser particles have a higher velocity than the fine particles.

The head of the flow is unstable and breaks up with the coarsest particles starting to saltate and finer particles begin to progressively aggrade. When this aggrading deposit is 1.13mm thick (at 0.30 seconds) the overrunning current to become more turbulent and unsteady, this then leads to rapid deposition and the thin deposit aggrades to 5.91mm thick.

Gradually aggrading beds, started depositing from the initial flow head at 0.176 seconds, show slight reverse grading as the lower most deposit in each bed consists of 45-90 µm particles which have fallen out of suspension and the coarser particles from the current deposit above these. A pulse of coarser material entrains fine particles from the surface of the deposited material (at 0.32 seconds). Fine particles also fall out of suspension into the pulse; and layers of fines are observed depositing between gradually aggrading coarse beds (at 0.38 to 0.76 seconds) resulting in reverse grading throughout the lower beds.

Gradually the basal layer energy decreases and most transport is in the highly turbulent overriding plume; however, a 1.97mm basal layer is still transporting and depositing material with most deposition appearing to come from the fallout of coarser particles in the plume above.

Quad-disperse currents

Experiment 22

The current initially contains a steady flow head with overriding cloud, with the body of the flow containing breaking waves 8 cm after the flow head. The breaking waves are followed by a pulse of coarser material 20 cm after the flow head (at 0.364 time), this pulse contains breaking waves with a larger overriding cloud than the initial flow head.

As the unsteady body of the flow overtakes the steady flow head and the pulse over runs the tail of the previous unsteady flow, there is progressive aggradation (from 0.74 seconds) forming a large 20 cm long bedform (63-83 cm) which starts off as a forward bed and becomes a backset bed as aggradation progresses. This aggradation then intensifies around 60cm before progressive aggradation occurs towards the end of the flume; while the deposit is aggrading the flow appears to be laminar with an overriding cloud of fines.

Experiment 23

Preceding the main flow head between 0.150 and 0.334 seconds transport of coarse grains entirely by saltation and there was a cloud of fine particles. These saltating particles have a vertical offset of 27.24 mm and the horizontal distance travelled is greater than 85 mm.

The initial flow head (0.154 seconds) is steady but slightly unstable with fines separating and elutriating into the overriding cloud and coarse grains saltating through the main flow. Greater than 12 cm after the initial flow head a denser pulse is generated; this pulse is unsteady and rich in fine

material, with some of the saltating particles entrained which made the pulse richer in coarser particles.

The deposit progressively aggrades (from 0.4 seconds) which is followed by the flow to becoming more turbulent. As the flow propagates fine particles fell out of suspension and were incorporated into the current. Some of these suspended particles also deposited forming beds of fine material between beds of coarser material from the current.

After this deposition the flow becomes more stable with the majority of transport occurring in the overriding cloud. A 3rd pulse is present, this is unstable and shows vertical stratification (fine base, coarse surface) with an overriding cloud 40.1 mm ahead of the pulse, that has the same shape as the flow. During this 3rd pulse between 0.84 seconds and 1 second, recirculation of coarse particles can be observed.

The flow then progressively aggrades before a 4th pulse is generated with lateral and vertical segregation, possibly fines rich due to fall out from overriding cloud; this flow is unstable and progressively aggrades.

Experiment 24

In the current, between 0.13 and 0.388 seconds, there was a very large flow of saltating particles. There were multiple grain sizes within the saltating particles where the coarser particles (500-710µm) tend to have a vertical offset of 24mm while the finer particles (125-335µm) have a vertical offset of at least 58.5mm, where they go out of frame. At 0.118 seconds the finest particles (45-90µm) formed an overriding cloud.

These saltating particles and overriding cloud is followed (0.388 seconds) by an unsteady flow head which entrains some of these coarser materials. This flow is fines rich showing lateral and vertical normal grading, and above the main flow body, the overriding cloud becomes larger and turbulent.

Following the initial unsteadiness in the current leads there is the generation of a 2nd pulse of material (at 0.554 seconds) which is unsteady and mainly consists of coarser materials, with the fine particles travelling faster than the coarser particles. As the flow propagates the flow then becomes laminar with a fast and turbulent overriding cloud.

Deposition of the flow begins with reverse aggradation and some deposition of fine particles falling out of suspension from overriding cloud. Once these backset beds had developed and formed a wedge the deposition became progressive.

Experiment 25

As the flow impinges on the baseplate of the flume an overriding cloud is generated. This overriding flow initially is in line with the highly unsteady and turbulent basal layer before preceding the flow by 2cm at 60cm along the flume and by 4cm at 66cm along the flume.

Following the initial unsteady flow 2 pulses are generated within the current. The 1st pulse generates at 0.41 seconds, 10cm behind the flow head, and the 2nd pulse generates at 0.478 seconds, 20cm behind the initial flow head, following the generation of unsteadiness in the 1st pulse. At this point the overriding cloud is fed directly from the hopper and is 11.74cm high from the top of the basal layer.

After the 2nd pulse, after 0.6 seconds, the flow shows vertical grading and becomes laminar. At 0.606 seconds the flow is 1.385cm thick and at 1.038 seconds the flow is 0.37cm thick as it flows over the deposit at 33cm along the flume (26.7% reduction in flow thickness).

Reverse aggradation occurs in the laminar flow and on the backwall there is some turbulence like experiment 14. As the deposit aggrades the flow over the deposit decreases to 12% of the previous flow thickness where the ramp meets the base (1.605cm to 0.197cm). As the reverse aggradation continues, the wedge at the beginning of the flume underneath the hopper becomes unstable and a laminar flow is generated leading to slight progressive aggradation.

Appendix IV: Videos

Table IV.1: Table providing the links to the high-speed video for each experiment described in Chapter 4

Experiment Number	Description	Link
6	Fine bi-disperse. Close up showing 60-100 cm	https://youtu.be/Jsbr5nC5A-8
8	Fine bi-disperse. Wide angle lens showing the first 130 cm	https://youtu.be/zciBtyi5DJw
9	Monodisperse. Wide angle lens showing the first 125 cm	https://youtu.be/ZGHY1VeMNF0
10	Coarse bi-disperse. Wide angle lens showing the first 130 cm	https://youtu.be/znitI2mjrJg
11	Coarse bi-disperse. Close up showing 60-100 cm	https://youtu.be/BvR9fgUkhc8
12	Coarse bi-disperse. Close up showing 60-100 cm	https://youtu.be/HxLy9GnnwzQ
13	Monodisperse current. Wide angle lens showing the first chamber	https://youtu.be/8qHl9bsUWKQ
14	Fine tri-disperse. Close up showing 60-100 cm	https://youtu.be/WbuLY2hKGvg
15	Fine tri-disperse. Close up showing 60-100 cm	https://youtu.be/J3MNzn-zwug
16	Fine tri-disperse. Close up showing 60-100 cm	https://youtu.be/05uUGjzji3g
17	Fine tri-disperse. Wide angle lens showing the first chamber	https://youtu.be/_9vA5bA7ZAc
18	Coarse tri-disperse. Wide angle lens showing the first chamber	https://youtu.be/GYHHeabk4E4
19	Coarse tri-disperse. Close up showing 60-100 cm	https://youtu.be/MT46MMO6JOs
20	Coarse tri-disperse. Close up showing 60-100 cm	https://youtu.be/2uYLYc0T2Hg
21	Coarse tri-disperse. Close up showing 40-50 cm	https://youtu.be/5QgdZfsKpck
22	Quad-disperse. Close up showing 60-100 cm	https://youtu.be/_sFrdIaeWCI
23	Quad-disperse. Close up showing 40-50 cm	https://youtu.be/MdTngx-pkXU
24	Quad-disperse. Close up showing 60-70 cm	https://youtu.be/dxD-PH5fe74

25	Quad-disperse. Wide angle lens showing the first chamber	https://youtu.be/OfISBFyXsog

Table IV.2: Table providing the links to the GoPro video for each experiment described in Chapter 4

Experiment Number	**Description**	**Link**
6	Fine bi-disperse	https://youtu.be/39s_1TiD4Xk
8	Fine bi-disperse	https://youtu.be/4LbuyYIHLn8
9	Monodisperse	https://youtu.be/ga5CX-vDUBs
10	Coarse bi-disperse	https://youtu.be/3RAiAseLfqk
11	Coarse bi-disperse	https://youtu.be/rEO5vBzgqRc
12	Coarse bi-disperse	https://youtu.be/pDh3UePDoaQ
13	Monodisperse current	https://youtu.be/HBS1BiVIyCc
14	Fine tri-disperse	https://youtu.be/-sSjA1ROQx0
15	Fine tri-disperse	https://youtu.be/_btv_UynlyA
16	Fine tri-disperse	https://youtu.be/Qjbq4kWxK3Y
17	Fine tri-disperse	https://youtu.be/H2kJGB--QMU
18	Coarse tri-disperse	https://youtu.be/vQJmbgiN7xU
19	Coarse tri-disperse	https://youtu.be/vv4veNCmAoM
20	Coarse tri-disperse	https://youtu.be/wgl9YbF9a5g
21	Coarse tri-disperse	https://youtu.be/z1rD8SLHyqM
22	Quad-disperse	https://youtu.be/FE2Q2uLxCJ8
23	Quad-disperse	https://youtu.be/DJ6GlvIHW04
24	Quad-disperse	https://youtu.be/7kjrbE8PwCA
25	Quad-disperse	https://youtu.be/0QT1_VuGfKg

Appendix V: Deposit Photographs

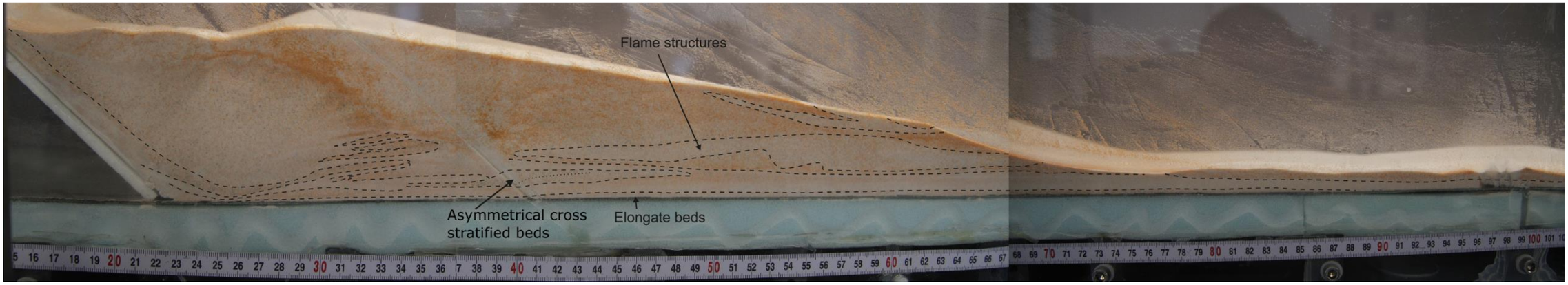

Figure V.16: The deposit from Experiment 8 – Fine bi-disperse current

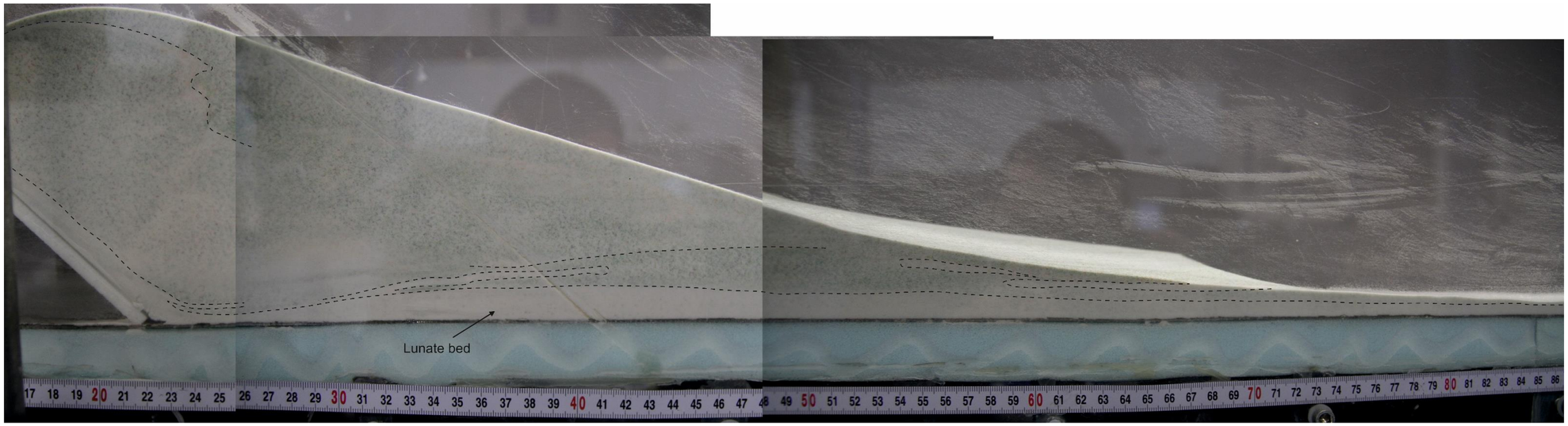

Figure V.17: The deposit from Experiment 10 – Coarse bi-disperse current

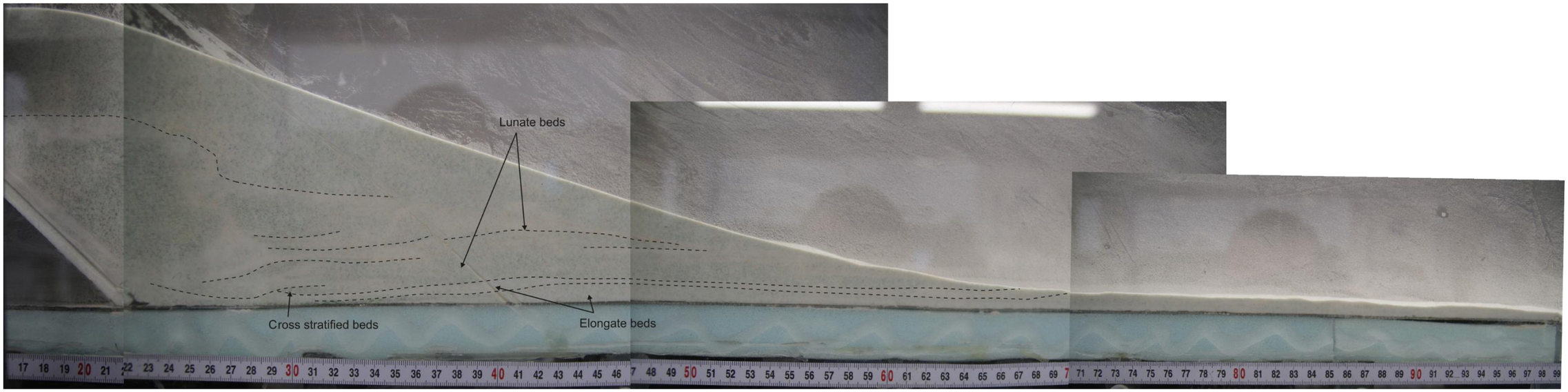

Figure V.18: Deposit from Experiment 11 – Coarse bi-disperse current

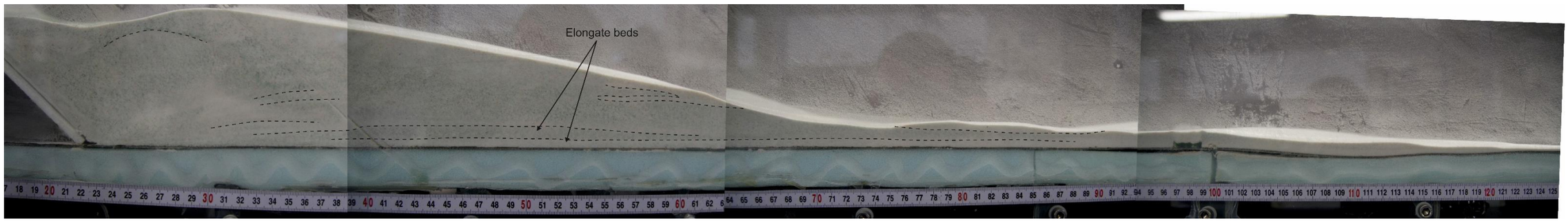

Figure V.19: Deposit from Experiment 12 – Coarse bi-disperse current

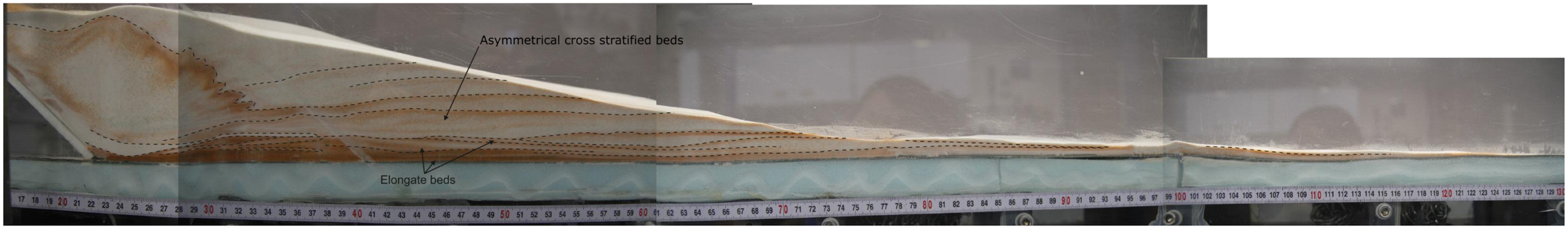

Figure V.20: Deposit from Experiment 14 – Fine tri-disperse current

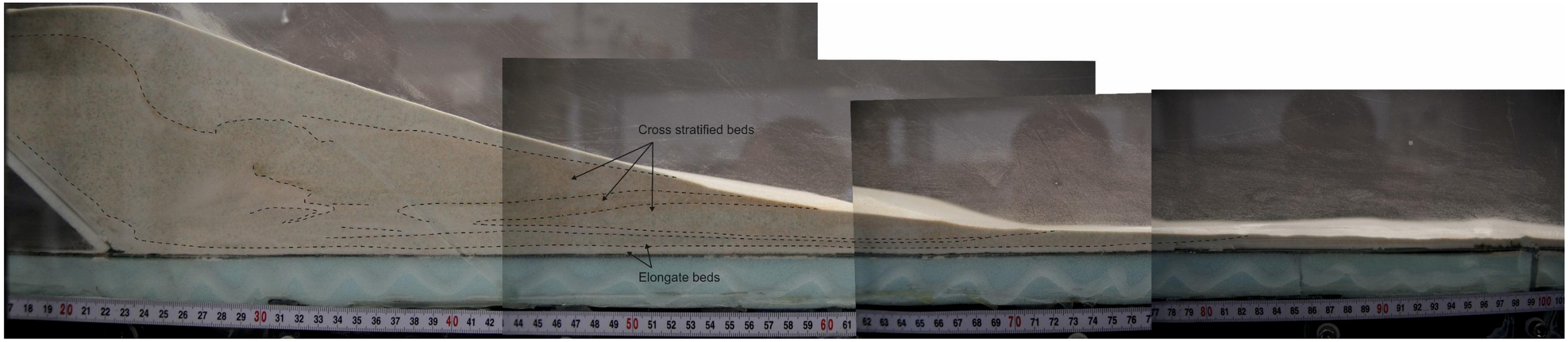

Figure V.21: Deposit from experiment 15 – Fine tri-disperse current

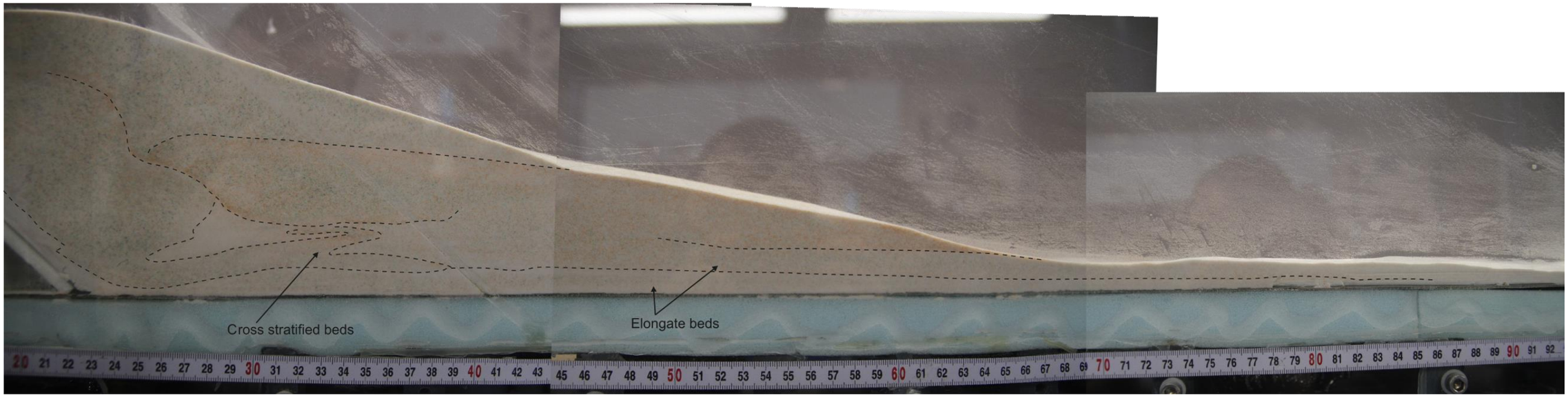

Figure V.22: Deposit from Experiment 16 – Fine tri-disperse current

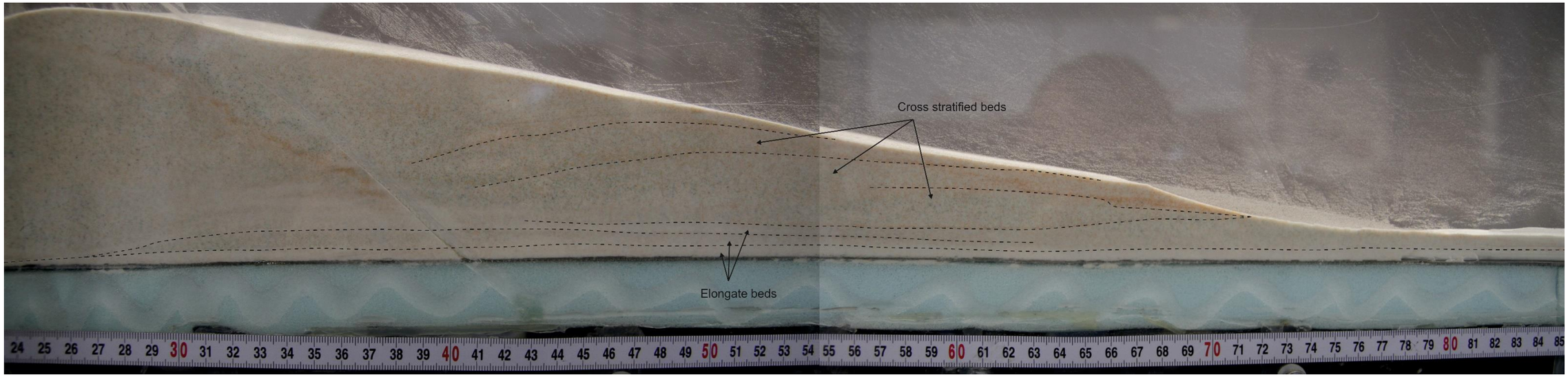

Figure V.23: Deposit from Experiment 17 – Fine tri-disperse current

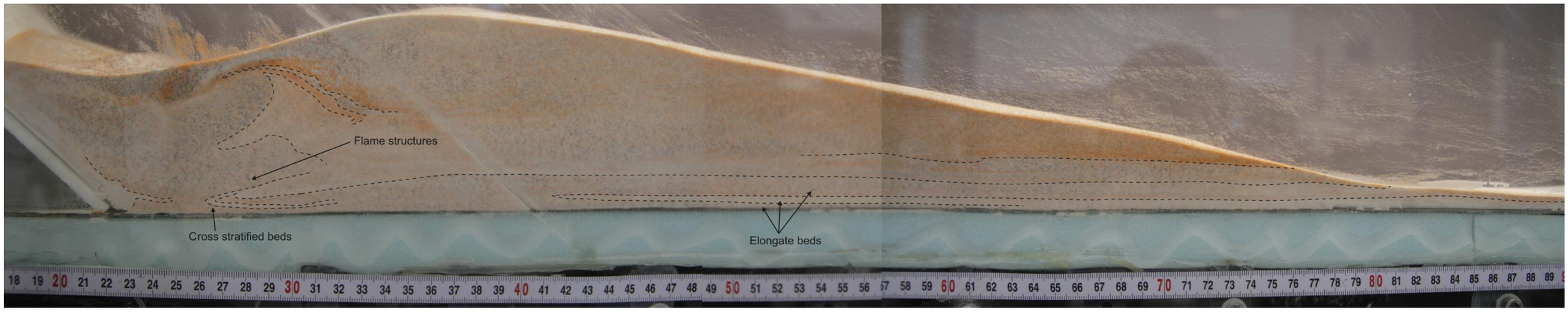

Figure V.24: Deposit from experiment 18 – Coarse tri-disperse current

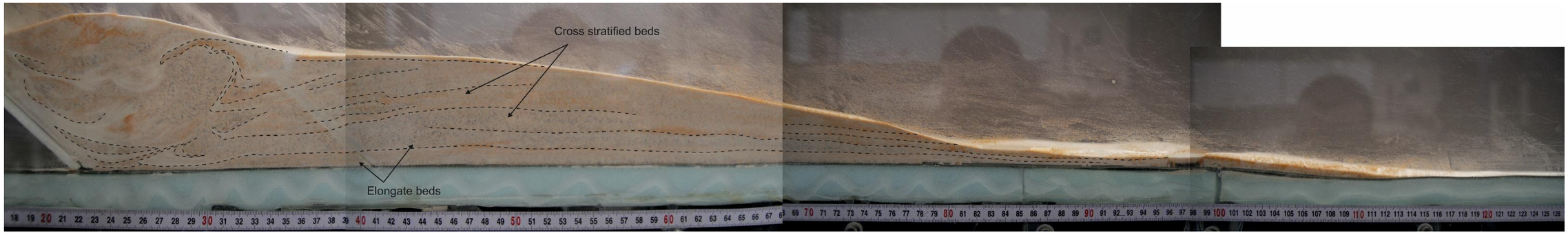

Figure V.25: Deposit from Experiment 19 – Coarse tri-disperse current

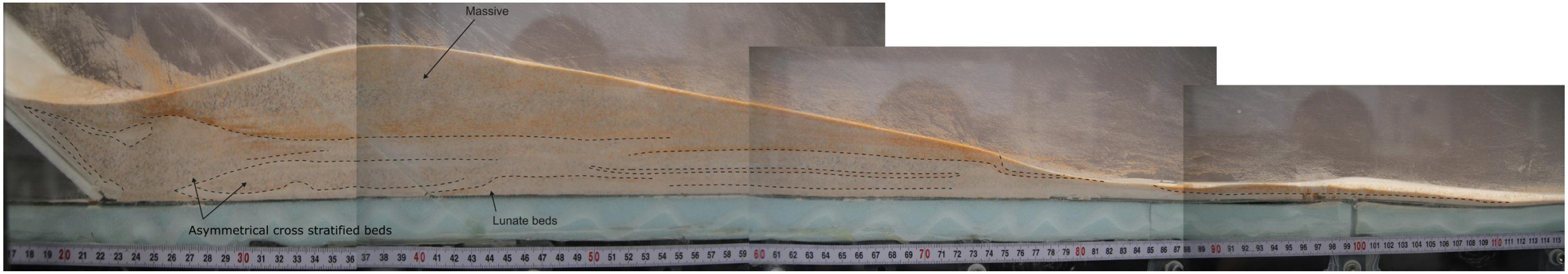

Figure V.26: Deposit from Experiment 20 – Coarse tri-disperse current

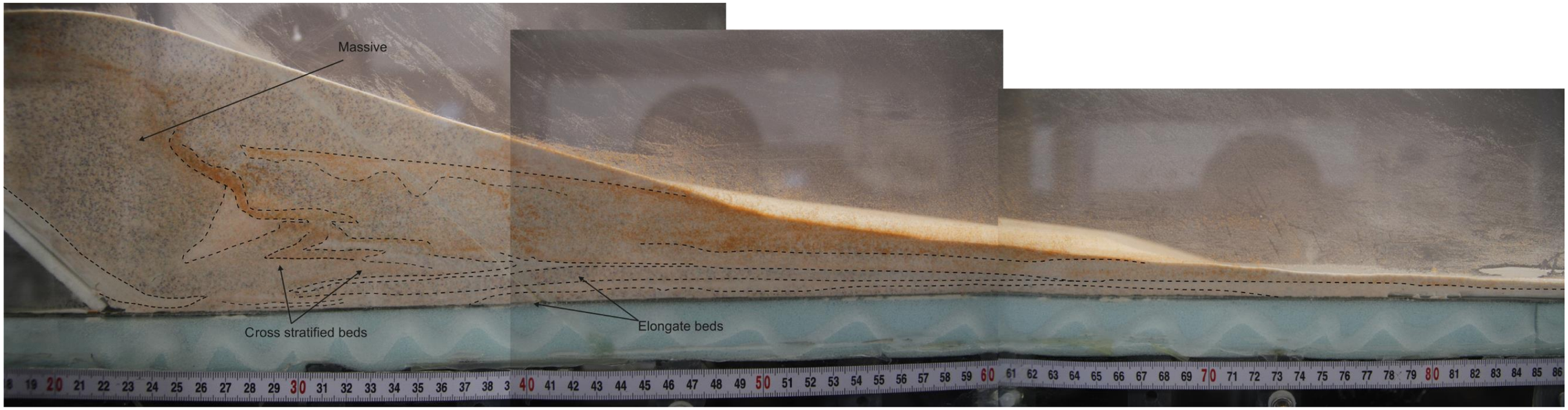

Figure V.27: Deposit from Experiment 21 – Coarse tri-disperse current

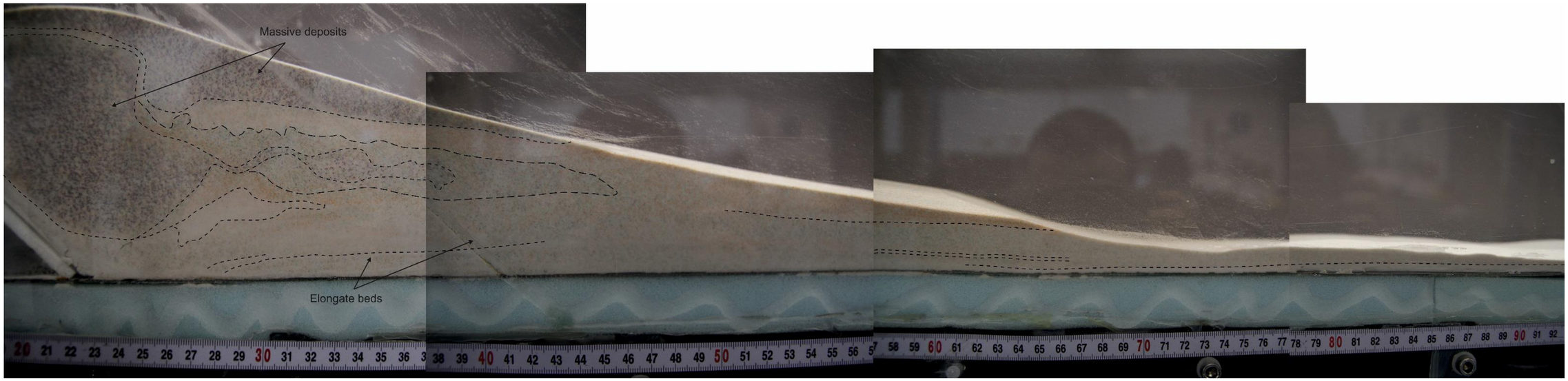

Figure V.28: Deposit from Experiment 22 – Quad-disperse current

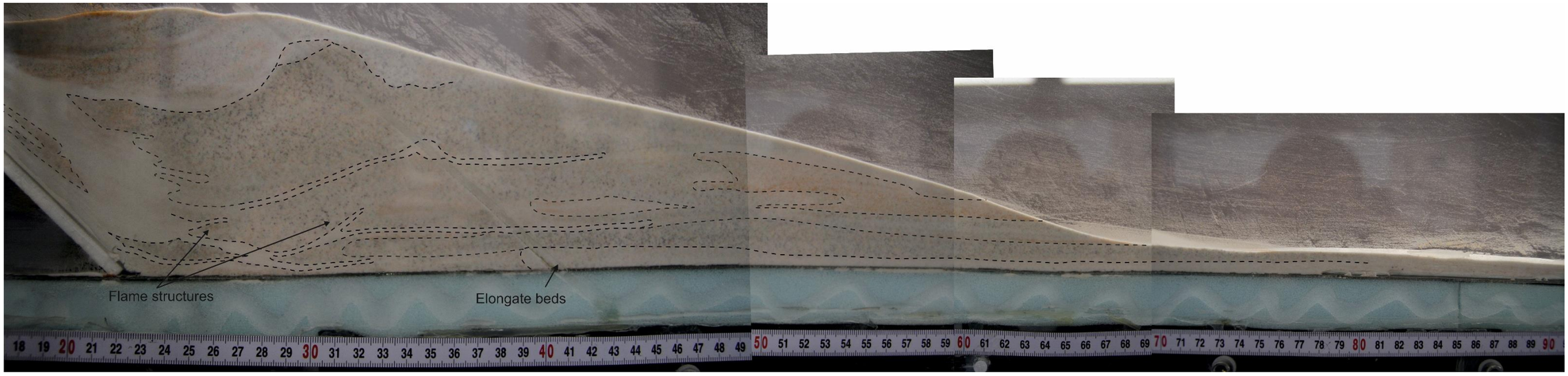

Figure V.29: Deposit from Experiment 23 – Quad-disperse current

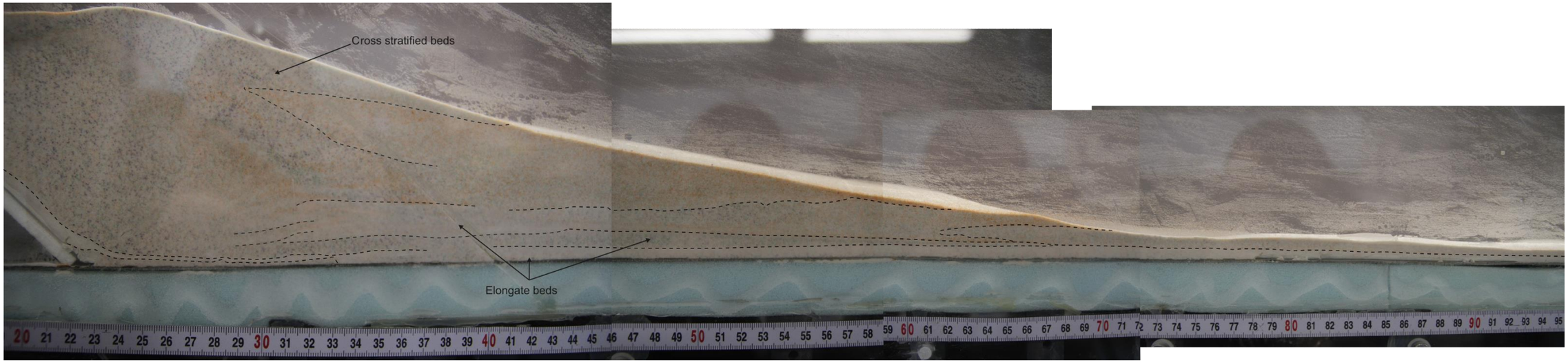

Figure V.30: Deposit from Experiment 24 – Quad-disperse current

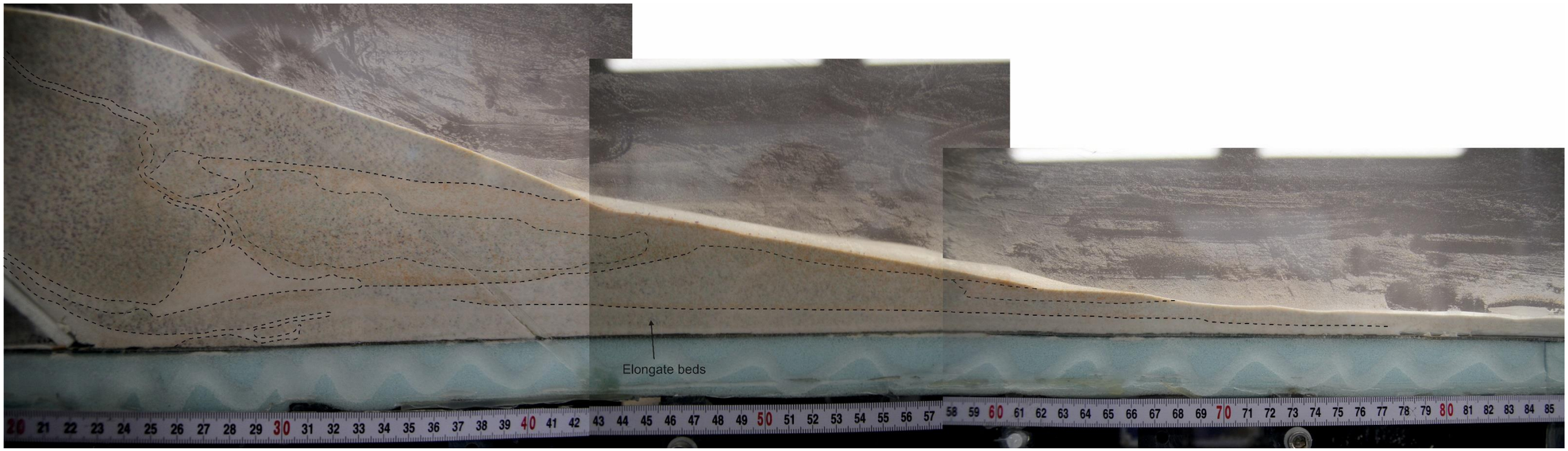

Figure V.31: Deposit from Experiment 25 – Quad-disperse current